CYTOPLASMIC DYNEIN AND DYNACTIN COORDINATE MICROTUBULE DYNAMICS AT THE GROWING PLUS END

Jacob Eric Lazarus

A DISSERTATION

In

Cell and Molecular Biology

Presented to the Faculties of the University of Pennsylvania

in

Partial Fulfillment of the Requirements for the

Degree of Doctor of Philosophy

2012

Supervisor of Dissertation

____

Erika LF Holzbaur

Professor, Physiology

Graduate Group Chairperson

____

Erfei Bi, Professor of Cell and Developmental Biology

Dissertation Committee

Morris Birnbaum, Professor of Medicine

Kathryn Ferguson, Associate Professor of Physiology

Michael Ostap, Professor of Physiology

CYTOPLASMIC DYNEIN AND DYNACTIN COORDINATE MICROTUBULE DYNAMICS AT THE GROWING PLUS END

COPYRIGHT

2012

JACOB ERIC LAZARUS

ABSTRACT

CYTOPLASMIC DYNEIN AND DYNACTIN COORDINATE MICROTUBULE DYNAMICS AT THE GROWING PLUS END

Jacob Eric Lazarus

Erika L.F. Holzbaur

Microtubules are cytoskeletal polymers that serve as long-distance tracks for intracellular transport. However, microtubules are not static tracks; they undergo dynamic instability, a non-equilibrium behavior which allows them to continually remodel. Microtubules must remodel to adapt to the changing needs of the cell, yet they must also be stable enough to allow long-distance transport by kinesins and by cytoplasmic dynein and its partner complex dynactin. Microtubule dynamics are strongly influenced by microtubule-associated proteins, which bind to microtubules and bias them toward growth or shrinkage. A pool of dynein and dynactin localizes to the microtubule plus end and to the cortex, where we hypothesized that they might not be solely poised to initiate retrograde runs, but might also act to modify microtubule dynamics. To test this, we reconstituted microtubule dynamic instability *in vitro* and visualized it using TIRF microscopy.

We show that dynein, when immobilized in an orientation recapitulating its membrane recruitment, can tether growing microtubules, reducing their lateral diffusion and delaying catastrophe. This effect does not represent mere microtubule binding; dynein tethers microtubules more effectively than kinesin or the plus end-tracking protein EB1, and we show that this ability of dynein is dependent on its ATPase activity. Modeling suggests that dynein may delay catastrophe by actively applying tension to straighten, and thus stabilize the microtubule. We also have examined the effects of the p150^{Glued} subunit of dynactin on microtubule dynamics. We find that to modify dynamics, p150^{Glued} must be dimerized, and it must bind tubulin, an interaction that requires its CAP-Gly and basic domains in tandem. p150^{Glued} is alternatively spliced in vivo, with the isoform including both these domains expressed primarily in neurons. Accordingly, depletion of p150^{Glued} in a non-polarized cell line does not alter microtubule dynamics, while p150^{Glued} RNAi in neurons leads to a dramatic increase in microtubule catastrophe. Strikingly, a Parkinson syndrome-associated mutation blocks this microtubule-stabilizing activity both in vitro and in neurons. Together, these data provide novel mechanistic insight into how cytoplasmic dynein and dynactin, the principle minus end-directed motor complex in the cell, also act at the plus end to coordinate microtubule dynamics.

Table of contents

List of tables……….………………………………………………………...……ix

List of illustrations…...……………………………………………………..…….….x

1. Introduction………………………………………………………………………..1

1.1 Microtubules…………………………………..……………………………1

1.1.1 Historical background……………………………………………………….1

1.1.2 Current Knowledge…………………….……………………………………2

1.2 Dynein……………………………………………………………………………4

1.2.1 Historical background……………………………………………………….4

1.2.2 Current Knowledge…………………….……………………………………5

1.3 Dynactin………………………………………………………………………….8

1.3.1 Historical background……………………………………………………….8

1.3.2 Current Knowledge…………………….……………………………………9

1.4 Thesis aims and overview…………………………………………………14

2. Methods……………………………………..…………………………15

2.1 Methods for Chapter 3……………………………..……………………………15

2.1.1 Protein purification and labeling……………………..……………………………15

2.1.2 Microtubule-binding assays………………………..……………………………15

2.1.3 Microtubule seeds…………………………………………………….……16

2.1.4 Microtubule plus-end tracking assays……………………………………...……16

2.1.5 Image analysis and statistics……………………………………………………….17

2.2 Methods for Chapter 4……………………………………………………….……18

2.2.1 Protein purification…………………………………………………………...18

2.2.2 In vitro tethering assays………………………………………………………18

2.2.3 TIRF assays for microtubule dynamics………………………………………19

2.2.4 Computational modeling……………………………………………………...20

2.3 Methods for Chapter 5.…………………………………………………………21

2.3.1 Protein purification…………………………………………………………...21

2.3.2 Glutaraldehyde cross-linking…………………………………………………23

2.3.3 Analytical size exclusion chromatography…………………………………...23

2.3.4 Light scattering assay…………………………………………………………24

2.3.5 TIRF microtubule elongation assay…………………………………………..24

2.3.6 TIRF microtubule nucleation assay…………………………………………..25

2.3.7 Microtubule binding assays…………………………………………………..25

2.3.8 Live cell imaging and analysis……………………………………………….26

2.4 Methods for Chapter 6………………………………………………………….26

2.4.1 Protein purification..………………………………………………………….26

2.4.2 COS7 assays………………………………………………………………….27

2.4.3 Knock-in mouse characterization…………………………………………….27

2.4.4 Recombinant p150 interaction with bovine dynein.………………………………27

3. Microtubule plus-end tracking by CLIP-170 requires EB1…………………………...29

3.1 Introduction……………………………………………………………………..30

3.2 Results……………..…………………………………………………………….32

3.2.1 EB1 targets growing microtubule plus-ends independently of other proteins……..32

3.2.2 CLIP-170 requires EB1 for +TIP activity……………………………………….33

3.2.3 Both EB1 and CLIP-170 rapidly turnover at microtubule plus-ends……………...35

3.2.4 GMPCPP abolishes +TIP activity of EB1 and CLIP-170…………………………36

3.3 Figures…..……..……………………………………………………………………..38

3.4 Discussion………..………………………………………………………………….46

4. Dynein tethers and stabilizes dynamic microtubule plus ends……………………….51

4.1 Introduction…………………………………………………………………………52

4.2 Results……………………………………………………………………………….52

4.2.1 Dynein tethers Taxol-stabilized microtubules……………………………………52

4.2.2 Dynein motor tethers and stabilizes dynamic microtubules………………………54

4.2.3 Modeling suggests dynein inhibits catastrophe by straightening protofilaments….56

4.3 Figures…..……..……………………………………………………………………..58

4.4 Discussion…………………………………………………………………………….63

5. Dynactin regulates neuronal microtubule dynamics by binding to soluble tubulin...…66

5.1 Introduction……………………………………………..……………………67

5.2 Results……………………………………………………..……………………69

5.2.1 p150^{Glued} dimer potently promotes microtubule formation…...……………………70

5.2.2 p150^{Glued} increases the rate of microtubule polymerization and inhibits catastrophe………………………………………………………………………….71

5.2.3 p150^{Glued} modifies microtubule dynamics independently of EB1…………………72

5.2.4 p150^{Glued} catalyzes microtubule nucleation……………………………………73

5.2.5 p150^{Glued} promotes microtubule formation by binding to soluble tubulin…………74

5.2.6 Neuron-specific p150^{Glued} isoform stabilizes microtubules……………………………75

5.2.7 p150^{Glued} is a tissue-specific microtubule modifier………………………………………77

5.2.8 A Parkinson disease mutation abolishes p150^{Glued} activity……………………………78

5.3 Figures…..…………………………………………………………………………………80

5.4 Discussion…………………………………………………………………………………94

6. Dynein activation by dynactin……...………….…………97

6.1 Introduction………………………………………………………………………………98

6.2 Results……………..……………………………………………………………………100

6.3 Figures…..………………………………………………………………………………105

6.4 Discussion………………………………………………………………………………115

7. Conclusion……………………………………………………………………………...116

7.1 Microtubule plus end reconstitution……………………………………………………..116

7.2 Dynein tethering…………………………………………………………………………120

7.3 Dynactin plus end regulation……………………………………………………………124

8. Future directions…………………………………………………………………………127

8.1 Dynein tethering…………………………………………………………………………127

8.2 Dynactin plus end regulation……………………………………………………………129

8.3 Dynein activation by dynactin………………………………………………………….130

Bibliography………………………………………………………………………………134

List of tables

Chapter 3

Table S1 Dynamic instability properties of in vitro polymerized microtubules in the presence and absence of +TIPs……………………………………………………………..…45

List of illustrations

Chapter 3

Figure 1 Microtubule plus-end tracking by the human EB1 protein…………………….38

Figure 2 CLIP-170 requires EB1 for +TIP activity…………………………………...39

Figure 3 Rapid turnover of single EB1 and CLIP-170 molecules on the growing ends of microtubules…………………………………………………………………………...40

Figure 4 Effect of GMPCPP on CLIP-170-GFP plus-end tracking activity……………..41

Figure 5 Model for plus-end tracking activity of mammalian EB1 and CLIP-170……...42

Figure S1 Microtubule binding and labeling of +TIP proteins…………………………..43

Figure S2 Single molecule kinetics of EB1-Alexa 488 and CLIP-170-GFP at growing microtubule plus ends…………..…………………………………………………..…44

Chapter 4

Figure 1 Dynein tethers microtubule plus ends in vitro………………..………………...58

Figure 2 Dynein-mediated tethering of dynamic microtubule plus ends is ATP dependent

Figure 3 Cortically localized dynein tethers and stabilizes microtubules…..…………….59

Figure S1 Dynein bound to beads can drive translocation of free microtubules; dynein-bound beads released from the trap translocate on bound microtubules..……………….60

Figure S2 Dynein stabilizes interactions of dynamic microtubule plus ends with a bead.61

Chapter 5

Figure 1 p150^{Glued} promotes microtubule formation…………………...………………...80

Figure 2 p150^{Glued} catalyzes microtubule nucleation……………………………………81

Figure 3 p150^{Glued} forms a complex with soluble tubulin….……………………………82

Figure 4 Tissue-specific p150^{Glued} isoforms differentially modify microtubule dynamics………………………………………………………………………………83

Figure 5 p150^{Glued} stabilizes microtubules in neurons…………………………………...84

Figure 6 A Parkinson syndrome mutation abrogates p150^{Glued} activity…………………85

Figure S1 Characterization of recombinant dimeric and monomeric p150 polypeptides……………………………………………………………………………...86

Figure S2 Characterization of complex formation between the p150 Nt and tubulin…...88

Figure S3 Characterization of recombinant Δ5-7 Nt-GCN4 and p135 Nt-GCN4 representing endogenous isoforms…………………………………………...…….90

Figure S4 Characterization of p150^{Glued} role in modulating microtubule dynamics in cells………………………………………………………………………………91

Figure S5 Characterization of Q74P mutant construct…………………………...…...93

Chapter 6

Figure 1 Coarse mapping of the p150^{Glued} binding region for dynein…………………105

Figure 2 Yeast 2 hybrid analysis of the p150^{Glued} binding region for dynein…………..106

Figure 3 Secondary structure prediction for p150^{Glued} CC1 region……………………107

Figure 4 Fine mapping of the p150^{Glued} binding region for dynein……………………109

Figure 5 Depiction of the splicing of the DIC1 and DIC2 genes………………………110

Figure 6 Isoform-specific differences in dynein-dynactin binding……………………..111

Figure 7 Characterization of DIC1-GFP-FLAG knockin mice by immunoprecipitation…………………………………………………………………....112

Figure 8 Characterization of DIC1-GFP-FLAG knockin mice by density centrifugation……………………………………………………………………...113

Figure 9 Characterization of the ability of recombinant p150^{Glued} to bind native dynein…………………………………………………………………………...114

1. Introduction

In large eukaryotic cells, simple diffusion is not sufficient to allow timely transport of small vesicular cargo or large organelles. Instead, active transport occurs along the cytoskeleton, a network of dynamic biological polymers. Of these polymers, microtubules are the most important in facilitating long-distance transport. However, microtubules are not static tracks; they must continually remodel to adapt to changing cellular conditions, yet they must also be stable enough to allow kinesins and cytoplasmic dynein and its partner complex dynactin to travel long distances.

1.1 Microtubules

1.1.1 Historical background

Microtubules had been described by anatomists and histologists since the beginning of the 20th century, but their ubiquity was only recognized after aldehyde fixation became widely adopted for use in electron and light microscopy (Sabatini et al., 1963). Early work focused primarily on cilia and flagella, where microtubules are arranged in regular, geometric arrays. This allowed careful electron microscopists to infer that microtubules were actually polymers made up of regular and repeating protomers (Grimstone and Klug, 1966). At the same time, workers studying the mitotic apparatus, also thought to be composed of microtubules, were able to isolate an abundant protein constituent that sedimented at 6S. This 6S subunit bound to colchicine, a well-characterized microtubule poison. This, then, was tubulin (Borisy and Taylor, 1967a, b; Shelanski and Taylor, 1967). Its essential qualities were quickly revealed.

It was found that microtubules contained bound guanine nucleotides (Stephens et al., 1967; Yanagisawa et al., 1968). With the development of techniques to better resolve proteins by gel electrophoresis, it became clear that the tubulin protomer was actually a heterodimer consisting of an alpha- and a beta-tubulin subunit (Bibring and Baxandall, 1971; Bryan and Wilson, 1971; Feit et al., 1971). Reliable purifications of tubulin from brain tissue were devised, and the ionic and nucleotide optima for in vitro polymerization deduced (Lee and Timasheff, 1977; Olmsted and Borisy, 1975).

This allowed the systematic study of the microtubule polymer. Though initial studies proposed that microtubules might treadmill in a way similar to actin (Margolis and Wilson, 1981), subsequent work revealed that in fact, microtubules behaved quite differently. They found that microtubules exist in both growing and shrinking states, and at least in vitro, they can do this from both the plus and minus ends (Horio and Hotani, 1986; Mitchison and Kirschner, 1984). In ways that we are only now beginning to fully understand, this process depends on the incorporation of hydrolysable GTP into the microtubule lattice (Carlier et al., 1984).

1.1.2 Current knowledge

Microtubules, then, are dynamic polymers that, in purified systems, add subunits at both the slow-growing minus and fast-growing plus ends. However in cells, after the formation of a stable nucleus, canonically at the centrosome, the minus-end is somehow capped and stabilized (Evans et al., 1985; Mitchison and Kirschner, 1985). In this way, growth occurs selectively from the plus end.

We now know that both alpha- and beta-tubulin are part of large, multi-gene families (Cleveland et al., 1978; Cleveland et al., 1980). During and after translation, the nascent alpha- or beta- tubulin requires a diverse array of cellular chaperones to attain its final shape and unite into a dimer. Some of the tubulin chaperones are general cofactors, while others are completely devoted to folding tubulin (Gao et al., 1993).

In solution, the tubulin protomer exists overwhelmingly in a GTP-bound state. We now think that in this state, tubulin is mostly straight and extended along the alpha-beta longitudinal axis. Though microtubule polymerization does not require GTP hydrolysis, dynamic instability does (Hyman et al., 1992; Muller-Reichert et al., 1998). Tubulin catalyzes its own hydrolysis; upon incorporation into the microtubule, contacts with residues in the previously incorporated protomer triggers GTP hydrolysis in the newly incorporated protomer. The preferred conformation of GDP-bound tubulin is not straight; it is curved, but because the microtubule is straight, GDP-tubulin is prevented from adopting this conformation (Nogales et al., 1999; Nogales et al., 1998; Wang and Nogales, 2005). In this way, the energy from GTP hydrolysis in individual tubulin subunits is stored by the microtubule as mechanical strain (Caplow et al., 1994). This stored energy can be used to perform work, either through microtubule polymerization (Dogterom and Yurke, 1997; Koshland et al., 1988) or depolymerization (Grishchuk et al., 2005; Molodtsov et al., 2005; Westermann et al., 2005; Westermann et al., 2006).

Though microtubules polymerized in vitro may contain anywhere from 11-15 protofilaments, cytoplasmic microtubules predominantly contain 13 tubulin protofilaments (McIntosh et al., 2009). At the single filament level, microtubules undergo alternating phases of slow polymerization followed by rapid depolymerization (Salmon et al., 1989; Walker et al., 1988). The transition from polymerization to depolymerization is termed "catastrophe," while the opposite transition is termed "rescue" (Mitchison and Kirschner, 1984).

Recently, we have also begun to understand microtubule dynamics at the single protofilament, and the single protomer level. After incorporation into the microtubule, hydrolysis of the bound GTP rapidly occurs, resulting in a small cap of un-hydrolyzed GTP-tubulin (Seetapun et al., 2012). This small cap is sufficient to prevent the rest of the microtubule from adopting the lower energy curved conformation. P_i is then slowly released (Maurer et al., 2012). At some point, defects due to active microtubule depolymerases (Gardner et al., 2011b; Helenius et al., 2006; Varga et al., 2006) or poorly-understood stochastic errors in tubulin incorporation (Gardner et al., 2011b) lead to loss of the GTP cap, and to catastrophe. It is thought that through this cycle of microtubule growth and shrinkage, the cell can organize a dynamic, yet productive cytoskeleton (Holy and Leibler, 1994).

1.2 Dynein

1.2.1 Historical background

Dynein – in fact, a whole diversity of axonemal dyneins – had been isolated from cilia and flagella starting as early as the 1960's (Gibbons, 1963). Ironically, as axonemal dynein became better characterized, it had the impact of breeding skepticism toward reports of cytoplasmic dynein-like activities; it was thought these reports resulted from contamination (Stebbings, 1988).

In the late 1980's, stimulated by the excitement generated from the characterization of kinesin (Vale et al., 1985), a burst of papers proved convincingly that there was indeed a cytoplasmic dynein. A previously identified high molecular weight microtubule associated protein was found to translocate microtubules and have similar nucleotide-hydrolyzing properties to axonemal dynein (Paschal et al., 1987). This translocation was subsequently determined to proceed toward the microtubule minus-end (Paschal and Vallee, 1987). Finally, scanning transmission electron micrographs were obtained that clearly show structurally equivalency to axonemal dynein (Shpetner et al., 1988). Around the same time, cytoplasmic dyneins from different organisms and organs were also characterized (Euteneuer et al., 1988; Lye et al., 1987).

1.2.2 Current knowledge

Parts of this section were adapted from:
Dynein at odd angles? (News & Views), Hendricks AG, Lazarus JE, Holzbaur EL., Nat Cell Biol. 2010 Dec;12(12):1126-8. Epub 2010 Nov 21.

We now know that cytoplasmic dynein is a complex motor, with two dimerized heavy chains made up of motor, linker and tail domains. In addition, the dynein complex includes intermediate, light intermediate and light chains that assemble onto the tail domain of the heavy chain and together form the main cargo-associating domain of the complex (Gill et al., 1994; Hughes et al., 1995; Paschal et al., 1992).

When compared with motors from the kinesin and myosin superfamilies, dynein is distinct. Kinesins and myosins involved in vesicular transport possess relatively small, compact motor domains that hydrolyse ATP and bind directly to their cognate cytoskeletal tracks (Kull et al., 1996). In contrast, each of the two dynein motor domains is a large 13-nm diameter ring consisting of six concatenated AAA modules (ATPase associated with various cellular activities) (Mikami et al., 1993; Mocz and Gibbons, 2001). At least two of these modules are known to bind nucleotides and affect motility. Improbably, the microtubule-binding domain of dynein is not located within its AAA modules, but is instead located at the tip of a stalk that projects from the ring (Carter et al., 2008; Gee et al., 1997). Thus, the dynein microtubule-binding site is as much as 15 nm away from the primary site of nucleotide hydrolysis, requiring long-range structural rearrangements that we are now only beginning to understand (Roberts et al., 2012; Roberts et al., 2009)

With respect to function, cytoplasmic dynein is also unique. The kinesin and myosin superfamilies are composed of many diverse members with biophysical distinctions that suggest functional specialization. In contrast, a single form of cytoplasmic dynein performs a wide variety of roles in mammalian cells ranging from spindle assembly and nuclear migration to retrograde vesicular transport. Thus, the mechanical properties of dynein arising from its unique structure may reflect evolutionary tradeoffs allowing one motor to perform a diverse array of cellular roles.

Single-molecule studies have begun to clarify how dynein performs these diverse roles. The emerging view is that of a flexible motor capable of stepping along the microtubule in a variety of ways. Dynein primarily takes 8 nm steps towards the minus end of the microtubule, but these steps can range from 8 to 32 nm (Mallik et al., 2004; Toba et al., 2006). Dynein even has a tendency to step backward or sideways to an adjacent protofilament (Ori-McKenney et al., 2010; Ross et al., 2006; Wang et al., 1995). This suggests that, unlike for myosin or kinesin, the coupling between dynein motor domains is flexible, or possibly variable.

Compared to myosin or kinesin, mammalian dynein is also a relatively weak motor. Although there is not yet complete agreement (Toba et al., 2006), the general consensus is a unitary stall force of 1 pN (Mallik et al., 2004; Schroeder et al., 2010). In contrast to dynein, the major anterograde motor for axonal transport, kinesin-1, moves processively in 8 nm steps along a single protofilament, only very rarely taking backwards or sideways steps, and the stall force is close to 6 pN (Yildiz et al., 2008; Yildiz et al., 2004).

Cytoplasmic dynein from yeast is a much slower and stronger motor with less variable stepping, but detailed studies have provided insight into a (presumably conserved) mechanical behaviour. Gennerich et al. (2007) observed that large steps (> 8 nm) were often followed by backward steps, resulting in periods of highly processive, 8 nm steps towards the minus end interspersed with periods of large forward and backward steps. Recent single-molecule experiments that simultaneously visualized both motor domains confirm this, and show that even for the relatively processive yeast dynein, coordination between the motor domains is weak (DeWitt et al., 2012; Qiu et al., 2012).

Taken together, these studies portray dynein as a large, flexible motor, capable of many types of stepping that correlate with its role as a molecular multi-tasker. While under low loads, it may take processive steps to efficiently transport cargos over long distances. But at high loads, dynein may act as a stationary tether by taking back and forth steps (Ross et al., 2008),

1.3 Dynactin

1.3.1 Historical background

Though we now know cytoplasmic dynein is the major motor that translocates minus end-directed cargo, for a short period after its discovery in the late 1980's, the evidence for this was actually quite circumstantial. Because methods at the time to inhibit dynein in cells were so crude, cell-free systems were developed to test this hypothesis.

Using video-enhanced differential interference contrast light microscopy (Schnapp, 1986), salt-washed organelles were imaged on microtubules in the presence of purified dynein. It was found that the purified dynein motor could not translocate vesicles by itself, but instead required an unknown activity from added-back cytosol (Schnapp and Reese, 1989; Schroer et al., 1989).

This was an important result. It implied that the cargo receptor for dynein was likely not contained within the dynein complex itself, but instead provided by a soluble adaptor. In this way, multiple adaptors could provide specificity for the variety of cargoes it might encounter in the cell and need to transport. It might also be that, instead, dynein might inherently be capable of interacting with cargo, but in some other way, it might need to be “activated.”

A report soon emerged of just such a dynein activating factor (Schroer and Sheetz, 1991). The authors discovered it by first isolating dynein and co-purifying factors via microtubule-pelleting, ATP release, and subsequent centrifugation over a sucrose gradient. In contrast to previous reports (Schroer et al., 1989), this sucrose gradient-purified dynein was competent to power organelle movements, likely because of the higher protein concentrations achieved. However, after further purification of dynein from co-migrating complexes by ion exchange chromatography, the authors once again found that this highly pure dynein was unable to translocate organelles (Schroer and Sheetz, 1991).

One of the fractions off the ion exchange column was found to drastically increase the ability of dynein to transport organelles. This dynein activating factor came to be known as dynactin (Gill et al., 1991; Schroer and Sheetz, 1991).

1.3.2 Current knowledge

Dynactin was subsequently characterized as a large multi-protein complex with its largest 150 kD subunit showing extensive homology to the Drosophila protein Glued (Gill et al., 1991), and a previously identified mammalian homolog (Holzbaur et al., 1991, 1992). We now know that the dynactin complex is a necessary for most dynein-dependent processes in the cell. However, due to its structural complexity, its ubiquitous localization, and its multiple activities, exactly how it aids dynein is still surprisingly mysterious.

Quantitative Western blotting (Gill et al., 1991; Schafer et al., 1994) and low-resolution structural analysis of dynactin have allowed us to at least begin to gain a picture of the overall complex. Most of the work has been accomplished via isolation of dynactin from brain (either mammalian (Bingham et al., 1998) or avian (Schroer and Sheetz, 1991)) followed by platinum-replica- and immuno-electron microscopy (Schafer et al., 1994) or negative stain electron microscopy with single particle reconstruction (Hodgkinson et al., 2005; Imai et al., 2006).

The most prominent feature of dynactin is a short, 40 nm rod consisting of 7-9 copies of the actin-related protein, Arp1 (Clark and Meyer, 1992; Schafer et al., 1994). Arp1 has a ~50% sequence identity to actin (Lees-Miller et al., 1992), which has allowed the rod to be reconstructed using high-resolution structures of canonical actin (Hodgkinson et al., 2005). From these reconstructions, and from biochemical evidence (Bingham and Schroer, 1999), it is clear that the Arp1 filament is a polar structure resembling F-actin, but what allows its length to be so precisely regulated is currently unknown.

The primary function of the Arp1 filament and an associated subcomplex at its pointed end (Yeh et al., 2012; Zhang et al., 2011), is believed to be in allowing dynactin to associate with cellular cargo. Similar to one mode whereby F-actin is thought to interact with the cell cortex, Arp1 has been shown to interact with spectrin, including the β3 isoform of organelle-associated spectrin (Holleran et al., 2001; Holleran et al., 1996).

This may help dynactin interact with intracellular vesicles and the Golgi (Muresan et al., 2001).

The other major structural feature of dynactin is a broad, triangular density emanating from the barbed end of the Arp1 filament. This is the dynactin shoulder complex, which consists of a higher order assembly of the p50 and p24 subunits (Echeverri et al., 1996; Gill et al., 1991; Karki et al., 1998). Extending from the shoulder complex is a thin, long, flexible structure, with globular densities at its very tip. This projection is the dimeric $p150^{Glued}$ subunit described above. The C-terminus of $p150^{Glued}$ has been reported to interact with the Arp1 rod directly (Waterman-Storer et al., 1995), but complex reciprocal interactions between the $p150^{Glued}$ and the rest of the shoulder complex, all of which are highly helical, likely serves to cement dynactin together (Burkhardt et al., 1997; Valetti et al., 1999).

A large, extended coiled-coil domain (CC1) of $p150^{Glued}$ binds directly to the dynein intermediate chain, and is the only known interface between dynein and dynactin (Karki and Holzbaur, 1995; King et al., 2003; Vaughan and Vallee, 1995). Though earlier studies indicated that an extended C-terminal region of $p150^{Glued}$ was necessary for dynein-binding (Karki and Holzbaur, 1995; Vaughan and Vallee, 1995; Vaughan et al., 2002), more recent work has shown that an isolated CC1 polypeptide is sufficient for stable complex formation with the dynein intermediate chain (King et al., 2003). Interaction of CC1 with dynein in a physiological context appears sufficient for dynactin to activate dynein (Dixit et al., 2008a; Kardon et al., 2009; Kim et al., 2007; Moore et al., 2009). However, whether this is due to a direct influence of dynactin on the mechanochemistry of dynein, or alternatively through linking dynein to the dynactin cargo-binding domain is unknown.

The N-terminus of p150^{Glued} contains the globular projections, its dimeric CAP-Gly domains (Riehemann and Sorg, 1993), which can bind microtubules directly (Waterman-Storer et al., 1995). The N-terminus also contains an extended, highly-basic and serine-rich region which undergoes phosphoregulation (Li et al., 2010; Rome et al., 2010) and can bind microtubules independently of the CAP-Gly domain (Culver-Hanlon et al., 2006). It was thought that the ability of p150^{Glued} to bind to microtubules as well as dynein could act as a second binding site for dynein, tethering it to microtubules and increasing its processivity (Culver-Hanlon et al., 2006; King and Schroer, 2000; Waterman-Storer et al., 1995).

However, we now know that both experimental and physiological truncations of this domain have only minor effects on interphase cargo transport by dynein. In cells, cargo run length, directionality, and velocity are not appreciably affected (Dixit et al., 2008a; Kardon et al., 2009; Kim et al., 2007; Lloyd et al., 2012; Moore et al., 2009; Moughamian and Holzbaur, 2012). The p150^{Glued} N-terminus may instead play a specialized role during mitosis, where it may aid in dynein generating and sustaining the high forces necessary to rearrange the spindle and nucleus (Kim et al., 2007; Moore et al., 2009). The p150^{Glued} N-terminus may also play a role in the initiation of dynein transport, particularly at the microtubule plus-end, where a pool of dynactin has long been observed (Lloyd et al., 2012; Moore et al., 2009; Moughamian and Holzbaur, 2012; Vaughan et al., 2002; Xiang et al., 2000; Zhang et al., 2003). Finally, at the microtubule plus-end, the p150^{Glued} N-terminus may directly modify dynamics through interactions with the microtubule or through other plus end-tracking proteins (Berrueta et al., 1999; Goodson et al., 2003; Hayashi et al., 2005; Lansbergen et al., 2004; Ligon et al., 2003; Ligon et al., 2006).

1.4 Thesis overview

In the research leading to this dissertation, I have investigated the influence of both the dynein complex and the dynactin complex on microtubule dynamics. In the last two decades, we have become comfortable with the notion of dynein-dynactin translocating small vesicles and organelles along microtubules. The experiments here show that, in addition, dynein and dynactin both affect microtubules directly, altering the very tracks on which they walk. You will find those investigations in Chapters 4 and 5.

Before we could test these hypotheses, we needed an in vitro system to interrogate them. The in vitro polymerization of microtubules has been possible for almost 40 years, but when I started this work, we could only image it with visible light microscopy. Our new ability to visualize microtubule dynamics in real time with fluorescence microscopy has given us the ability to gain new spatial and temporal information about the properties of microtubules, and about the proteins that interact with them, particularly those at the growing microtubule plus end. This is described in Chapter 3.

As a final synthesis of this work, I have also begun to determine how dynactin directly affects dynein. In Chapter 6, you will find preliminary data investigating isoform-specific interactions between dynein and the $p150^{Glued}$ subunit of dynactin, and the initial characterization of a recombinant $p150^{Glued}$ polypeptide and the dynein complex from a new knock-in mouse that will enable us to directly observe the influence of dynactin on the stepping and force-generating ability of dynein.

The methods used to perform these experiments are grouped in the next chapter. Figures are also grouped together, and follow the results described in each data chapter. This work was performed in a highly collaborative environment. I list the contributions of other members of the Holzbaur lab at the beginning of each chapter.

2. Materials and Methods

2.1 Methods for Chapter 3

2.1.1 Protein purification and labeling

His-tagged recombinant GFP-labeled CLIP-170(H2) was affinity purified using a nickel column and subsequently desalted using a PD-10 column (Amersham Biosciences) and exchanged into BRB80 buffer (80mM PIPES, 1 mM $MgCl_2$, 1 mM EGTA, pH 6.8) supplemented with 50 mM NaCl. Recombinant GST-tagged full-length EB1 protein was purified using the PreScission expression system (GE Healthcare). Briefly, the fusion protein was purified using glutathione sepharose beads and the GST tag subsequently cleaved via site-specific cleavage with the PreScission protease. The released EB1 protein was further purified using a NAP-10 gel filtration column and exchanged into BRB80 buffer supplemented with 50 mM NaCl. Purified proteins were flash frozen and stored at –80° C until use. Purified EB1 protein was fluorescently labeled at cysteine residues using Alexa-Fluor 488 maleimide (Invitrogen) in BRB80 buffer. The degree of labeling was estimated to be about 70% by spectroscopic analysis.

2.1.2 Microtubule binding assays

Microtubule binding assays were conducted by co-incubating increasing concentrations of rhodamine-labeled microtubules with purified recombinant CLIP-170(H2), CLIP-170(H2)-GFP, EB1, or EB1-Alexa 488 proteins for 30 minutes at 37° C. The samples were then centrifuged at 35,000 g for 20 min and the resultant supernatant and pellet fractions were analyzed by SDS-PAGE and densitometry. Under our experimental conditions, both tagged and untagged EB1 bound weakly to microtubules and did not reach saturation.

2.1.3 Microtubule seeds

Rhodamine-labeled and biotinylated GMPCPP microtubule seeds were prepared by polymerizing 50 µM tubulin (at a ratio of 22.5: 1.5: 1 of bovine tubulin: rhodamine-tubulin: biotin-tubulin) in the presence of 1 mM GMPCPP (Jena Bioscience GmbH) at 37 ºC for 30 min. The assembled microtubules were harvested by centrifuging at 35, 000 g for 20 min and resuspended in BRB80 buffer supplemented with 1 mM GMPCPP. These microtubules were sheared with a 100 µl Hamilton syringe to generate short seeds prior to use.

2.1.4 Microtubule plus-end tracking assays

The in vitro reconstitution experiments were conducted in flow cells (15 µl in volume) constructed using slides and silanized coverslips (Repel silane, Amersham Biosciences) attached with double sided adhesive tape. The flow cell was coated with 20 % monoclonal anti-biotin antibody (Clone BN-34, Sigma) and then blocked with 5% Pluronic F-127 (Sigma). 125 nM sheared GMPCPP microtubule seeds were then introduced in the flow cell. Tubulin polymerization was initiated by introducing 22 µM 1:30 rhodamine-labeled bovine tubulin in BRB 80 buffer supplemented with 0.1% methyl cellulose (4000 cP, Sigma), an oxygen scavenging system containing glucose oxidase, catalase and glucose, 100 mM DTT, 1mM GTP-Mg and +TIP proteins. We used 250 nM

EB1-Alexa 488 and 25 nM CLIP-170(H2)-GFP, unless otherwise stated. Microtubule dynamics was visualized at 22 °C using total internal reflection fluorescence (TIRF) microscopy outfitted on an inverted microscope (Nikon TE-2000U). TIRF excitation was achieved using a 488-nm optically pumped semiconductor laser (Sapphire, Coherent) and a 532-nm diode-pumped solid-state laser (CrystaLaser) to visualize Alexa 488 and rhodamine, respectively. The lowest laser light intensities were used for imaging and under these conditions, the photobleaching rates were slow compared to the fluorescence lifetimes. Images were captured with a back-illuminated electron multiplier-CCD camera (Cascade-512B, Photometrics) using either time-lapse capture at 2 sec intervals for two-color microscopy or burst mode at 10 frames per second for analysis of +TIP dynamics at the single molecule resolution. Control experiments showed that the dwell time of single molecule binding events was the same at a low concentration of labeled protein and at a higher total protein concentration of unlabeled protein containing a labeled fraction.

2.1.5 Image analysis and statistics

Plus-end tracking of EB1-Alexa 488 and CLIP-170(H2)-GFP was analyzed using kymographs generated with the “Multiple Kymograph” plug-in for ImageJ submitted by J. Rietdorf and A. Seitz (European Molecular Biology Laboratory, Heidelberg, Germany). Microtubule growth rates and +TIP dwell tips were extracted from these kymographs. The length of the +TIP comet tails was defined as the distance from the peak fluorescence intensity at microtubule tips to the baseline lattice intensity and was measured from line profiles of fluorescence intensities of EB1-Alexa 488 and CLIP-

170(H2)-GFP. For analyzing the diffusional movement of CLIP-170(H2)-GFP, we used manual tracking to trace the displacement of single molecules on the microtubule lattice. Dwell time and mean squared displacement data were fitted using KaleidaGraph (Synergy Software) and statistical significance was determined using the Student's t-test.

2.2 Methods for Chapter 4

2.2.1 Protein Purification.

Cytoplasmic dynein and tubulin were purified from bovine brain as described (Castoldi and Popov, 2003). Labeled tubulin was purchased from Cytoskeleton, Inc. Recombinant kinesin-1 (K560) and EB1 were expressed in E. coli and purified as described (Dixit et al., 2009; Dixit et al., 2008b).

2.2.2 In vitro tethering assays.

Polarity-marked microtubules were prepared by polymerizing brightly-labeled tubulin onto more dimly-labeled, biotinylated, Taxol-stabilized microtubule seeds. Flow chambers were constructed with a silanized coverslip and a glass slide. Biotinylated microtubules were bound to the coverslip with anti-biotin (Sigma, clone BN-34). Chambers were blocked with pluronic F-127 (Sigma) then rinsed with 2-3 chamber volumes of motility assay buffer (MAB: 10 mM PIPES, 50 mM K+ acetate, 4 mM MgCl2, 1 mM EGTA, pH 7.0, supplemented with 20 µM taxol). Protein-A-coated beads (polystyrene, 1 µm diameter, Polysciences) were incubated with either BSA or dynein on ice for 10 minutes (Perlson et al., 2009). Beads were diluted in motility buffer (MAB supplemented with 0.6 mg/ml BSA, 6 mM DTT, 10 mg/ml glucose, 1 µg/ml glucose oxidase, 0.5 µg/ml catalase, 1 mM ATP, 20 µM Taxol) and added to the chamber. The sample was illuminated using a 532 nm laser and imaged with an EM-CCD camera (Photometrics Cascade II). The lateral thermal fluctuations of the nonbiotinylated plus-ends of microtubules was observed. Then, an optical trap was used to position a dynein- or BSA-coated bead to interact with the plus-end of the microtubule. Kymographs of lateral diffusion were prepared in ImageJ, at the same axial location along the microtubule before and after introduction of the bead. A custom Matlab routine was used to calculate the variance of positions from each kymograph. Independent force traces were acquired using an optical trap for dynein-bound beads interacting with microtubules stably bound to the coverslip (Takagi et al., 2006). The following criteria were used to identify stalls in the force trace data: stall force > 0.5 pN, stall plateau time > 10 ms, pre-stall velocity > 50 nm/s, snapback velocity > 100 nm/s.

2.2.3 TIRF assays for microtubule dynamics.

Microscopy chambers were prepared and dynein was purified as above. YG Beads (polystyrene, 1 µm diameter, Polysciences) were incubated with biotinylated-BSA and protein A and attached to the coverslip via anti-biotin. Dynein or BSA was then bound to the beads, followed by washing with 3 chamber volumes. Biotinylated microtubule seeds stabilized with GMPCPP (Jena Biosciences) were incubated in the chamber in polymerization buffer (80 mM K-PIPES, 1 mM MgCl2, 1 mM EGTA, 1 mM ATP, 3 mg/mL BSA, pH 6.8); the chamber was then washed to remove unbound seeds. Polymerization was initiated with 10 µM tubulin in polymerization buffer supplemented with 0.15% methyl cellulose, 0.5% F-127, 5% deoxy enzyme mix, 22.5 mg/mL glucose, 50 mM DTT, 3 mM GTP. For the no-ATP condition, ATP was not included in the buffers and residual ATP was depleted with a hexokinase-glucose system. Objective-type TIRF illumination (Nikon Ti with house-built TIRF illuminator and 1.49 NA apochromatic TIRF objective) was used to image the microtubules and beads. Images were collected every 2 seconds using an EM-CCD camera (Cascade Photometrics) and analyzed in ImageJ.

2.2.4 Computational Modeling.

3D computational simulations of microtubule assembly were developed using MATLAB (Natick, MA) as previously described (VanBuren et al., 2002). Briefly, outward curling of GDP-tubulin subunits when exposed at a microtubule tip leads to mechanical strain between neighboring tubulin subunits, thus reducing the stability of the subunits in the lattice. Simulations were performed by allowing microtubules to grow for ~20 sec real-time before contacting a stiff barrier which stalled further growth (Schek et al., 2007). Then, the time to a catastrophe event was recorded for each microtubule. To simulate protofilament straightening mediated by dynein, the GDP-tubulin preferred angle was adjusted to 0 deg. (rather than 22 deg.) for an assigned number of randomly selected protofilaments. 3-25 events were simulated for each case.

2.3 Methods for Chapter 5

2.3.1 Protein Purification.

Amino acids 1-210 of human p150^{Glued} (DCTN1, NM_004082.4) were inserted into pET-29a (Novagen) with a short linker (AAAADPPVAT) before the C-terminal 6x-His tag. Dimeric constructs contained a GCN4 sequence (VMKQLEDKVEELLSKNYHLENEVARLKKLVGE) (Trybus et al., 1997) before the linker and 6x-His. Δ5-7 dimer was deleted for exons 5-7 (RGLKPKKAPTARKTTTRRPK). The p135 dimer encodes an N-terminal MMRQ (replicating the endogenous expressed spliceform) appended to p150^{Glued} AA 139-210. Q74P Nt-GCN4 was constructed from the p150 Nt-GCN4 backbone and previously used plasmids (Moughamian and Holzbaur, 2012). The accuracy of inserts was verified by sequencing.

For expression, transformed Rosetta *E. coli* (Novagen) were grown in LB at 37C and 300 RPM under standard chloramphenicol and kanamycin selection. At OD600 of ~0.8, cultures were cooled to 15 C and induced with 0.5 mM IPTG. After 16 hours, cells were harvested and resuspended in binding buffer (500 mM NaCl, 20 mM Tris-HCl pH 7.9, 20 mM imidazole, 1 mM TCEP, supplemented with complete protease inhibitor cocktail from Sigma, TAME, leupeptin, and PMSF). At that point, cells were either flash-frozen in liquid nitrogen, or lysed via French press (Thermo) at 18,000 psi. Nucleic acids were cleaved with DNAse I and RNAse H treatment (Roche) and the lysate was cleared at 45,000 g for 20 minutes at 4C. The supernatant was filtered through a 0.22 um polysulfone membrane (PALL Life Sciences) and applied to a 2 mL V_b Ni Sepharose Fast Flow column by gravity or a 1 mL HisTrap column (GE Healthcare) by FPLC. The column was washed with binding buffer until the UV absorbance had settled, then eluted with binding buffer plus 0.5 M imidazole. Protein-containing fractions were then diluted in 100 mM NaCl binding buffer, loaded into a 50 mL Superloop (GE Healthcare), and injected onto a Mono S 5/50 GL column (GE Healthcare), and eluted with a linear gradient of 0.1 M NaCl to 1 M NaCl in binding buffer. Finally, the protein was exchanged into BRB80 (80 mM PIPES pH 6.8, 1 mM $MgCl_2$, 1 mM EGTA) with 75 mM KCl and 10% glycerol (v/v) by gel filtration on a Superdex 200 10/300 GL column (GE Healthcare), aliquoted, and flash-frozen and stored in liquid N_2. Protein concentration was determined by BCA assay (Pierce) with BSA as a standard. We found that for the p150 constructs, concentration determined in this way differed by only ~10% when compared to concentration determined spectrophotometrically with a calculated extinction coefficient.

Unlabeled tubulin was purified from bovine brain through two cycles of polymerization and depolymerization in high molarity PIPES buffer as described (Castoldi and Popov, 2003). Tau23 was purified as previously reported (Dixit et al., 2008b). EB1 was purified as previously reported (Dixit et al., 2009), except 0.5 M NaCl and 10% glycerol were present throughout, and protein was gel-filtered as for p150 constructs before aliquotting. DCX-GFP was purified after Bechstedt and Brouhard (Bechstedt and Brouhard, 2012).

2.3.2 Glutaraldehyde cross-linking

Dimeric constructs were diluted to 0.5 μM and the p150 monomer was diluted to 1 μM in BRB20 with 125 mM NaCl and 1 mM DTT and incubated on ice with 0.5% glutaraldehyde (Thermo) for 2 hours. The reactions were quenched with an equal volume of 1 M glycine, denatured, and analyzed by SDS-PAGE and colloidal Coomassie staining (Invitrogen).

2.3.3 Analytical size exclusion chromatography

Recombinant polypeptides were thawed and incubated at the molar ratio indicated in the text with 30 μM tubulin or mock-incubated for 10' on ice, then loaded into a 50 μL loop with 80 μL final volume, and injected onto a Superdex 200 10/300 GL column pre-equilibrated with BRB20 (pH 7.1) supplemented with 125 mM KCl and 10 mM imidazole, or indicated concentrations of KCl for Figure 3C. Polypeptides were eluted isocratically at 4 C and 0.4 mL/min in the equilibration buffer and collected in 250 μL fractions. The column was calibrated with gel filtration molecular weight standards (ferritin, β-amylase, alcohol dehydrogenase, bovine serum albumin, and carbonic anhydrase) from Sigma. The void volume was at ~7.5 mL. We did not detect any material in the void for any experiments.

Subtilisin cleavage was performed for the indicated times at room temperature in a 1:350 mass ratio to tubulin after Knipling et al (Knipling et al., 1999) and Gupta et al (Gupta et al., 2010).

2.3.4 Light scattering assay

Assay was performed in BRB80 supplemented with 35 mM KCl, 5% glycerol (v/v), 1 mM DTT, 1 mM GTP, and 1 mg/mL casein (to prevent nonspecific adsorption) mixed in a 96 well half area UV transparent plate (Corning) on ice. The plate was read in kinetic absorption mode at 340 nm in a SynergyMx platereader (BioTek) that had been prewarmed to 37 C. We confirmed that the p150 constructs described here were stable over the time course of the assay and did not contribute to light scattering in the absence of tubulin (Fig S1D). The heat quench in this set up is relatively slow, and we found that it corresponded to the limit of the exponential fit in Fig 2C. Accordingly, when we added 1 μM p150 directly to warm tubulin we observed the instant appearance of light scattering (Fig S1F).

2.3.5 TIRF microtubule elongation assay

Experiments were conducted in flow cells (~8 μL in volume) constructed using slides and silanized coverslips (Amersham Biosciences) attached with double sided adhesive tape and bordered with vacuum grease. The flow cell was coated with 25% monoclonal anti-biotin (Clone BN-34, Sigma) and then blocked with 5% pluronic F-127 (Sigma). The chamber was then washed with 1 mg/mL casein in BRB80, and 6.25 μg/mL freshly-thawed double-cycled GMPCPP (Jenna) (Gell et al., 2010) microtubule seeds were then introduced in the flow cell. These seeds were labeled 1:1:33 with biotin and Alexa488 (Cytoskeleton Inc). The chamber was then washed with 1 mg/mL casein in BRB80.

Polymerization was initiated by introducing polymerization buffer (as described previously (Dixit et al., 2009)) with 7.5 μM tubulin labeled 1:50 with rhodamine tubulin (Cytoskeleton). The final buffer composition was BRB80 supplemented with 28 mM KCl and 3.75% glycerol (v/v). Imaging was performed at 37 C.

2.3.6 TIRF microtubule nucleation assay

Flow cells constructed as above were coated with 15% anti-tetraHis (Qiagen). The chamber was blocked with 5% pluronic F-127. p150 constructs were adsorbed to the chamber at 250 nM, and unbound constructs were removed with copious washing with BRB80 supplemented with 1 mg/mL BSA. Imaging was initiated and nucleation buffer perfused consisting of 3.5 μM tubulin in BRB80 supplemented with 1 mg/mL BSA, 2.5 mM GTP, 50 mM DTT, 140 mM glucose, glucose catalase/oxidase anti-fade system, and 0.25% F-127. Imaging was performed at 37 C.

2.3.7 Microtubule binding assays

Unlabeled tubulin was polymerized at 5 mg/mL in BRB80 and 1 mM GTP and stabilized with 20 μM Taxol on the day of the experiment. Increasing concentrations of microtubules were incubated at 37 C for 20 minutes with 0.4 μM dimeric constructs or 0.8 μM monomeric construct, and centrifuged at 100k rpm in the TLA 120.1 rotor (Beckman) at 37 C for 20 minutes. The supernatant and the pellet were then separated, denatured, and analyzed by SDS-PAGE and densitometry.

2.3.8 Live cell imaging and analysis

Isolation, culture, nucleofection, and imaging of dorsal root ganglion neurons was performed as done previously (Moughamian and Holzbaur, 2012). GFP-EB3 comets were imaged in both the mid- and distal axons, taking care to image only cells that were expressing at appropriately low levels. Kymographs were constructed and quantitated in ImageJ. The X-axis displacement of the comet we computed as the distance until catastrophe, while the slope of the line that the comet makes was taken as the polymerization velocity. COS7 cells were cultured, and transfected per previously (Dixit et al., 2008a), and imaged as for neurons above. Cells expressing appropriate levels of GFP-EB3 were quantitated using the PlusTipTracker software package (Applegate et al., 2011) using the following tracking parameters: search radius of 3-15 pixels; minimum sub-track length of 3 frames; maximum gap length of 5 frames; maximum shrinkage factor (relative to growth speed) of 1.5; maximum angle of 30 degrees forward and 10 degrees backward; and fluctuation radius of 1.0 pixels.

2.4 Methods for Chapter 6

2.4.1 Protein Purification.

p150 1-210-CC1 (AA 1-550 of p150 appended with a FLAG tag – DYKDDK – and an AviTag) was cloned into a viral packaging construct, and virus was generated, and insect cells were infected, harvested, and lysed per previous (Lewis et al., 2012). After clarification at 205,000 g, 1h, 4C, the supernatant was applied to a 5 mL M2-agarose column by gravity (Sigma). The column was then washed with PBS until the absorbance had settled, and eluted with FLAG peptide. Protein-containing fractions were pooled and loaded directly onto a MonoQ 5/50 column (GE Healthcare) that had been pre-equilibrated with 150 mM NaCl, 10 mM Tris HCl, pH 7.5. Contaminants were washed off, and p150 eventually eluted by a linear salt gradient. The peak fractions were desalted into 10 mM Tris pH 7.5, 150 mM KCl, 1 mM DTT, and 10% glycerol. Protein quality was confirmed by running a 100 uL fraction off the MonoQ column on a Superdex 200 10/100 column (GE Healthcare) pre-equilibrated in 10 mM Tris pH 7.5, 300 mM KCl.

2.4.2 COS7 assays

Indicated plasmids were transfected, or co-transfected with 9 ug total DNA per 10 cm plate of nearly-confluent COS7 cells. Transfection was performed with Fugene 6 reagent (Roche). The next day, fully confluent plates were lyed and immunoprecipitation was performed as per previous (Moughamian and Holzbaur, 2012). Quantitation was performed by densitometrically calculating in ImageJ the average of 3 independent experiments. The final number was expressed as a ratio of the IP to the load for a given isoform, and then normalized to the lowest isoform (DIC 2c). The trend was similar if quantitation was done by merely taking the signal for the IP.

2.4.3 Knock-in mouse characterization

To confirm that the endogenously expressed DIC1-GFP was incorporated normally into the dynein complex, we homogenized brains from homozygous mice in ice cold homogenization buffer (BRB80 supplemented with 1 mM DTT, 1 mM ATP and protease inhibitor cocktail), clarified the lysate for 30 minutes at 122,000 rcf, and bifurcated the resulting sample for analysis by immunoprecipitation and by sucrose gradient centrifugation. Sucrose gradient centrifugation was performed as previously described (Ross et al, 2006), and fractions were collected and analyzed by Western blot. For immunoprecipitation, anti-FLAG (M2, Sigma), anti-DIC (1618, Millipore), and anti-Myc as a negative control (Invitrogen), were coupled according to manufacturer's instructions to Protein G dynabeads (Invitrogen). The coupled beads were then incubated with equal volumes of the clarified lysate at room temperature for 60 minutes with intermittent agitation, followed by washing in homogenization buffer, and boiling in Laemlli denaturing buffer to collect the immunoprecipitated proteins.

2.4.4 Recombinant p150 interaction with bovine dynein

Immunoprecipitation was performed as above against the His-tag of p150 1-210-GCN4 or against the FLAG tag of 1-210-CC1. This was done after incubation of approximately 30 ug recombinant proteins with approximately 3 ug of bovine cytoplasmic dynein in BRB80 + 1 mg/mL BSA + 1 mM ATP for 60 minutes at room temperature with intermittent agitation, followed by 3 washes in the incubation buffer.

CHAPTER 3.

Microtubule plus-end tracking by CLIP-170 requires EB1

This work was originally published as:

Proc Natl Acad Sci U S A. 2009 Jan 13;106(2):492-7.

Dixit R, Barnett B, Lazarus JE, Tokito M, Goldman YE, Holzbaur EL.

Contributions:

During my initial rotation in the lab, I was able to advance previous attempts at reconstituting microtubule dynamics, and I purified CLIP-170 (H2). After I returned to medical school, Ram Dixit optimized the protocol, and with Brian Barnett, collected the data in the main text of the paper. When I returned to graduate school, I helped with revisions by performing additional control experiments.

3.1 Introduction

Microtubules are highly dynamic polymers of tubulin that are essential for a variety of fundamental processes within eukaryotic cells, including vesicle transport, cell division, and cell motility. In most mammalian cells, microtubules are nucleated at the microtubule organizing center (MTOC) where their minus-ends may remain stably anchored (Dammermann et al., 2003). Microtubule plus-ends growing out from the MTOC are highly dynamic, undergoing stochastic switching between growing and shortening phases (Howard and Hyman, 2003). These dynamics allow microtubule plus-ends to explore the cellular environment. A ‘search and capture’ model has been proposed in which the randomly directed outgrowth of a microtubule from the MTOC may lead to a chance encounter with a binding target such as an organelle or the cell cortex (Kirschner and Mitchison, 1986). Interaction of the microtubule plus-end with a target protein may lead to preferential stabilization of end dynamics; the transiently stabilized microtubule may then serve as a marker for the establishment of cell polarity or act to stabilize a cellular protrusion or extension (Siegrist and Doe, 2007). Stabilized microtubules may also serve as preferential tracks for intracellular transport, allowing localized delivery within the cell (Jaworski et al., 2008). Or, locally captured microtubules may have a more active role, transmitting a force between the cell cortex and the MTOC. This generation of force may further facilitate cell polarization (Levy and Holzbaur, 2007). Thus, spatial and temporal regulation of microtubule plus-end dynamics is critical for controlling microtubule architecture and function in the cell.

Cellular studies have revealed a specialized class of microtubule binding proteins, known as plus-end tracking proteins (+TIPs), that accumulate at and track with growing microtubule plus-ends (Akhmanova and Steinmetz, 2008). These proteins participate in various processes including regulation of microtubule dynamics, interactions between microtubules and other cellular structures, and delivery of signaling molecules (Lansbergen and Akhmanova, 2006). The cytoplasmic linker protein-170 (CLIP-170) was the first identified +TIP (Perez et al., 1999; Pierre et al., 1992). Since then, numerous structurally unrelated +TIP proteins have been identified that are evolutionarily conserved in most eukaryotes. Genetic and biochemical studies have revealed that many of these proteins interact with each other and may form higher order plus-end complexes (Akhmanova and Hoogenraad, 2005). One member in particular, the end-binding 1 (EB1) protein, interacts directly with the majority of other known +TIPs and therefore has been proposed to form the core of the microtubule plus-end complex (Lansbergen and Akhmanova, 2006; Vaughan, 2005).

Most +TIPs can directly bind to microtubules, but the molecular basis for their dynamic plus-end localization remains unresolved. In the copolymerization model for +TIP localization, it is suggested that +TIPs copolymerize with tubulin and hence incorporate preferentially at growing microtubule plus-ends (Arnal et al., 2004; Diamantopoulos et al., 1999; Folker et al., 2005; Ligon et al., 2006; Slep and Vale, 2007). Alternatively, the end-recognition model posits that +TIPs have an increased affinity for the microtubule plus-end due to its distinct structural and/or biochemical state (Bieling et al., 2007; Dragestein et al., 2008).

To dissect the mechanisms underlying plus-end tracking, we developed a cell-free, in vitro reconstitution system to observe mammalian EB1 and CLIP-170 proteins and their interactions with microtubules. Using time-lapse total internal reflection fluorescence (TIRF) microscopy, we show that mammalian EB1 can dynamically track growing microtubule plus-ends. The presence of EB1 is necessary for CLIP-170 to localize specifically to the plus-end; in the absence of EB1, CLIP-170 moves diffusively along the entire microtubule lattice. Single molecule analysis indicates that the CLIP-170-EB1 complex undergoes multiple cycles of binding and dissociation from growing microtubule ends, an observation that is inconsistent with a co-polymerization model. We also show that the plus-end specificity of the EB1-CLIP-170 complex requires GTP hydrolysis. Together, these observations provide new insight into the dynamic and specific localization of these proteins seen in vivo, and indicate that EB1 preferentially binds to a distinct structural conformation at growing microtubule plus-ends.

3.2 Results

3.2.1 EB1 targets growing microtubule plus-ends independently of other proteins

To study the +TIP activity of human EB1 protein, we fluorescently tagged recombinant EB1 protein with Alexa 488. In vitro binding experiments showed that the Alexa 488-tagged EB1 protein bound to microtubules with affinity similar to untagged recombinant protein (Fig. S1A).

Reconstitution experiments with dynamic microtubules and EB1-Alexa 488 using TIRF microscopy showed that EB1-Alexa 488 alone is capable of +TIP activity. In these experiments, EB1-Alexa 488 labeled all growing microtubule plus-ends; in contrast, we observed no EB1-Alexa 488 labeling at depolymerizing microtubule ends (Fig. 1 and Movie S1). Also, we did not reproducibly detect EB1-Alexa 488 labeling of the more slowly growing microtubule minus-ends in our experiments. Increasing the EB1-Alexa 488 concentration in these experiments resulted in enhanced accumulation of EB1 at growing microtubule plus-ends (Fig. 1B). Thus, the robust and specific comet-like labeling of growing microtubule plus-ends shows that +TIP activity is an intrinsic property of mammalian EB1, similar to observations on the *S. pombe* EB1-homolog, Mal3 (Bieling et al., 2007).

3.2.2 CLIP-170 requires EB1 for +TIP activity

Next we examined the interaction of CLIP-170 with microtubules. In CLIP-170, the central coiled-coil domain allows the formation of intramolecular contacts between the N-terminal CAP-Gly microtubule-binding domain and the C-terminal zinc-finger motifs, resulting in a ‘closed’ conformation of CLIP-170 that inhibits microtubule binding (Lansbergen et al., 2004). Since the amino terminus alone is sufficient for +TIP activity in the cell, to avoid auto-inhibition we used a well-characterized carboxy-terminal truncation construct of CLIP-170 designated as the H2 fragment (Diamantopoulos et al., 1999). The H2 fragment is dimeric like the full-length CLIP-170 (Scheel et al., 1999). We purified recombinant GFP-tagged CLIP-170(H2) and found that CLIP-170(H2)-GFP did not differ significantly from untagged CLIP-170(H2) in microtubule binding affinity: we measured a K_d of 0.9 ± 0.5 μM for unlabeled H2 and 1.5 ± 0.6 μM for H2-GFP under our experimental conditions (Fig. S1A).

In contrast to EB1, CLIP-170(H2)-GFP alone did not show +TIP activity over a broad range of concentrations. Instead, CLIP-170(H2)-GFP bound nonspecifically along the length of the microtubule. At relatively high concentrations (150 nM), CLIP-170(H2) decorated dynamic microtubules uniformly during both the growth and shortening phases (Fig. S1B). Control experiments with GFP alone at similarly high concentrations did not result in detectable microtubule binding (Fig. S1C). At lower concentrations (25 nM), CLIP-170(H2) non-specifically bound along the microtubule length and time-lapse (Movie S2) and kymograph analysis (Fig. 2A) indicated that CLIP-170(H2) moved bidirectionally along the microtubule lattice. Mean-squared displacement analysis of single CLIP-170(H2)-GFP molecules moving over the microtubule surface showed that this movement is consistent with a one-dimensional random walk with an average diffusion coefficient, D, of $3.5 \pm 0.1 \times 10^{-11}$ cm^2 s^{-1} (Fig. 2B). This diffusive motion of CLIP-170 is similar to that of other microtubule end-binding proteins (Brouhard et al., 2008; Culver-Hanlon et al., 2006; Helenius et al., 2006), but did not result in +TIP accumulation of CLIP-170(H2)-GFP over time.

EB1 and CLIP-170 interact directly with each other (Komarova et al., 2005; Ligon et al., 2006; Mishima et al., 2007) and therefore we tested whether EB1 could significantly alter microtubule association of CLIP-170. In the presence of unlabeled EB1, CLIP-170(H2)-GFP dramatically changed localization from non-specific lattice labeling to selective targeting of growing microtubule plus-ends (Fig. 2C). Under these conditions, CLIP-170(H2)-GFP preferentially labeled all actively polymerizing microtubule plus-ends in a comet-like pattern similar to that observed for EB1-Alexa 488 (Movie S3). These results indicate that EB1 is both necessary and sufficient to recruit CLIP-170 to dynamic plus-ends.

Both EB1 and CLIP-170(H2), alone or together, did not significantly change the microtubule dynamic instability parameters as compared to the control values obtained in the absence of any +TIP proteins (Table 1). Therefore, EB1 and CLIP-170(H2) do not significantly affect the dynamics of microtubule assembly and disassembly in this minimal system.

3.2.3 Both EB1 and CLIP-170 rapidly turnover at microtubule plus-ends

Fluorescence intensity profiles along growing microtubule plus-end structures show that the spatial distribution of labeling are similar for both EB1-Alexa 488 and CLIP-170(H2)-GFP (Fig. 3A). These data are consistent with a model in which EB1 regulates CLIP-170 recruitment and dissociation at microtubule ends (Dragestein et al., 2008; Komarova et al., 2005). Based on the integrated fluorescence intensity in a 1 μm x 1 μm region at growing microtubule plus-ends, we estimate an average of 10 EB1 molecules and 5 CLIP-170(H2) molecules to be present in the comet-like structure. To determine the turnover of individual EB1 and CLIP-170 proteins at microtubule plus-ends, we used single molecule imaging conditions and greater temporal resolution (Fig. S2). Single

EB1-Alexa 488 molecules rapidly exchanged at microtubule plus-ends with an average dwell time of 0.81 ± 0.06 s (n = 184). In our experiments, the average lifetime of the labeled region (calculated as the ratio of comet tail length to microtubule growth speed) at microtubule plus-ends is 8.3 ± 0.1 s (n = 50). Therefore, single EB1-Alexa 488 molecules exhibit multiple rounds of binding and unbinding over the lifetime of the microtubule plus-end structure.

In the absence of EB1, single CLIP-170(H2)-GFP molecules have an average dwell time of 2.69 ± 0.16 s (n = 800) as they diffuse along the microtubule surface. However, when imaged together with unlabeled EB1, the dwell time of single CLIP-170(H2)-GFP molecules is reduced to 1.03 ± 0.03 s (n = 753), which is similar to that of single EB1-Alexa 488 molecules. Therefore, EB1 appears to directly influence the turnover of CLIP-170 at microtubule plus-ends. In contrast to the effects of EB1 on CLIP-170 dynamics, the presence of unlabeled CLIP-170(H2) did not significantly affect either the comet tail length or average dwell time of EB1-Alexa 488 at microtubule plus-ends (data not shown). Therefore, the inherent +TIP dynamics of EB1 are not altered by association with CLIP-170.

3.2.4 GMPCPP abolishes +TIP activity of EB1 and CLIP-170

During the reconstitution experiments, we observed that the +TIP activity of both EB1-Alexa 488 and CLIP-170(H2)-GFP did not require pre-incubation with monomeric tubulin prior to microtubule polymerization. This observation and the dwell time dynamics discussed above suggest that while EB1 and CLIP-170 can form a complex with free tubulin dimers (Ligon et al., 2006), formation of such a complex is not required nor does it enhance the targeted concentration of these proteins at plus-ends. Thus, our data support an end-recognition mechanism for +TIP activity, in which these proteins bind with higher affinity to the newly polymerized end of the microtubule, due to biochemical and/or structural differences between the new end and the older lattice structure.

To test this mechanism directly, we conducted reconstitution experiments using GMPCPP instead of GTP. GMPCPP is a slowly hydrolysable analog of GTP that promotes microtubule assembly and results in an overall microtubule lattice structure that mimics the GTP-bound microtubule cap structure at growing plus-ends (Caplow et al., 1994).

Microtubule polymerization with GMPCPP abolished +TIP activity of CLIP-170(H2)-GFP in the presence of EB1 and led to non-specific binding of CLIP-170(H2)-GFP along the entire microtubule lattice (Fig. 4 and Movie S4). Under these conditions, the CLIP-170(H2)-EB1 complex showed one-dimensional diffusion along the microtubule surface with an average dwell time of 0.79 ± 0.02 s (n = 440). Therefore, we conclude that EB1 and CLIP-170 selectively accumulate at growing microtubule plus-ends because of their ability to recognize a structural or chemical discontinuity along the polymer generated by nucleotide hydrolysis. In the absence of GTP hydrolysis, no plus-end specific localization is observed.

3.3 Figures

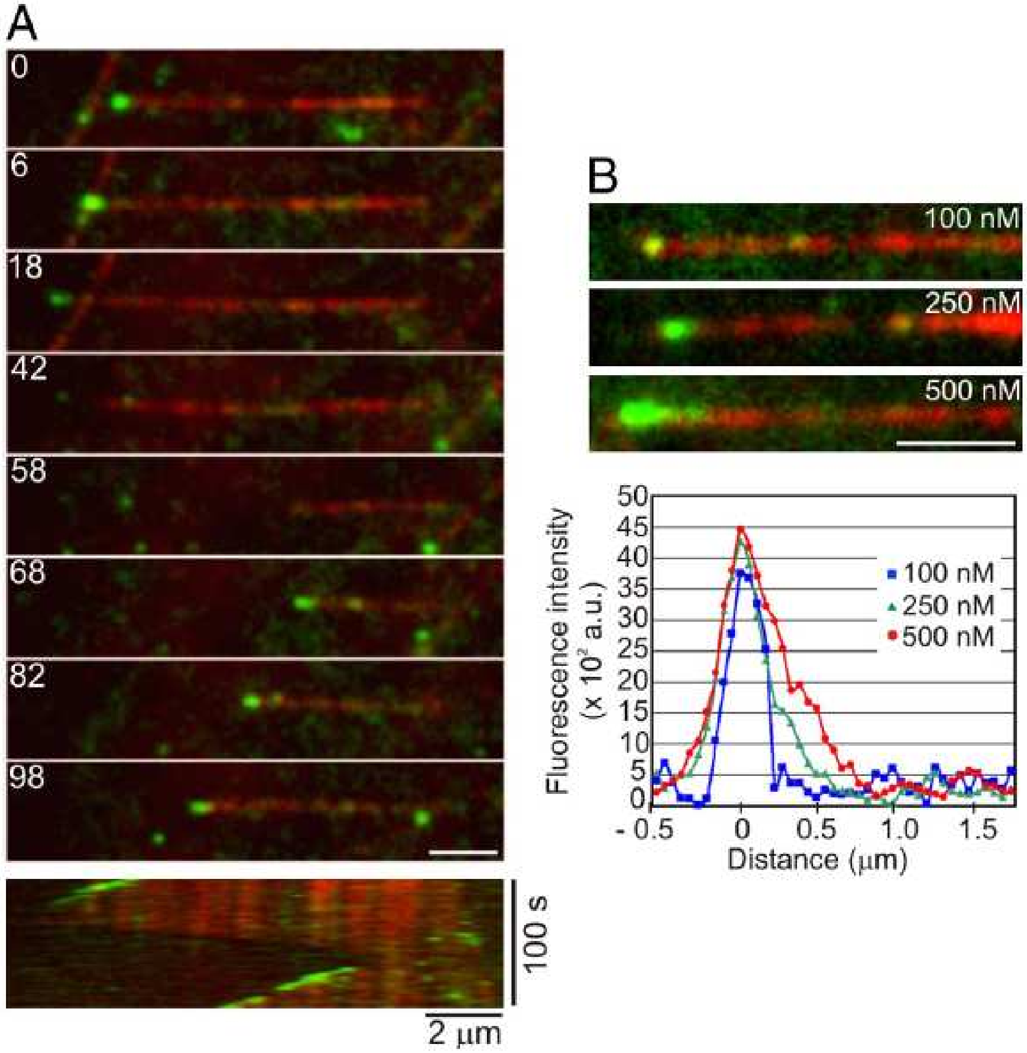

Fig. 1. Microtubule plus-end tracking by the human EB1 protein. (*A*) Montage depicting the specific decoration of growing microtubule plus-ends by 250 nM EB1–Alexa 488. The kymograph at the bottom shows the same microtubule over the duration of the observation period. Microtubule depolymerization is accompanied by loss of EB1–Alexa 488 at the plus-ends, and subsequent rescue of microtubule growth restores plus-end tracking of EB1–Alexa 488. The numbers on each frame represent time in seconds. (*B*) Images showing the microtubule plus-end decoration pattern at increasing concentrations of EB1-Alexa 488. (Scale bar, 2 μm). The graph shows the corresponding distribution of the fluorescence intensity of EB1–Alexa 488 at the microtubule tip.

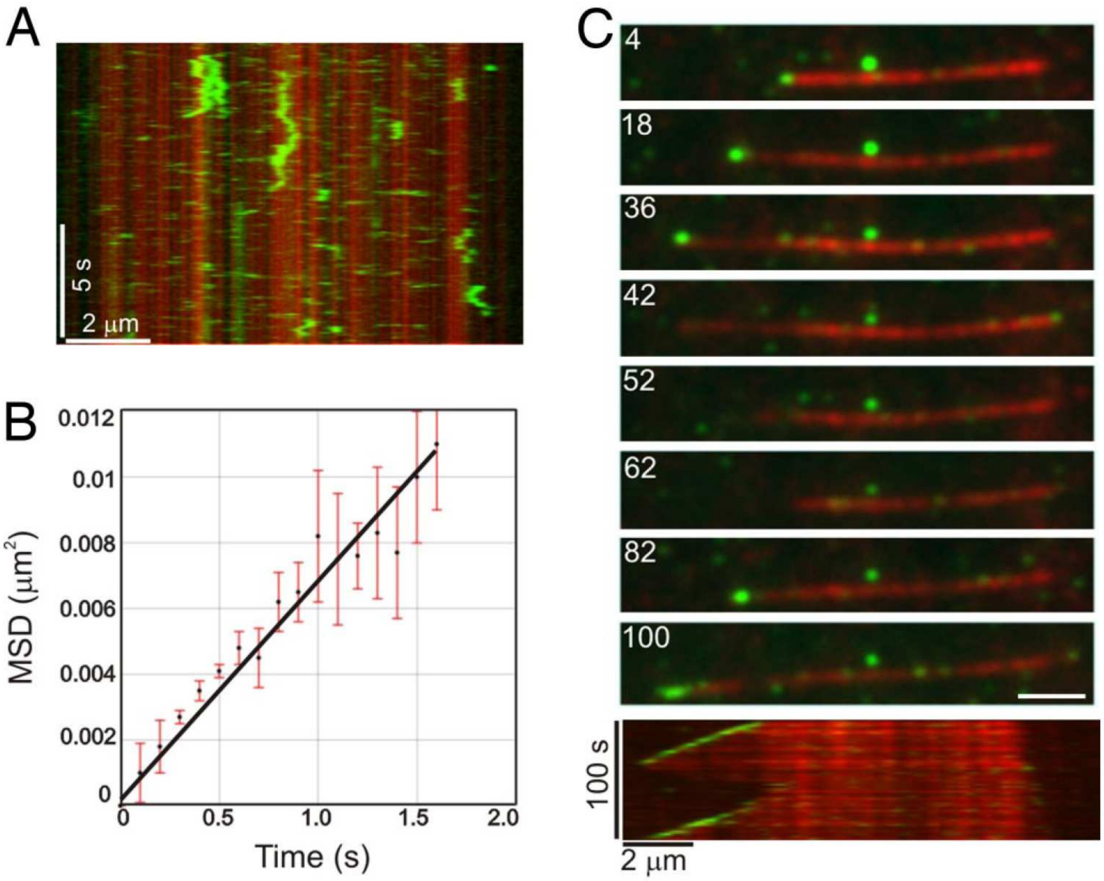

Fig. 2. CLIP-170 requires EB1 for +TIP activity. (*A*) Kymograph showing the microtubule binding and diffusive movement of CLIP-170(H2)–GFP at 25 nM. Note the transient binding of CLIP-170(H2)–GFP along the length of the microtubule lattice. (*B*) Plot of the mean squared displacement (MSD) of CLIP-170(H2)–GFP against time. A linear fit to the data yields a diffusion coefficient, D, of $3.5 \pm 0.1 \times 10^{-11}$ $cm^2\ s^{-1}$ ($MSD = 2Dt$). Error bars represent the SEMs of the squared displacement values ($n = 38$). (*C*) The montage at the top depicts the specific decoration of growing microtubule plus-ends by 25 nM CLIP-170(H2)–GFP in the presence of 250 nM of unlabeled EB1 protein. The kymograph at the bottom shows the same microtubule over the duration of the observation period. Microtubule depolymerization is accompanied by loss of CLIP-170(H2)2–GFP at the plus-ends and subsequent rescue of microtubule growth restores plus-end tracking of CLIP-170(H2)–GFP. The numbers on each frame represent time (in seconds). (Scale bar, 2 μm.)

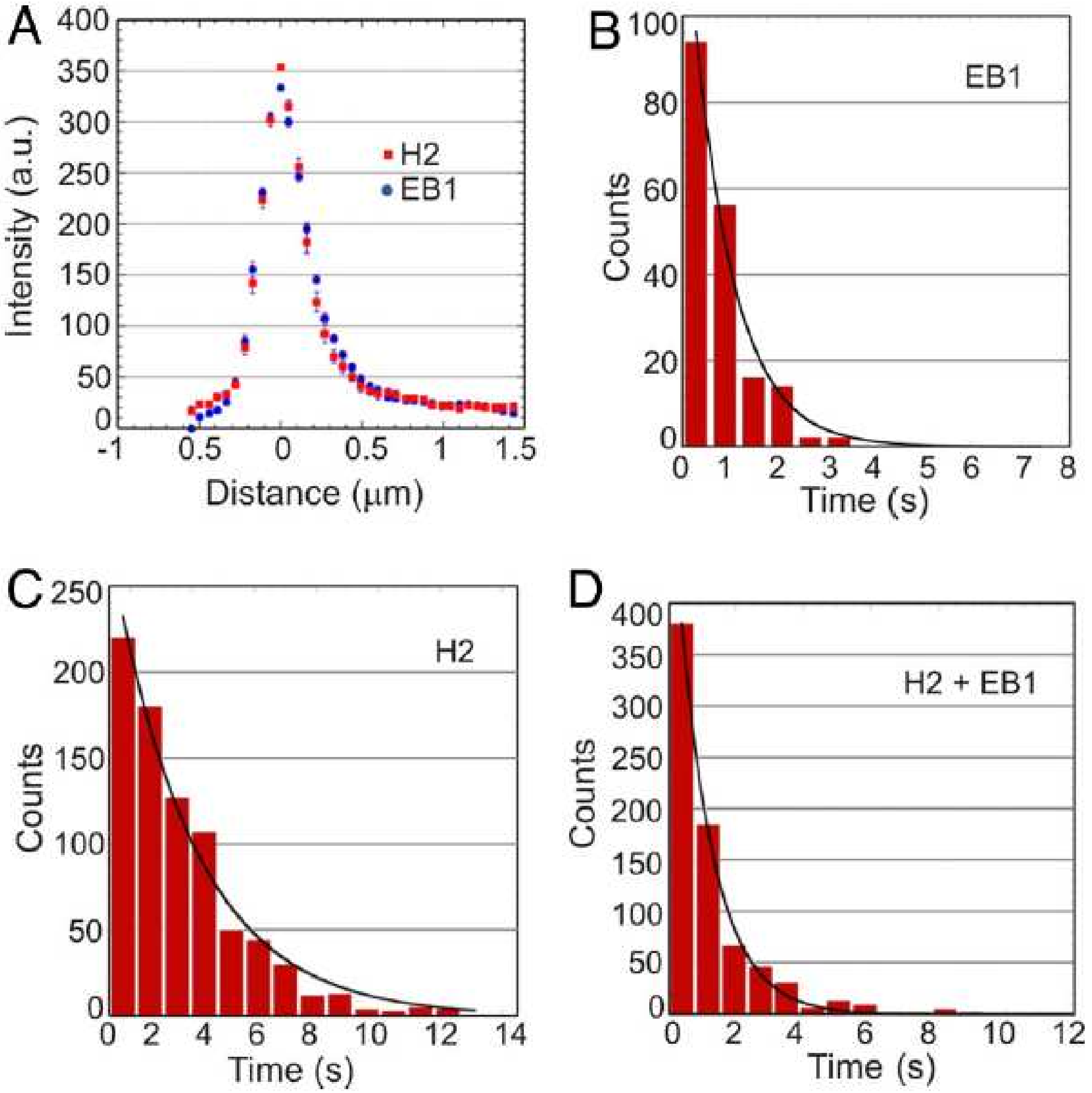

Fig. 3. Rapid turnover of single EB1 and CLIP-170 molecules on growing ends of microtubules. (*A*) Averaged intensity profiles of EB1–Alexa 488 and CLIP-170(H2)–GFP microtubule plus-end decoration (*n* = 20 for both). The concentrations of EB1–Alexa 488 and CLIP-170(H2)–GFP were 250 nM and 25 nM, respectively. (*B–D*) Histograms of dwell times of single binding events of 10 nM EB1–Alexa 488 (*B*), 5 nM CLIP-170(H2)–GFP in the absence of EB1 (*C*), or 5 nM CLIP-170(H2)–GFP in the presence of 250 nM unlabeled EB1 (*D*). Exponential fits to the data yielded mean lifetimes of interactions of 0.81 ± 0.06 s for EB1–Alexa 488 (*n* = 184), 2.69 ± 0.16 s for CLIP-170(H2)–GFP alone (*n* = 800), and 1.03 ± 0.03 s for CLIP-170(H2)–GFP in combination with EB1 (*n* = 753).

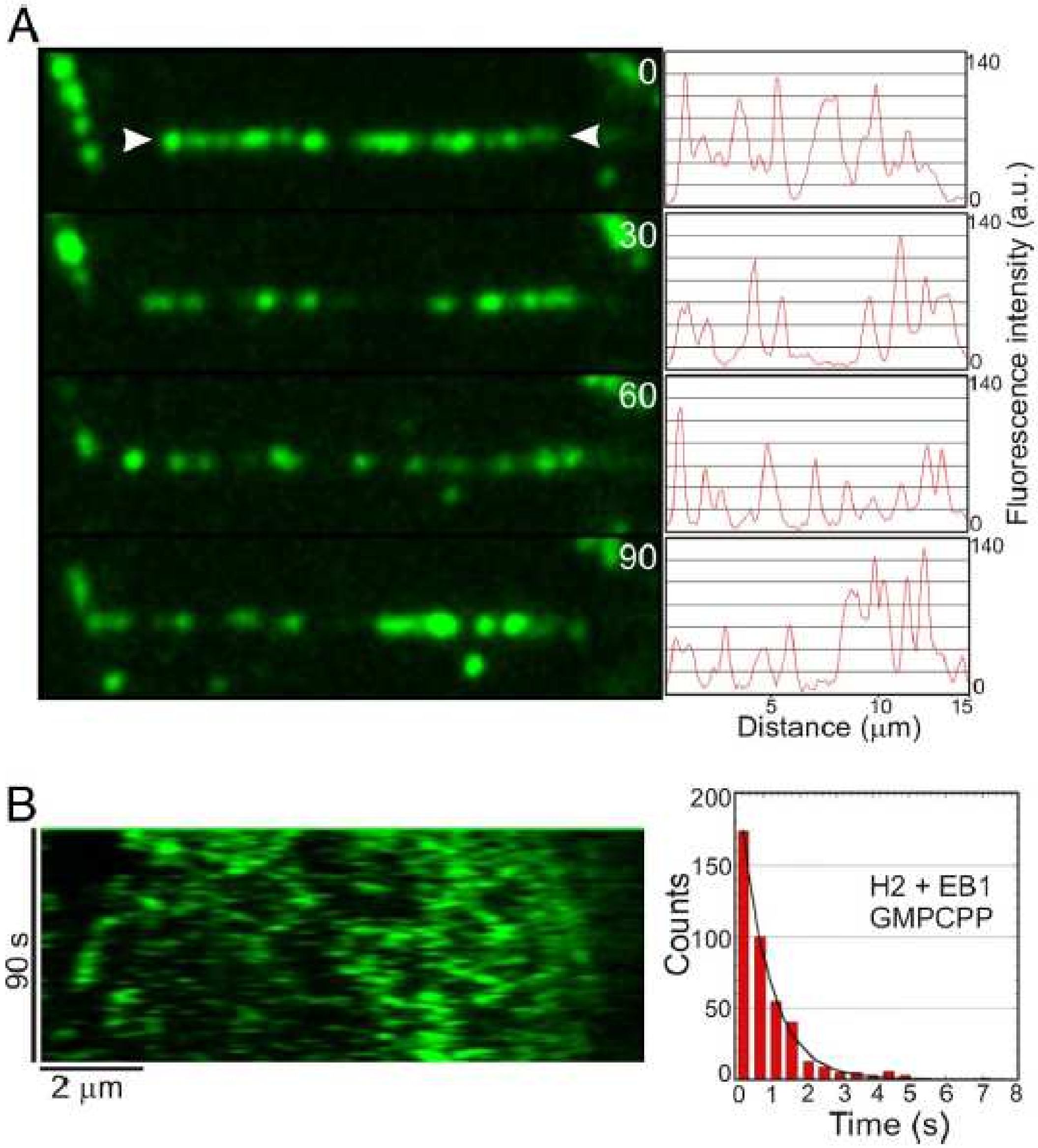

Fig. 4. Effect of GMPCPP on CLIP-170–GFP plus-end tracking activity. (*A*) Montage showing a dynamic microtubule (arrowheads) polymerized with GMPCPP-tubulin in the presence of 25 nM CLIP-170(H2)–GFP and 250 nM unlabeled EB1. The numbers indicate time (in seconds). Each image is accompanied by an intensity profile of the CLIP-170(H2)-GFP fluorescence along the microtubule length. (*B*) Kymograph showing the same microtubule over the duration of the observation period. Note that CLIP-170(H2)–GFP does not show plus-end tracking, but rather binds indiscriminately along the entire length of the GMPCPP microtubule. The accompanying histogram shows the distribution of dwell times of single binding events. An exponential fit to the data yields a mean lifetime of interaction of 0.79 ± 0.02 s (n = 440) for the CLIP-170–EB1 complex.

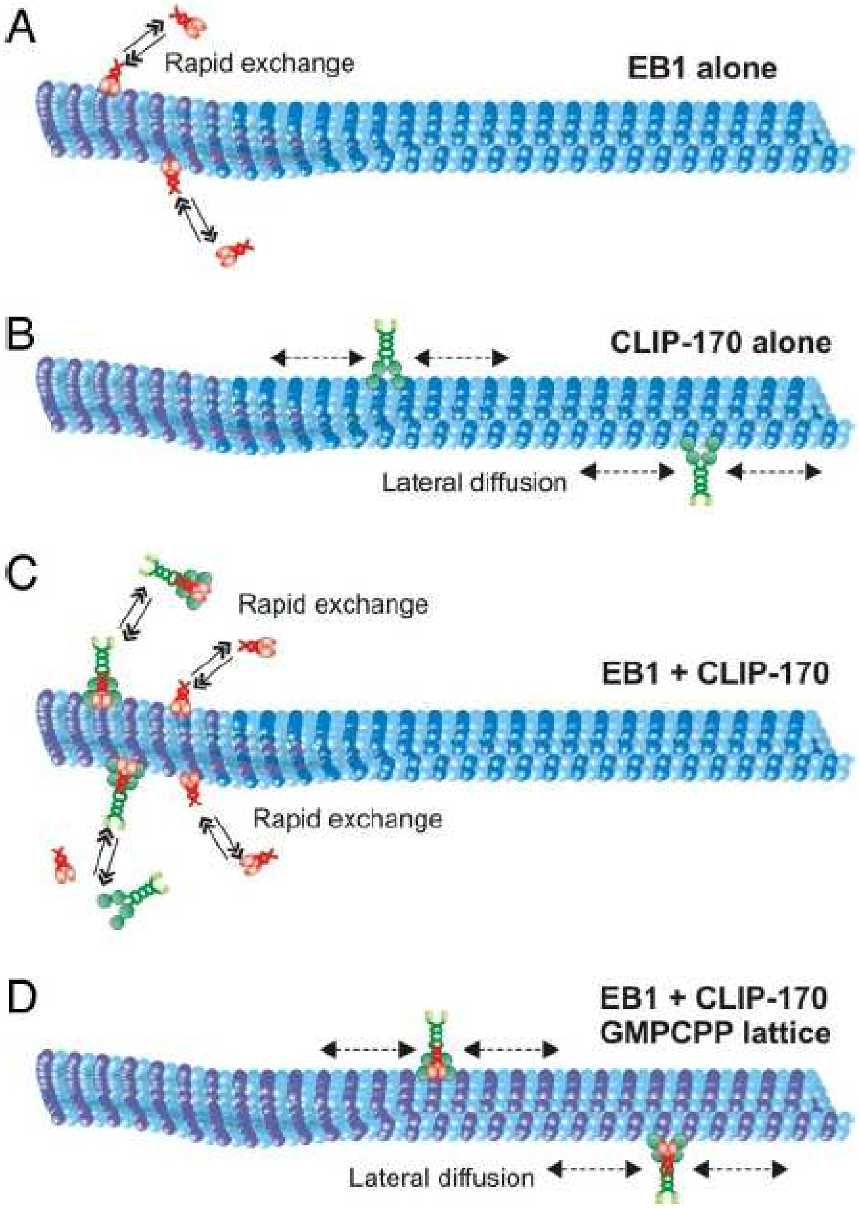
A
Rapid exchange
EB1 alone
B
CLIP-170 alone
Lateral diffusion
C
Rapid exchange
EB1 + CLIP-170
Rapid exchange
D
EB1 + CLIP-170
GMPCPP lattice
Lateral diffusion

Fig. 5. Model for plus-end tracking activity of mammalian EB1 and CLIP-170. (*A*) EB1 (red) is an intrinsic +TIP protein that specifically decorates growing microtubule plus-ends by targeting the plus-end structure (purple). (*B*) In the absence of EB1, CLIP-170 (green) binds nonspecifically along the length of the microtubule and exhibits 1-dimensional diffusion on the microtubule surface. (*C*) EB1 is required for +TIP activity of CLIP-170, either by binding to the microtubule plus-end as a preformed complex with CLIP-170 or by recruiting CLIP-170 to the microtubule plus-end. +TIP activity of both proteins is characterized by rapid exchange of these proteins at the growing microtubule tips. (*D*) GMPCPP (purple microtubule lattice) eliminates plus-end tracking of the CLIP-170–EB1 complex and results in its binding along the length of the microtubule, as well as 1-dimensional diffusion along the lattice.

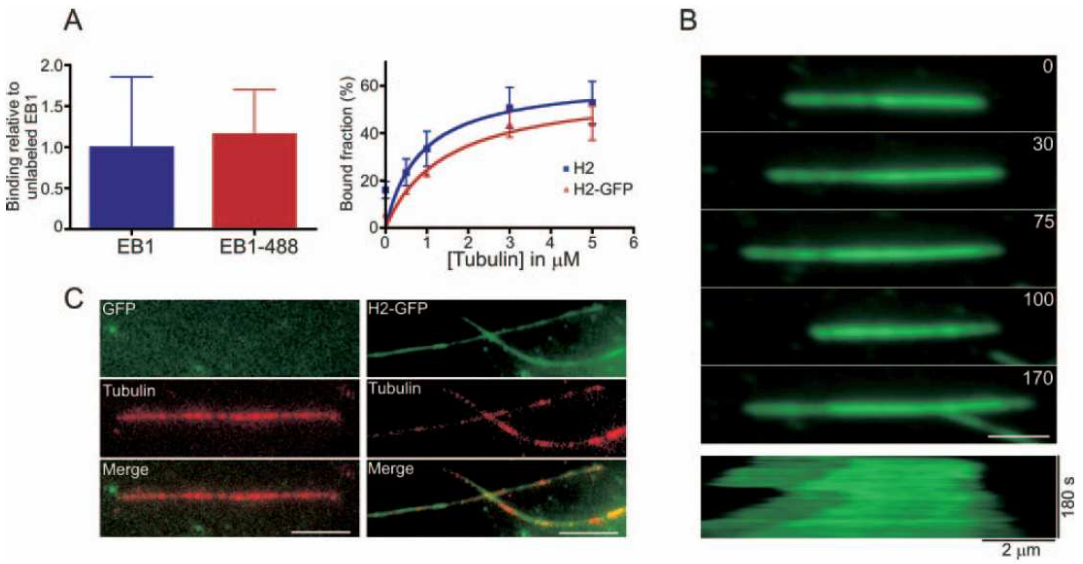

Fig. S1. Microtubule binding and labeling of +TIP proteins. (*A*) The bar graph on the left shows the average (±SD) from 3 or more replicates of the microtubule bound fraction of 3 µM unlabeled EB1 and EB1–Alexa 488 proteins at 5 µM microtubules normalized to the extent of binding observed for unlabeled EB1. The binding curves on the right show the percentage of microtubule bound fraction (±SD) from 3 independent experiments with 3 µM unlabeled CLIP-170(H2) and CLIP-170(H2)–GFP proteins at increasing microtubule concentrations. These data were fit to a K_d of 0.9 ± 0.5 µM for unlabeled CLIP-170(H2) and 1.5 ± 0.6 µM for CLIP-170(H2)–GFP. In both cases, there is no statistical difference between the microtubule binding activities of unlabeled protein and fluorescently tagged protein. (*B*) The montage at the top shows the microtubule labeling pattern of 150 nM CLIP-170(H2). At the bottom is a kymograph of the same microtubule over the duration of the observation period. At this relatively high concentration, CLIP-170(H2) shows indiscriminate labeling of the entire microtubule length during both the polymerization and depolymerization phases of microtubule dynamics. The numbers in each frame indicate time (in seconds). (*C*) Comparison of the microtubule-binding activity of 150 nM GFP alone (*Left*) and 150 nM CLIP-170(H2)–GFP (*Right*). GFP alone, even at relatively high concentrations, exhibits no detectable binding to the microtubule lattice under our experimental conditions. (Scale bar, 2 µm.)

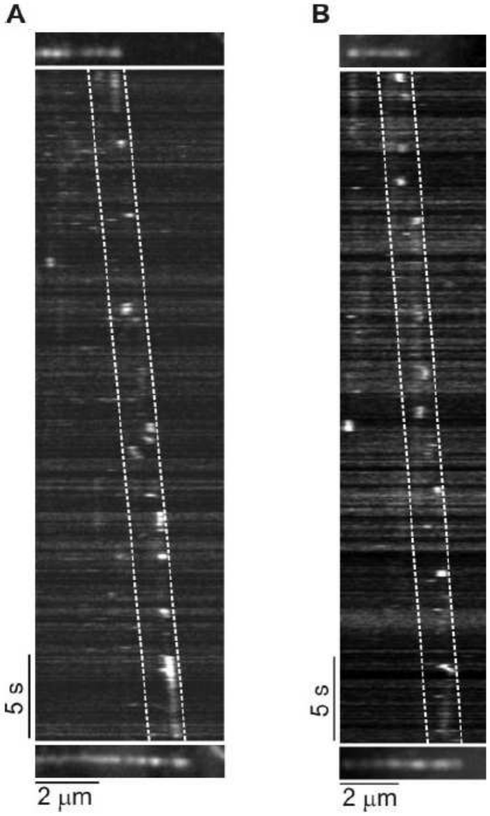

Fig. S2. Single-molecule kinetics of EB1–Alexa 488 and CLIP-170-GFP at growing microtubule plus-ends. In vitro reconstitution experiments were conducted with either 10 nM EB1–Alexa488 (*A*) or 5 nM CLIP-170(H2)–GFP together with 250 nM unlabeled EB1 (*B*) at a temporal resolution of 10 frames/s. The kymographs show binding and unbinding events of single EB1–Alexa488 (*A*) and CLIP-170(H2)–GFP (*B*) molecules at the plus-end of a growing microtubule (shown above and below the kymograph). Dwell times were determined for binding events occurring within a 1-µm region along the growing microtubule tip (dotted lines).

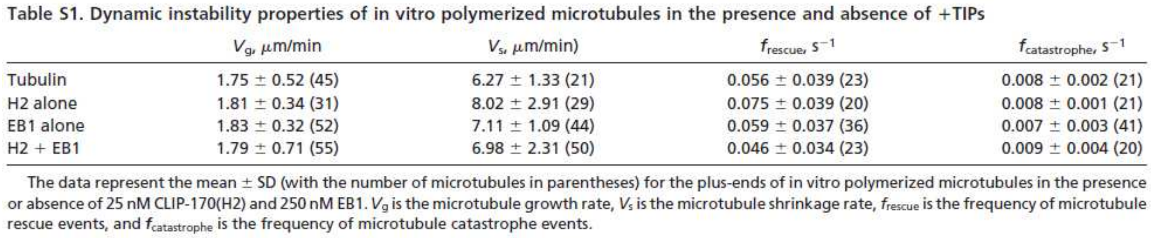

Table S1. Dynamic instability properties of in vitro polymerized microtubules in the presence and absence of +TIPs

	V_g, μm/min	V_s, μm/min)	f_{rescue}, s^{-1}	$f_{catastrophe}$, s^{-1}
Tubulin	1.75 ± 0.52 (45)	6.27 ± 1.33 (21)	0.056 ± 0.039 (23)	0.008 ± 0.002 (21)
H2 alone	1.81 ± 0.34 (31)	8.02 ± 2.91 (29)	0.075 ± 0.039 (20)	0.008 ± 0.001 (21)
EB1 alone	1.83 ± 0.32 (52)	7.11 ± 1.09 (44)	0.059 ± 0.037 (36)	0.007 ± 0.003 (41)
H2 + EB1	1.79 ± 0.71 (55)	6.98 ± 2.31 (50)	0.046 ± 0.034 (23)	0.009 ± 0.004 (20)

The data represent the mean ± SD (with the number of microtubules in parentheses) for the plus-ends of in vitro polymerized microtubules in the presence or absence of 25 nM CLIP-170(H2) and 250 nM EB1. V_g is the microtubule growth rate, V_s is the microtubule shrinkage rate, f_{rescue} is the frequency of microtubule rescue events, and $f_{catastrophe}$ is the frequency of microtubule catastrophe events.

3.4 Discussion

Here we reconstitute the microtubule plus-end tracking of the +TIPs EB1 and CLIP-170 in vitro in a minimal system, and demonstrate an intrinsic ability of the mammalian EB1 to bind specifically to the growing plus-end of a microtubule. A similar result was observed with the *S. pombe* EB1 homolog Mal3 (Bieling et al., 2007), highlighting the functional conservation of EB1 as a master regulator of +TIP function (Akhmanova and Steinmetz, 2008). We also find that an interaction between EB1 and CLIP-170 (Komarova et al., 2005; Ligon et al., 2006; Mishima et al., 2007) is sufficient to recruit CLIP-170 to dynamic microtubule plus-ends in vitro, an observation consistent with cellular RNAi studies in mammalian cells demonstrating a requirement for EB1 in the localization of CLIP-170 to dynamic plus-ends (Komarova et al., 2005; Watson and Stephens, 2006).

In contrast to our observation on these mammalian +TIPs, reconstitution of plus-end dynamics for the yeast homolog of CLIP-170, Tip1, required the presence of a plus-end directed kinesin, Tea2, in addition to Mal3; these in vitro observations are consistent with genetic data from yeast indicating a requirement for both Mal3 and Tea2 in the proper cellular localization of Tip1 (Browning et al., 2003). Thus, while CLIP-170 is structurally similar to Tip1, the mammalian and yeast proteins differ significantly in their mechanisms of plus-end localization. CLIP-170 on its own binds directly to the microtubule with an affinity of 0.2 to 1 µM (Folker et al., 2005; Ligon et al., 2006) and in TIRF assays we see diffusion along the microtubule lattice (Fig. 2). In contrast, Tip1 does not bind significantly to microtubules on its own and Mal3 is not sufficient to recruit

Tip1 to plus-ends (Bieling et al., 2007). One potential explanation for this functional difference is that there is a tandem repeat of the CAP-Gly domain at the N-terminus of CLIP-170, while there is a single CAP-Gly domain at the N-terminus of Tip1. It has been suggested that at least two microtubule binding domains may be required for +TIP activity (Slep and Vale, 2007).

The specificity of EB1 for the microtubule plus-end observed here in a minimal system indicates that EB1 binds differentially to the microtubule plus-end relative to the overall polymer lattice, due to either biochemical or structural differences at the microtubule tip. Experiments tracking the interactions of CLIP-170 and EB1 along microtubules polymerized in the presence of GMPCPP indicate that plus-end specificity is lost in the absence of GTP hydrolysis. Current thinking on the GTP cap suggests a depth of ~ 40-50 tubulin dimers (Schek et al., 2007; VanBuren et al., 2005; Voter et al., 1991), so a model in which EB1 binds specifically to GTP-bound dimers would not explain the ~0.5 μm length of EB1 comet tail-labeling observed here. While our observations therefore favor a model of conformationally-driven specificity, these results indicate that GTP hydrolysis serves as a critical regulatory switch for +TIP tracking.

Dwell-time analysis indicates that neither EB1 nor CLIP-170 remains stably bound to the growing microtubule end. Instead, both on- and off-rates are relatively high, leading to short dwell times. This in vitro observation closely parallels those made previously for EB1 binding to microtubules in Xenopus extracts (Tirnauer et al., 2002), and for the association of CLIP-170 with microtubule ends within mammalian cells (Dragestein et al., 2008). Together, these observations argue against a co-polymerization model (Diamantopoulos et al., 1999; Folker et al., 2005; Ligon et al., 2006), or a polymerization-chaperone model (Slep and Vale, 2007). Instead, the in vitro dynamics suggest a model in which EB1 alone, or the CLIP-170-EB1 complex, has a higher binding affinity for the tubulin structure found only at the growing plus-end. Interestingly, Bieling et al. (2007) noted a pronounced dependence of Mal3 comet tail length on the rate of microtubule polymerization, data that are consistent with our observations on the comet tail length of EB1 and the CLIP-170-EB1 complex. Thus, the structural transition that occurs following incorporation of newly polymerized subunits into the microtubule and which results in a significant decrease in the affinity of EB1 for the lattice structure, is not tightly linked to subunit incorporation into the polymer, but instead occurs as a subsequent event. In this way, it is similar to the hydrolysis of bound GTP that occurs with first order kinetics on newly incorporated subunits, although it remains to be determined if these events occur at similar rates. EB1 has been proposed to promote tubulin sheet closure during microtubule polymerization (Vitre et al., 2008). If EB1 does preferentially bind along the edges of microtubule sheets, as suggested by the seam binding seen by Sandblad et al. (2006), then tube closure would have the effect of dramatically reducing EB1-binding sites along the microtubule, leading to end-binding specificity such as that observed here.

EB1 enhances microtubule elongation (Ligon et al., 2003), but the mechanisms involved are not clear. In vitro, EB1 has been reported to suppress the shortening rate and the catastrophe frequency (Manna et al., 2008), or alternatively to promote both catastrophes and rescues (Vitre et al., 2008). Much of this experimental variation is likely due to differences in EB1 concentrations used in the assays, as at higher concentrations EB1 does not localize in a tip-specific manner but instead binds along the microtubule lattice both in vitro (Ligon et al., 2006; Vitre et al., 2008) and in the cell.

In vivo, deletion analysis of Mal3 or Tip1in *S. pombe* suggests that these proteins act to suppress the frequency of microtubule catastrophes (Browning et al., 2000; Brunner and Nurse, 2000; Busch and Brunner, 2004). In Xenopus extracts, EB1 was shown to decrease the frequency of catastrophes and increase the frequency of rescues (Tirnauer et al., 2002); in mammalian cells, CLIP-170 functions to promote rescue (Komarova et al., 2002). In our reconstitution experiments, neither EB1 nor CLIP-170, acting alone or as a complex, significantly altered the microtubule dynamic instability parameters that we observed in the presence of tubulin alone. This result suggests that using these minimal components, both EB1 and CLIP-170 are not sufficient to modulate microtubule dynamics when localized to growing microtubule plus-ends and that other cellular factors are needed for this function.

We propose a model in which EB1 dynamically recruits CLIP-170 to growing microtubule plus-ends by recognizing the distinct conformation of the plus-end (Fig. 5). This model is consistent with a growing theme that EB1 is the master plus-end tracking protein, capable of recruiting multiple distinct +TIPs to the dynamic plus-end (Lansbergen and Akhmanova, 2006). The relatively weak binding affinities measured for associations among the +TIPs suggests that these proteins function in rapidly changing networks of interactions (Akhmanova and Steinmetz, 2008; Lansbergen and Akhmanova, 2006), consistent with observations that +TIPs function in a wide array of cellular processes, such as cell polarization, cell migration, and cell division. The enrichment of these +TIPs at the microtubule plus-end is likely to facilitate microtubule search-and-capture, in which dynamic microtubules search the cellular space and become captured by specific targets such as adherens junctions or other cortical sites of contacts (Jaworski et al., 2008; Levy and Holzbaur, 2007; Siegrist and Doe, 2007). Future in vitro reconstitution studies modeling the dynamics of these diverse +TIPs are likely to provide further insights into the cellular mechanisms of the plus-end complex.

CHAPTER 4.

Dynein tethers and stabilizes dynamic microtubule plus ends

This work was originally published as:

Curr Biol. 2012 Apr 10;22(7):632-7.

Hendricks AG*, Lazarus JE*, Perlson E, Gardner MK,

Odde DJ, Goldman YE, Holzbaur EL. *Denotes equal contributions

Contributions:

I performed all experiments with dynamic microtubules, analyzed data, and wrote the paper. Adam Hendricks performed all experiments with stable microtubules, analyzed data, and wrote the paper. Melissa Gardner adapted a previous computational model of the microtubule to test our hypothesis on the mechanism of dynein tethering.

4.1 Introduction

Strong evidence that cortically-localized dynein can mediate interactions between microtubules and the cell periphery comes from studies in S. cerevisiae, where dynein’s primary role is to exert tension on microtubules projecting from the spindle pole body in order to properly position the nucleus at the bud neck (Heil-Chapdelaine et al., 2000; Moore and Cooper, 2010). A parallel mechanism also functions in higher eukaryotes, as cortically-localized dynein has been implicated in the proper positioning of the spindle in dividing cells in C. elegans, Drosophila, and human cells (Gonczy et al., 1999; Samora et al.; Siller and Doe, 2009). In interphase cells as well, cortically-localized dynein mediates microtubule capture and tethering, primarily at sites of cell-cell interaction such as adherens junctions and the immunological synapse (Combs et al., 2006; Ligon et al., 2001). Here, we explored the mechanistic basis of microtubule tethering by mammalian dynein, using in vitro assays employing optical trapping, reconstitution of microtubule dynamics, and TIRF microscopy.

4.2 Results

4.2.1 Dynein tethers Taxol-stabilized microtubules

We first asked if dynein-bound polystyrene beads could tether projecting microtubule plus-ends. We anchored polarity-marked Taxol-stabilized microtubules to a coverslip via their biotinylated seeds, so that the microtubule minus-ends were fixed. This geometry allows the unbiotinylated and thus unattached plus-ends to undergo lateral diffusive movements (Fig. 1A). Then, in the presence of 1 mM MgATP, we used an optical trap to bring dynein- or BSA-coated beads, one at a time, to the mobile plus-end of a microtubule. When BSA-coated beads were brought near the microtubule plus end, the variance in the lateral position did not decrease (Fig. 1B and Supplementary Movie S1). In contrast, when dynein-coated beads were brought near the microtubule plus end, the microtubule became tethered, resulting in a pronounced decrease in the variance in the lateral position of the microtubule tip (Fig. 1B and Supplemental Movie S1).

When released from the trap, beads moved towards the minus end, consistent with dynein motor function (Supplemental Fig. S1). We used the optical trap to measure the force exerted by the dynein-bound beads on microtubules stably attached to the cover slip along their length, and found forces ranging from 2-8 pN (Fig. 1C). As mammalian cytoplasmic dynein has a unitary stall force of ~1.1 pN and the force applied by multiple dynein motors is close to additive under these conditions (Mallik et al., 2004; Schroeder et al.), this suggests that 2-8 dynein motors may simultaneously interact with an individual microtubule in this assay.

Next, we asked whether these effects were unique to dynein, or if other microtubule-associated proteins might have the same effect of dampening the lateral mobility of the microtubule plus-end, consistent with tethering. We independently compared the effects of either purified recombinant kinesin-1 or the plus end-tracking protein EB1 on microtubule mobility using the optical trap assay. Both kinesin-1- and EB1-bound beads were able to bind to the microtubule, decreasing the lateral variance of the microtubule plus-end as compared to BSA-bound control beads. However, neither kinesin-1 nor EB1 decreased the lateral variance of the microtubule as effectively as dynein (Fig. 1D). Further, we observed distinct effects of these proteins on the microtubule plus end relative to dynein (Supplemental Movie S1). While the microtubule remained in contact with the bead, the plus-end continued to "search" the surface of either kinesin-1-bound or EB1-bound beads resulting in less-effective tethering (Supplemental Movie S1). In the case of kinesin-1, we occasionally observed microtubule buckling, consistent with the application of a compressive load on the microtubule by a plus end-directed motor. This was not seen with EB1-bound beads, where the microtubule plus end remained in contact with the bead but continued to search the surface (Supplemental Movie S1), likely due to individual binding and release events from multiple EB1 molecules bound to the surface. In contrast, dynein-bound beads induced a more stable attachment with the microtubule end, exerting tension that appeared to stiffen the microtubule, decreasing lateral fluctuations along its length (Supplemental Movie S1).

4.2.2 Dynein motor tethers and stabilizes dynamic microtubules

Microtubules in the cell are dynamic, undergoing periods of growth and shrinkage known as dynamic instability due to the addition and loss of tubulin subunits, primarily at their plus ends (Dixit et al., 2009). These dynamics allow the plus-ends to sample the cytoplasm over time, exploring cellular space. We next asked whether dynein-bound beads could tether dynamic microtubule plus ends (Fig. 2A). In a flow chamber maintained at 37 °C, we bound biotinylated microtubule seeds and BSA- or dynein-coated beads to the coverglass surface. We next added 10 μM tubulin dimers to the chamber, reconstituting dynamic instability. Microtubule dynamics were monitored by total internal reflection fluorescence (TIRF) microscopy.

Interactions of dynamic microtubules with BSA-coated beads often led to rapid catastrophe in this assay (Fig. 2B and Supplemental Movie S2), consistent with previous observations demonstrating induction of catastrophe by contact with a rigid barrier (Janson et al., 2003). In contrast, microtubules that encounter dynein-bound beads in the presence of ATP did not often rapidly catastrophe. Instead, the initial encounter of the microtubule with the bead was stabilized. In some encounters with dynein-bound beads, the microtubule remained tethered (Fig. 2C, left panels). In other encounters, the microtubule plus-end continued to polymerize past the bead while bead-bound dynein maintained a lateral interaction with the microtubule lattice (Fig. 2C, right panels and see Supplemental Movie S3). Importantly, when a growing microtubule plus-end encountered a dynein-bound bead in the presence of 1 mM ATP, we observed a marked decrease in the variance of lateral position consistent with dynein-mediated tethering (Fig. 2D,E), similar to the dynein-mediated tethering observed in the optical trap assays (Fig. 1B).

To determine the effects of dynein-mediated tethering on microtubule stability, we measured the time from initial contact to catastrophe for dynein-coated beads as compared to control beads. We found that in the presence of ATP, the mean time from contact to catastrophe was 161±25 s for dynein-bound beads, as compared to 67±13 s for BSA-coated beads (Figs. 2G and S2, $P<0.02$). Only microtubules making direct contact with beads were affected, as no significant differences were detected in microtubule dynamics away from the beads under any of the conditions tested (Fig. 2F).

Strikingly, although dynein is known to bind tightly to microtubules in the absence of ATP (apo state), encounters between microtubule ends and dynein-coated beads in the absence of ATP were not significantly different than microtubule ends encountering BSA-coated beads (Fig. 2G, $P>0.7$). Thus, the ATP-dependent motor activity of dynein, and not just the high affinity binding of dynein to microtubules, is required to stabilize interactions of dynamic microtubules with a barrier.

4.2.3 Modeling suggests dynein inhibits catastrophe by straightening protofilaments

To further probe the tethering mechanism of dynein, we adapted a previously described three-dimensional computational model that explicitly considers the forces within the microtubule lattice exerted through lateral and longitudinal bonds between each tubulin subunit (Schek et al., 2007; VanBuren et al., 2005) (Fig. 3A). In this model, the nucleotide state of each tubulin subunit determines its preferred angle in the microtubule lattice: GTP-bound tubulin subunits form straight protofilaments while protofilaments with GDP-tubulin subunits tend to curl outwardly when exposed (Wang and Nogales, 2005), destabilizing the polymer and encouraging catastrophe (Fig. 3A). We hypothesized that minus-end directed dynein can stabilize microtubule plus-ends by exerting tension to straighten curled microtubule protofilaments. The force required to straighten a single protofilament is ~1.25 pN (Gardner et al., 2005; Grishchuk et al., 2008), similar to the unitary stall force of mammalian dynein (~1.1 pN; (Mallik et al., 2005; Schroeder et al., 2010; Soppina et al., 2009)). We simulated this situation by allowing microtubule tips to grow against a barrier (Fig. 3A), and then randomly selected individual protofilaments to be straightened by the action of dynein pulling near the plus-end. We found that the time to undergo a catastrophe event was prolonged when dynein applied force to straighten individual protofilaments (Fig. 3B). The length of time that a microtubule plus-end was stabilized (time to catastrophe) was found to increase as a function of the number of protofilaments that were acted on by dynein (Fig 3C).

4.3 Figures

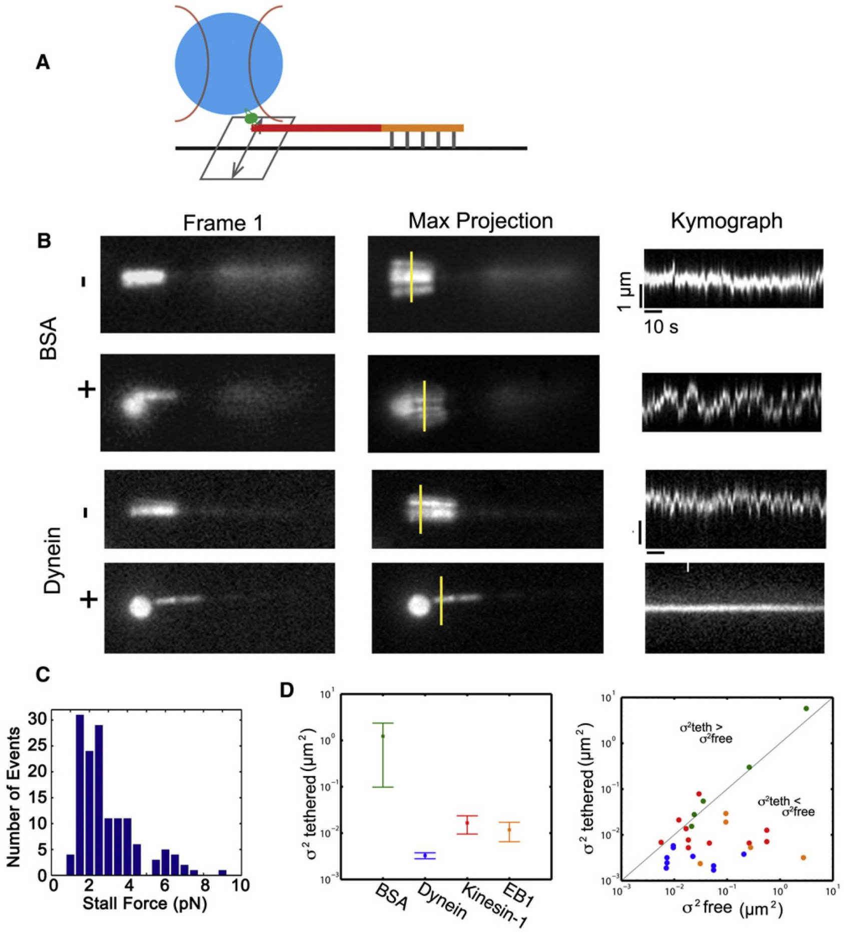

Figure 1. Dynein Tethers Microtubule Plus Ends In Vitro

(A) Microtubules polymerized from dimly labeled, biotinylated seeds were attached to a coverslip via an anti-biotin antibody. The bright, plus ends of the microtubule were not biotinylated and thus free to diffuse.

(B) BSA-coated beads do not decrease the lateral variance of the microtubule plus end. Shown are the initial frame of the movie, the maximum projection image of the sequence, and kymographs taken along the yellow line segments, showing variation in lateral position over time. In contrast, interactions with dynein-bound beads result in decreased lateral mobility of microtubule plus ends.

(C) Histogram of stall forces for dynein-bound beads interacting with stably bound microtubules. Stall forces ranged from 2 to 8 pN, suggesting that two to eight dynein motors on the bead are able to simultaneously interact with a microtubule.

(D) Dynein-bound beads induce stable microtubule tethering, as indicated by the variance in the presence ($\sigma^2_{tethered}$) of the bead. For kinesin-1 and EB1, the microtubule searches the bead surface, resulting in greater lateral diffusion. Error bars indicate SEM. The scatter plot compares the lateral diffusion in the presence ($\sigma^2_{tethered}$) or absence (σ^2_{free}) of the bead.

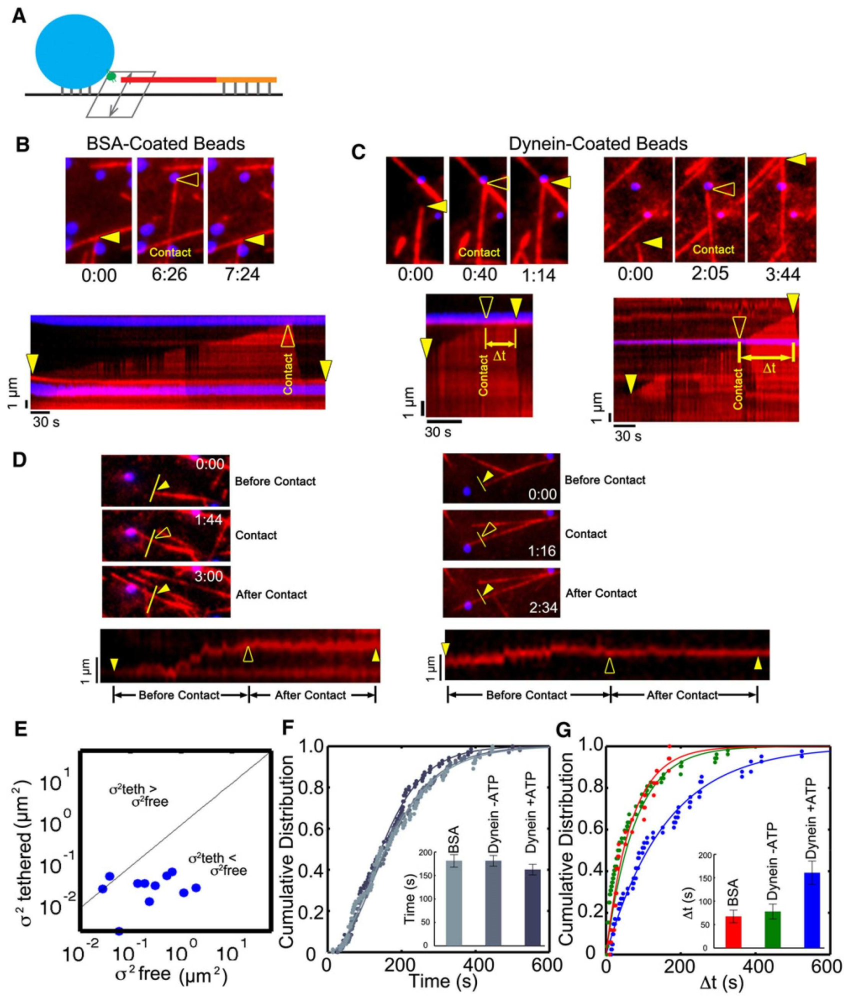

Figure 2. Dynein-Mediated Tethering of Dynamic Microtubule Plus Ends Is ATP Dependent

(A) Dynein- or BSA-bound beads and biotinylated microtubule seeds were attached to the surface of a flow chamber, and microtubule polymerization was initiated by the introduction of 10 μM tubulin. Interactions of growing microtubule plus ends with protein-bound beads were monitored over time.

(B) Dynamic microtubules contacting BSA-coated beads rapidly undergo catastrophe. A time series is shown at the top, with the point of contact highlighted by the open arrowhead. A corresponding kymograph is shown below; the solid arrowheads mark initial and final positions of the microtubule end, and the open arrowhead marks the point of contact with the bead.

(C) In contrast, microtubules become tethered when encountering dynein-coated beads, as measured by an increased time to catastrophe (Δt). Closed arrowheads mark initial and final positions of the microtubule plus end, and open arrowheads mark the point of contact with the bead.

(D) Two examples of the effects of dynein-mediated tethering on the lateral variance of dynamic microtubules. Time series (top three panels) and corresponding kymographs (bottom panels, taken along the indicated yellow line) show that interaction with dynein-coated beads reduces the lateral diffusion of the growing microtubule. Solid arrowheads mark the starting and ending positions, and the open arrowhead marks the initiation of contact with the bead. In the kymograph on the left, note that the bottom line results from the intersection of a second microtubule with the yellow line.

(E) Lateral diffusion for growing microtubules before (σ^2_{free}) and after ($\sigma^2_{tethered}$) contact with dynein-bound beads.

(F) Time to catastrophe for microtubules that do not contact beads is similar across different experimental conditions. Solid lines show fits to a gamma distribution. Error bars indicate SEM.

(G) The mean time between initial contact with the bead and catastrophe for dynein-coated beads in the presence of 1 mM MgATP is significantly longer than for encounters with a dynein-coated bead in the absence of ATP or with a BSA-coated bead ($p < 0.02$). Solid lines show fits to a single exponential. Error bars indicate SEM.

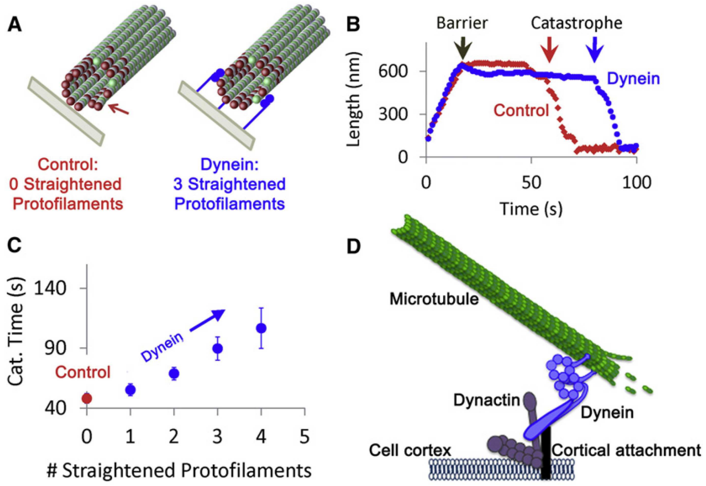

Figure 3. Cortically Localized Dynein Tethers and Stabilizes Microtubules

(A) Three-dimensional model simulations assume that GDP-tubulin subunits (green, with GTP-tubulin subunits in red) have an intrinsic preference for curving outward in the microtubule lattice, and so extended protofilaments with exposed GDP-tubulin subunits near the tip have the tendency to curl outwardly (left). This curling destabilizes the microtubule tip, leading to catastrophe events. However, cortex-anchored dynein could straighten individual protofilaments as dynein exerts tension on the microtubule tip (right, three dynein molecules shown in blue).

(B) In the 3D model simulations, once a microtubule contacts the barrier, the microtubule has a catastrophe event after ~30 s in this simulation run. However, if three random protofilaments are targeted for straightening in the simulation, the time to undergo a catastrophe event is increased to ~70 s.

(C) The mean simulated time to catastrophe after contact with a barrier is given as a function of the number of protofilaments that are targeted for straightening in the simulation. For three targeted protofilaments, simulated catastrophe time increases about 2-fold, consistent with experimental observations. Error bars indicate SEM.

(D) In a proposed model, cortically anchored dynein can actively tether and stabilize projecting microtubule plus ends.

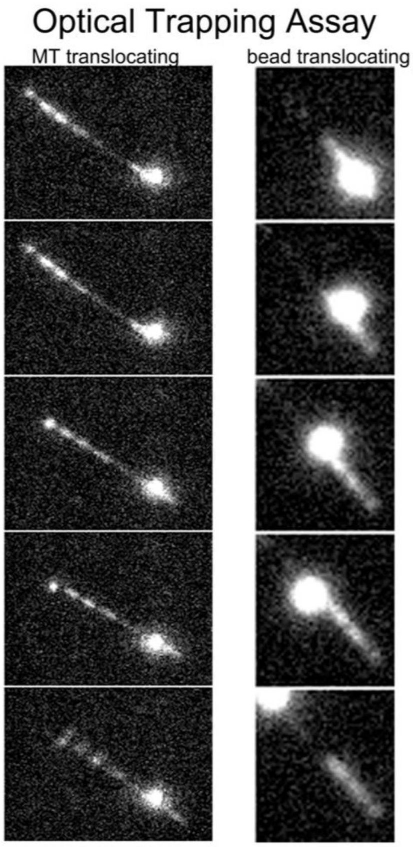
Optical Trapping Assay
MT translocating
bead translocating

Figure S1 (Related to Figure 1). Dynein Bound to Beads Can Drive Translocation of Free Microtubules; Dynein-Bound Beads Released from the Trap Translocate on Bound Microtubules

If a microtubule releases from the coverslip, it can translocate along dynein-bound beads (MT translocating). Alternatively, if the dynein-bound bead is released from the optical trap, it will translocate towards the minus end of the microtubule (bead translocating).

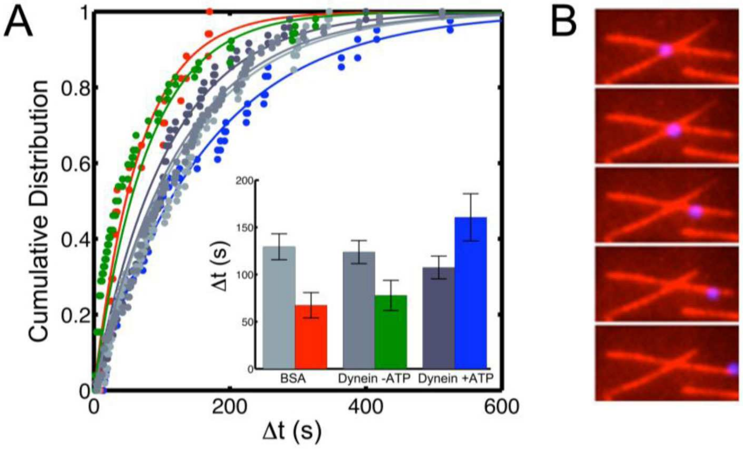

Figure S2 (Related to Figure 2). Dynein Stabilizes Interactions of Dynamic Microtubule Plus Ends with a Bead

(A) To compare the dynamics of microtubules that do and do not contact beads, we must take into account that microtubules polymerize for some time before contacting a bead (the median time is ~150 s). Microtubule plus ends are less likely to catastrophe at short times (<100 s after initiation of polymerization), resulting in a lag phase such that the time to catastrophe can be fit with a gamma distribution [1]. Subsequently, the time to catastrophe can be fit by a single exponential (solid lines, $p>0.7$). Changing this cutoff by ±40 s does not appreciably alter the results. By considering only the exponential phase for microtubules away from beads, the time to catastrophe can be compared directly to the time from initial contact to catastrophe for microtubules that encounter beads. Plotted in this manner, it is evident that encounters with BSA-coated beads (in red) decrease the time to catastrophe when compared to microtubules away from beads (in gray, $p<0.02$). In contrast, encounters with dynein-coated beads in the presence of ATP suppress catastrophe (in blue, $p<0.05$). The motor activity of dynein is required to suppress catastrophe at a barrier, as dynein-coated beads in the absence of ATP promote catastrophe similarly to BSA-coated beads ($p<0.01$). This analysis implies that dynein could be stabilizing microtubule plus ends in two ways. The primary effect of active dynein on the beads is to stabilize the initial interaction with the bead. This primary effect correlates to the difference in time to catastrophe between microtubules that encounter BSA-coated beads (red) and microtubules that do not encounter beads (gray), as BSA-coated beads are not able to stabilize the initial interaction with the microtubule plus end. Stabilization of the initial interaction with a barrier is likely to be most relevant in the cell, as dynein is anchored to the cell cortex, and thus the microtubule plus end would be prevented from polymerizing past the cortically-anchored dynein. However, in our system the microtubule is not constrained by a continuous barrier, and can continue to polymerize if the initial interaction with the bead is stabilized. In addition to stabilizing the initial contact with the bead, the time to catastrophe is delayed after contact with dynein beads when compared to microtubules that do not encounter beads. This suggests that after initial contact with the bead, lateral interactions of dynein with the microtubule delay catastrophe after the microtubule plus end has grown past the bead, possibly through decreased lateral fluctuations, which would decrease the amount of time the microtubule is in a strained geometry. Alternatively, tension exerted by dynein may contribute by stabilizing the microtubule lattice.

(B) Dynein is active and capable of driving motility in tethering assays. If the bead breaks free of the coverslip, dynein drives translocation towards the minus end of the microtubule.

4.4 Discussion

These simulations predict that minus-end directed dynein motors that are anchored at the cell cortex can transiently stabilize microtubule plus ends and delay catastrophe events by straightening individual protofilaments, resulting in dampened microtubule dynamics. Interestingly, the model predicts the number of engaged dynein motors required to stabilize microtubules is similar to the number of engaged motors estimated in our in vitro optical trap assays. Thus, even substoichiometric levels of dynein (1-4 molecules interacting with a 13-protofilament microtubule) would be expected to appreciably suppress catastrophe by counteracting the initial deforming force exerted on the microtubule as it encounters an organelle or the plasma membrane. Both the data and simulations predict that this stabilization requires active force production - high affinity binding alone would not be sufficient for this sort of microtubule capture, i.e. where catastrophe is delayed.

Our observations are consistent with previous observations that encounters between a growing microtubule plus end and a rigid barrier induce catastrophe (Janson et al., 2003). However, we show that when dynein is present, the microtubule plus end is stabilized, allowing the microtubule to continue to polymerize past the bead barrier. This stabilization requires dynein motor activity, as the observed stabilization is ATP-dependent. Thus, active generation of tension is required. Computational modelling suggests that dynein stabilizes the dynamic microtubule plus end through exertion of tension to straighten individual protofilaments. Also, active dynein motors may continuously remodel the connection between the microtubule and barrier, allowing the productive formation of a lateral contact as the microtubule grows past the bead.

The mechanochemistry of cytoplasmic dynein may be uniquely suited for a role in microtubule tethering. Mammalian cytoplasmic dynein has a relatively low stall force (Mallik et al., 2005; Schroeder et al., 2010; Soppina et al., 2009) compared to other motors such as kinesin-1, and a variable stepping pattern along the microtubule that includes both sideways and backward steps (Ross et al., 2008; Ross et al., 2006). The nature of the tethering may also be affected by the number of dynein motors acting on a microtubule plus end. Both our trapping assays and our simulations predict that substoichiometric levels of dynein (1-4 molecules interacting with a 13-protofilament microtubule) would suppress catastrophe by counteracting the initial deforming force exerted on the microtubule as it encounters the plasma membrane. However, either the activation of cortical dynein (Markus and Lee, 2011) or the recruitment of additional dynein motors to the cortex may lead to modulation of microtubule plus-end dynamics at the cell cortex.

Importantly, these results indicate that dynein not only captures and tethers dynamic microtubule plus ends, but can stabilize these ends and thus modulate microtubule dynamics. This influence on microtubule dynamics may promote the stabilization of specific microtubules, which could serve as preferred tracks for intracellular transport between cell center and subdomains at the cell periphery. As both motor and tether, dynein can also exert force on the cytoskeleton relative to the cortex. This mechanism is critical to spindle positioning in a number of systems (Moore and

Cooper, 2010), as dynein can mediate the association of astral microtubules with the cell cortex in dividing cells. However, dynein has also been localized to the cell cortex at sites of cell-cell adhesion (Combs et al., 2006; Ligon et al., 2001). Microtubule tethering at these sites may facilitate a connection between the dynamic microtubule cytoskeleton and intercellular adhesion molecules, creating a powerful mechanism for cells to react to stimuli in the extracellular environment (Fig. 3D). However, further studies to assess the role of dynein in mediating intercellular interactions will be necessary to determine whether the critical function of dynein at these sites is facilitated trafficking or the transduction of force.

CHAPTER 5.

p150^{Glued} regulates microtubule dynamics in neurons through tandem tubulin-binding domains

Under review at Developmental Cell.

Contributions:

Armen Moughamian performed live-cell imaging of primary neurons and analyzed those data. I performed all other experiments, analyzed data, and wrote the paper. Mariko Tokito accomplished all molecular cloning for the constructs used unless otherwise noted in Chapter 2.

5.1 Introduction

Microtubules are dynamic polymers of tubulin that serve as tracks for long-distance transport in eukaryotic cells. In neurons, transport along microtubules may be especially important, yet particularly vulnerable to disruption. These cells are long-lived and post-mitotic, and they contain elongated axonal processes that can extend for meters (Perlson et al., 2010). There is accumulating evidence that axonal transport is disrupted in multiple neurodegenerative diseases, including amyotrophic lateral sclerosis (ALS) and Huntington disease (HD) (Moughamian and Holzbaur, 2011). In neurodegeneration, defects in microtubule dynamics may actually precede transport defects (Cartelli et al., 2010). Reversing those defects by stabilizing microtubules has recently emerged as a viable therapeutic target (Barten et al., 2012; Zhang et al., 2012).

Like other biological polymers, the rate-limiting step in microtubule formation is nucleation from soluble tubulin, which in the canonical pathway is catalyzed by γ-TuRC enriched at the centrosome (Kollman et al., 2011). However, in large, post-mitotic cells like neurons, non-centrosomal nucleation may be particularly important (Nguyen et al., 2011; Stiess et al., 2010). Following nucleation, polymerization and depolymerization dynamics are strongly influenced by microtubule-associated proteins (MAPs). In particular, a spatially-specialized group of MAPs that localize to the microtubule plus end, the plus end-tracking proteins (+TIPs) are ideally poised to modulate dynamics in cells (Akhmanova and Steinmetz, 2008).

One of these +TIPs is dynactin (Vaughan et al., 2002), a large complex that binds and activates cytoplasmic dynein and also associates with microtubules through its dimeric p150^{Glued} subunit (Schroer, 2004). p150^{Glued} has two alternatively-spliced microtubule-binding domains at its N-terminus: a cytoskeleton associated protein glycine-rich (CAP-Gly) domain, followed by a serine-rich basic domain (Culver-Hanlon et al., 2006; Dixit et al., 2008a; Zhapparova et al., 2009). These domains were thought to be crucial for dynein activation by dynactin, but recent work has shown that the p150^{Glued} microtubule-binding N-terminus is dispensable for most dynein-mediated organelle transport (Dixit et al., 2008a; Kim et al., 2007; Lloyd et al., 2012; Moughamian and Holzbaur, 2012).

Because p150^{Glued} binds directly to two other canonical +TIPs, EB1 and CLIP-170, it may be uniquely positioned to coordinate microtubule dynamics (Goodson et al., 2003; Hayashi et al., 2005; Honnappa et al., 2006; Ligon et al., 2003). Previous biochemical studies concluded that p150^{Glued} alone does not markedly affect microtubule dynamics, but these investigations were limited to consideration of a monomeric CAP-Gly domain lacking the flanking basic domain (Hayashi et al., 2005; Manna et al., 2008). This basic domain of p150^{Glued}, though not necessary for microtubule- or dynein-binding, has nevertheless evolved specifically in vertebrates (Culver-Hanlon et al., 2006; Hammesfahr and Kollmar, 2012) and its expression is highly enriched in the nervous system (Dixit et al., 2008a; Zhapparova et al., 2009).

Here, using solution assays and direct visualization of microtubule dynamics using TIRF microscopy, we show that p150^{Glued} promotes the formation of microtubules by catalyzing nucleation from soluble tubulin, and by increasing the polymerization rate and decreasing the frequency of catastrophe. This ability of $p150^{Glued}$ to promote microtubule formation and stabilization is dependent on dimerization, and is restricted to the brain-enriched isoform that encodes both the N-terminal CAP-Gly and basic domains in tandem. In primary neurons, we found a significant increase in catastrophe upon depletion of $p150^{Glued}$ that was specifically rescued by expression of the neuronal isoform. Both *in vitro* and in neurons, we find that a mutation causative for Perry syndrome, a lethal form of Parkinsonism, abrogates the microtubule stabilizing activity of $p150^{Glued}$. In summary, these data identify an important function of $p150^{Glued}$ *in vivo* in the tissue-specific stabilization of microtubules, and indicate that disruption of this function may lead to neurodegeneration.

5.2 Results

We have previously shown that mammalian cytoplasmic dynein modifies microtubule dynamics (Hendricks et al., 2012). To investigate the effects of dynactin on microtubule dynamics independent of dynein, we designed N-terminal recombinant polypeptides truncated before the dynein binding site within the first $p150^{Glued}$ coiled-coil domain (CC1, Fig 1A) (King et al., 2003). Since CC1 is also required for endogenous dimerization of $p150^{Glued}$, and we wanted to conduct our investigations with physiologically relevant dimers, we replaced this domain with a short, well-characterized GCN4 coiled-coil (Trybus et al., 1997). To allow us to make comparisons between the activities of monomeric and dimer polypeptides, we also generated a corresponding construct lacking the dimerization domain, but including both of the N-terminal CAP-Gly and basic microtubule-binding domains.

Glutaraldehyde cross-linking and hydrodynamic analysis confirmed that p150 Nt-GCN4 was properly dimerized (Fig S1A, S1B). We also found that both constructs were monodisperse and highly elongated ($R_s/R_{min} > 1.9$, Fig S1B), consistent with previous analysis of dynactin by electron microscopy (Schafer et al., 1994). As a final initial validation, we determined the affinity of these constructs for microtubules. Both the dimer and monomer bound with moderate affinities (K_d = 340 nM, 890 nM, Fig S1C), which are typical for CAP-Gly proteins (Steinmetz and Akhmanova, 2008).

5.2.1 p150^{Glued} dimer potently promotes microtubule formation

Previous solution studies from our group suggested that the N-terminus of p150^{Glued} may promote bulk microtubule formation (Ligon et al., 2003). To confirm and extend this result, we first compared the activity of the monomeric p150 Nt and the dimeric p150 Nt-GCN4 to the well-characterized neuronal MAPs tau and doublecortin, both of which have been shown to promote the formation of microtubules, a function that appears defective in the setting of disease (Bechstedt and Brouhard, 2012; Lu and Wood, 1993). Like these classical neuronal MAPs, we found that p150 Nt-GCN4 lead to intense and rapid increases in signal in the classical light scattering assay (Fig 1B).

However, high light scattering readings can also result from microtubule bundling. To ensure that the assay was reporting true microtubule formation, we pelleted the early reaction mixtures and confirmed by SDS-PAGE that p150 Nt-GCN4 leads to a large increase in polymeric tubulin (Fig S1E). Additionally, we find that protein aggregation is also not responsible for the light scattering signal; in the absence of tubulin, light scattering is low and constant (Fig S1D).

Of note, though earlier workers found that monomeric p150 constructs could influence microtubule polymerization at high concentrations, we find that dimerization of p150 is clearly necessary for robust effects; in our assay, when compared to dimeric p150 Nt-GCN4 at equivalent concentrations, monomeric p150 Nt only marginally increased light scattering at later time points (Fig 1B), and we did not detect an increase in microtubules formed compared to a buffer control (Fig S1E).

5.2.2 p150^{Glued} increases the rate of microtubule polymerization and inhibits catastrophe

We hypothesized that p150^{Glued}, which localizes to the microtubule plus-end in the cell (Dixit et al., 2008a; Vaughan et al., 2002) and promotes the overall formation of microtubules *in vitro*, might, like other +TIPS (Akhmanova and Steinmetz, 2008), influence the parameters of dynamic instability. To test this hypothesis, we used total internal reflection fluorescence (TIRF) microscopy to directly observe microtubule polymerization from pre-formed GMPCPP-stabilized microtubule seeds (Fig 1C) (Dixit et al., 2009; Gell et al., 2010).

In the absence of p150, we saw that microtubules underwent their characteristic periods of slow growth alternating with rapid shrinkage (Fig 1D). In contrast, at low concentrations of p150 Nt-GCN4, microtubules grew more rapidly (Fig 1D), with the polymerization rate increased more than 2-fold at 200 nM p150 Nt-GCN4 (Fig 1E). We also observed that growth was more persistent, with the catastrophe frequency reduced 2-fold at 100 nM and 4-fold at 200 nM (Fig 1F). In agreement with the light scattering results above, here by direct observation we also see that dimerization of p150^{Glued} is necessary to modify dynamics; at 200 nM, the monomeric p150 Nt construct only had a very modest effect on microtubule polymerization, and we did not detect an effect on the catastrophe frequency (Fig 1E-F).

5.2.3 p150^{Glued} modifies microtubule dynamics independently of EB1

Previous studies with a monomeric p150^{Glued} CAP-Gly polypeptide suggested that EB1 was required for p150^{Glued} to modify microtubule dynamics (Hayashi et al., 2005; Manna et al., 2008). The constructs described here more faithfully recapitulate native p150^{Glued}, and we note strong effects on microtubule dynamics in the absence of EB1. However, we wondered if the presence of EB1 might modulate the effects we observed.

Using analytical size exclusion chromatography, we confirmed that, as expected (Hayashi et al., 2005; Honnappa et al., 2006; Weisbrich et al., 2007), p150 Nt-GCN4 forms a stable complex with recombinant full-length EB1 (Fig S1H, S1I). However, the ability of p150^{Glued} to promote microtubule formation appears to be independent of this interaction; the addition of 50 nM EB1, likely sufficient to saturate the plus end at the low tubulin concentrations in our assay (Bieling et al., 2008; Dixit et al., 2009), did not markedly alter the effect of $p150^{Glued}$ on either the microtubule polymerization rate or the catastrophe frequency (Fig S1J-K).

5.2.4 $p150^{Glued}$ catalyzes microtubule nucleation

Addition of p150 Nt-GCN4 increased the total amount of microtubule polymer that formed from soluble tubulin (Fig 1B, S1E). While this increase is partially due to the pro-polymerization and anti-catastrophe activities of p150 once microtubules have formed (Fig 1E, 1F), we suspected that p150 could also act to promote microtubule nucleation because we observed a decrease in the lag time for microtubule formation that was inversely dependent on the p150 Nt-GCN4 concentration (Fig 2A, 2B).

We designed a TIRF assay to directly test this hypothesis. We specifically oriented the p150 N-terminal microtubule-binding domains toward the microscopy chamber by immobilizing 250 nM p150 polypeptides on the coverslip via an antibody to the C-terminal His-tag (Fig 2C). We then washed the chamber to remove unbound p150, and perfused in 3.5 μM soluble tubulin, which is below the critical concentration for spontaneous microtubule nucleation.

Consistent with our hypothesis, in the presence of dimeric p150 Nt-GCN4 we observed the appearance of many short microtubules within 2 minutes (Fig 2D). We did not observe nucleation when monomeric p150 Nt was immobilized in the chamber (Fig 2D). When we reduced the amount of p150 Nt-GCN4 on the chamber surface so that we could observe the nucleation of individual filaments, we observed growth from both the microtubule minus- and plus-ends (Fig 2E). This suggested to us that p150 was not promoting nucleation via a template-and-capping mode like γ-TuRC (Kollman et al., 2011), but instead might stabilize an oligomeric tubulin species like doublecortin (Fourniol et al., 2010) or bind directly to soluble tubulin dimers.

5.2.5 p150^{Glued} promotes microtubule formation by binding to soluble tubulin

p150^{Glued} is well-characterized as a microtubule-associated protein, but we hypothesized that it might promote the formation of microtubules by also binding to soluble tubulin through its CAP-Gly domain. The CAP-Gly domains of other structurally related proteins, such as CLIP-170 and tubulin binding cofactors B and E, have been shown to bind soluble tubulin (Steinmetz and Akhmanova, 2008). Using analytical size exclusion chromatography, we assayed complex formation. To preclude microtubule formation, we performed all experiments at 4 C.

We observed a pronounced shift in the elution peak, indicating complex formation, when both p150 Nt-GCN4 and p150 Nt were incubated with tubulin (Fig 3A, Fig S2A-B). We varied the molar ratio of p150:tubulin until we no longer observed uncomplexed species after Al-Bassam et al. (2010). In this way, we found that p150 Nt-GCN4 formed a stable complex with tubulin in a 1:1 ratio (Fig S2C, E-F). However, we observed a tail trailing the elution peak of the 1:1 p150 Nt-GCN4:tubulin complex (Fig 3A) which could indicate an exchange process between free p150 Nt-GCN4 and tubulin during the elution. In agreement with this possibility, we found that when we incubated excess tubulin with p150 Nt-GCN4, the elution peak shifted further to the left (Fig 3A, Fig S2H-I), indicating that a larger complex had formed, and suggesting that p150 Nt-GCN4 might promote microtubule nucleation by transiently binding multiple tubulin subunits and encouraging the formation of a stable seed.

We know that the acidic tubulin C-termini are important for binding of p150^{Glued} to microtubules (Kobayashi et al., 2006; Weisbrich et al., 2007). To determine if p150^{Glued} also binds to the tubulin C-termini in their protomeric form, we cleaved tubulin C-termini with the protease subtilisin (Fig S2J-K) (Gupta et al., 2009; Knipling et al., 1999) and again assayed for complex formation via size exclusion chromatography. After cleavage, we could not detect a tubulin-p150 complex (Fig 3B), confirming that the p150 CAP-Gly domain interacts with the tubulin C-terminus in solution.

This orientation might leave the p150 basic domain free to stabilize the complex through electrostatic interactions. In support of this model, we found that when we eluted the tubulin-p150 Nt-GCN4 complex under increasing ionic strength, which should disrupt such an electrostatic interaction, the relative abundance of the complex was decreased at the expense of free tubulin (Fig 3C). This suggests that while either the p150 CAP-Gly or the basic domains are sufficient to bind microtubules (Culver-Hanlon et al., 2006; Dixit et al., 2008a; Zhapparova et al., 2009), both domains may be necessary to bind tubulin and modify microtubule dynamics.

5.2.6 Neuron-specific p150^{Glued} isoform stabilizes microtubules

We were able to take advantage of physiologically relevant p150^{Glued} spliceforms which lack either the CAP-Gly or basic domains to further test this model. p150^{Glued} is alternatively spliced in a tissue-specific manner with expression of full-length p150 containing both the CAP-Gly and basic domains restricted to the nervous system (Dixit et al., 2008a; Zhapparova et al., 2009) (Fig 4A). The two other predominant p150 spliceforms *in vivo* lack either the CAP-Gly domain or the basic domain. p135 is an isoform that, like p150, is enriched in the nervous system; it arises from an alternative start site and thus lacks the CAP-Gly domain and exon 5 (Tokito et al., 1996). In non-neuronal tissues, all or part of the basic domain is spliced out (Dixit et al., 2008a; Zhapparova et al., 2009). We produced recombinant dimeric polypeptides recapitulating p135 (p135 Nt-GCN4) and p150 lacking exons 5, 6, and 7 (the majority of the basic region, Δ5-7 Nt-GCN4) (Fig 4A and Fig S3A-D).

We found that when we co-incubated p135 Nt-GCN4 with tubulin, we did not observe complex formation by size exclusion chromatography (Fig 4B). This was unsurprising given the accepted role of CAP-Gly domains in binding to microtubules (and tubulin) (Steinmetz and Akhmanova, 2008). However, Δ5-7 Nt-GCN4 has a small 23 amino acid deletion that only slightly impacts its microtubule-binding affinity as measured by co-pelleting (K_d = 470 nM vs. 290 nM for p150 Nt-GCN4, Fig 4C) (Culver-Hanlon et al., 2006; Dixit et al., 2008a) and also leaves it able to bind EB1 as assessed by size exclusion chromatography (S4E-F) (Steinmetz and Akhmanova, 2008). Strikingly, we find that this isoform cannot bind tubulin (Fig 4D). Further, neither p135 NT-GCN4 nor Δ5-7 Nt-GCN4 were also able to promote the formation of microtubules (Fig 4E, Fig 4F). These results demonstrate that both the $p150^{Glued}$ CAP-Gly and basic domains are necessary to stably complex tubulin and to promote assembly dynamics.

5.2.7 p150^{Glued} is a tissue-specific microtubule modifier

To determine how the cellular role of p150^{Glued} corresponds to the biochemical activities we measured, we first depleted p150^{Glued} from COS7 cells (Fig S4A), a primate cell line derived from kidney that should express a minimal amount of the neuronal isoform (Zhapparova et al., 2009). Then, we transfected low levels of GFP-EB3 to allow us to visualize the growing microtubule plus end, and examined microtubule dynamics in an unbiased manner using the PlusTipTracker software package (Applegate et al., 2011). In the setting of >95% p150^{Glued} depletion, we did not observe an appreciable effect on either the average displacement of EB3-GFP comets before microtubule catastrophe, or on microtubule polymerization velocities (Fig S4A-B).

We next investigated the effect of p150^{Glued} depletion on microtubule dynamics in mammalian neurons, which express both the CAP-Gly and basic domains that we have identified as necessary for tubulin binding. Interestingly, though the CAP-Gly domain can be identified in organisms as diverse as humans, flies, and yeast, the basic domain has evolved only in vertebrates, with mammalian taxa expressing particularly basic regions downstream of the CAP-Gly domain (Fig S4C-D) (Hammesfahr and Kollmar, 2012).

Using RNAi, we depleted p150^{Glued} ~80% in mouse dorsal root ganglion neurons (Fig S4E), and visualized microtubule dynamics using GFP-EB3 at low levels. Because of the high levels of tubulin in mammalian neurons, we then quantitated microtubule dynamics manually using kymograph analysis (Fig 5A). In contrast to our results *in vitro*, we did not observe striking differences between polymerization rates in the absence or presence of p150^{Glued} (Fig 5A-B). However, we noted that when p150^{Glued} was depleted, there was a profound decrease in the distance GFP-EB3 comets traveled before catastrophe (Fig 5A, C). To confirm that this was a specific effect of p150^{Glued} knockdown and not a more general disruption due to dynein dysfunction, we quantitated dynamics in the setting of rescue with either the full-length neuronal p150 isoform, or with p135, which from our results *in vitro*, we would predict would not restore normal microtubule dynamics.

We observed that transfection of neurons with a plasmid encoding RNA-resistant p150 rescued the increase in microtubule catastrophe. In contrast, transfection with the p135 isoform, which lacks the N-terminal CAP-Gly domain, did not rescue defective polymerization dynamics (Fig 5C).

5.2.8 A Parkinson disease mutation abolishes p150^{Glued} activity

Mutations in the CAP-Gly domain of p150^{Glued} have been found to cause multiple neurodegenerative diseases, including lower motor neuron disease and Perry syndrome, which includes a constellation of Parkinsonism, weight loss, hypoventilation, and depression. Interestingly, human disease-associated mutations in p150^{Glued} are expressed throughout the body but only induce pathologies in the nervous system. (Moughamian and Holzbaur, 2011). We hypothesized that the tissue-specific ability of p150^{Glued} to stabilize microtubules might be disrupted in these diseases.

To test this hypothesis, we chose the Q74P mutation (Fig 6A), which causes Perry syndrome in humans (Farrer et al., 2009). The Q74P mutation has been shown to disrupt both the microtubule and EB1-binding activities of the p150 CAP-Gly domain but to have only a relatively modest effect on overall protein stability (Ahmed et al., 2010; Moughamian and Holzbaur, 2012). Still, to obviate any disease-induced aggregation, we expressed and purified recombinant Q74P Nt-GCN4 using a final gel filtration step to exclude higher order oligomers, and confirmed proper dimerization by glutaraldehyde cross-linking (Fig S5).

We observed by size exclusion chromatography that Q74P Nt-GCN4 could form a stable complex with tubulin (Fig 6B). We speculated that, instead of a complete loss of binding, Q74P Nt-GCN4 might instead bind tubulin in an altered conformation that was incompetent to encourage polymerization. Consistent with this possibility, Q74P Nt-GCN4 was unable to promote the formation of microtubules from soluble tubulin (Fig 6C-D), or to promote microtubule elongation (Fig 6E-F). In contrast to rescue with RNAi-resistant wild-type p150, transfection of p150-depleted primary neurons with a plasmid expressing Q74P did not restore normal microtubule dynamics, suggesting that this defect might contribute to neuropathology *in vivo* (Fig 6G).

5.3 Figures

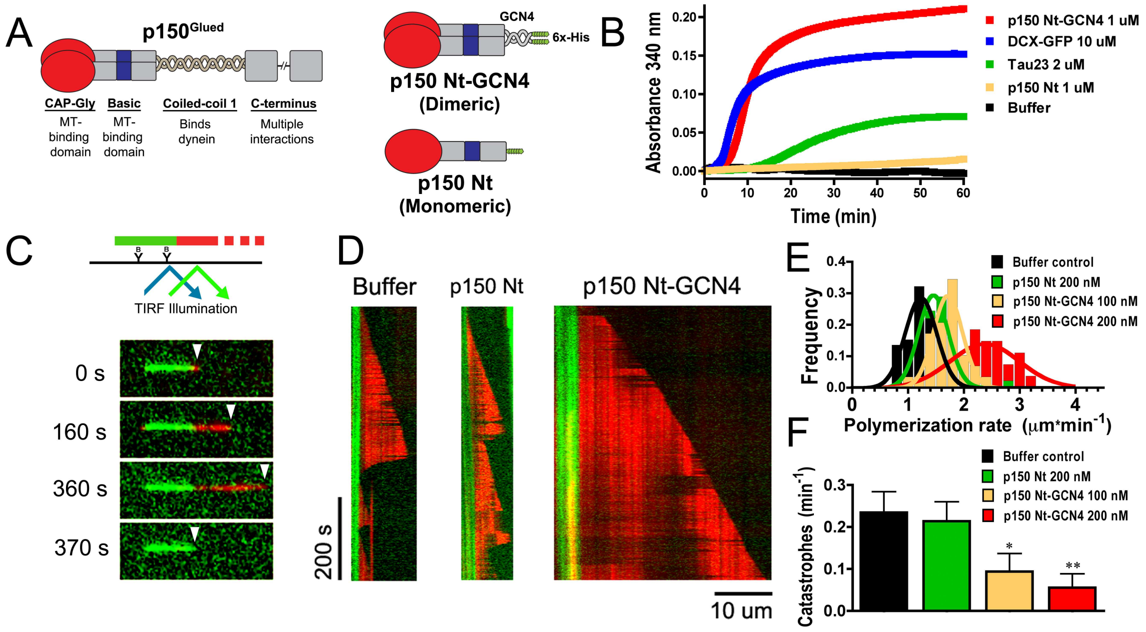

Figure 1. ***p150^{Glued} promotes microtubule formation.*** (A) Schematic depicting endogenous full-length p150^{Glued} and dimeric and monomeric constructs. (B) Light scattering traces for recombinant polypeptides or buffer control incubated with tubulin shows that the dimeric p150 Nt-GCN4 and neuronal MAPs tau23 and DCX-GFP robustly promote microtubule assembly, while monomeric p150 Nt does not. (C) Schematic of the TIRF elongation assay. Rhodamine-labeled tubulin is polymerized from biotinylated Alexa488-labeled GMPCPP microtubule seeds. Montage below shows free tubulin assembly (red) from a stabilized seed (green) in the absence of p150. Arrowhead identifies the microtubule plus-end. (D) Kymograph plots showing representative examples with buffer, 200 nM p150 Nt or p150 Nt-GCN4. (E) Polymerization rates and (F) catastrophe frequencies from seeded assembly shows that p150 Nt-GCN4 promotes polymerization and inhibits catastrophe. All error bars represent SEM of 3 or more independent experiments. Statistical testing was performed with a 2-tailed t-test. *, $p < 0.05$; **, $p < 0.01$.

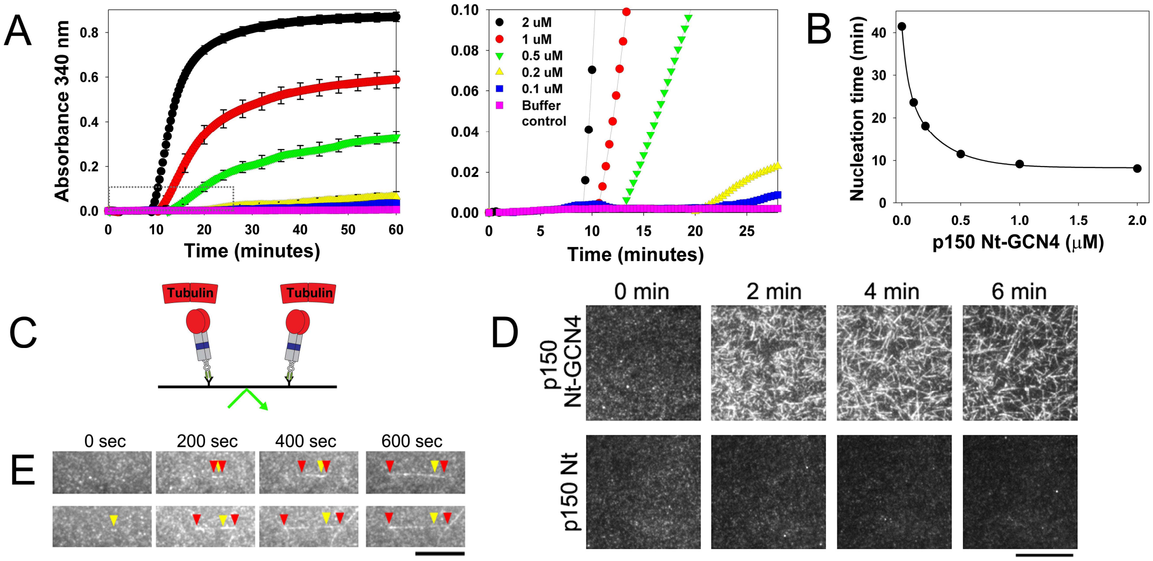

Figure 2. ***p150 catalyzes microtubules nucleation.*** (A) Light scattering traces for increasing concentrations of p150 Nt-GCN4. At right, the scale was magnified to illustrate the initial increase in light scattering observed with increasing concentrations of p150 Nt-GCN4. Error bars represent SEM of 3 or more independent experiments and are omitted for clarity at right. (B) p150 Nt-GCN4 decreases nucleation time, defined as initial appearance of signal over background. Fit is to a double exponential decay. Note that error bars are smaller than symbols. (C) Schematic of the TIRF nucleation assay. p150 constructs are immobilized and the chamber perfused with rhodamine-labeled tubulin. (D) Montage from TIRF nucleation assay shows that dimeric p150 Nt-GCN4 catalyzes microtubule nucleation in contrast to monomeric p150 Nt. Scale bar, 12.5 um. (E) Montage of representative microtubules nucleated in the presence of a low concentration of p150 dimer. Yellow arrows identify the site of nucleation. Red arrows identify the growing plus- and minus-ends. Scale bar, 5 um.

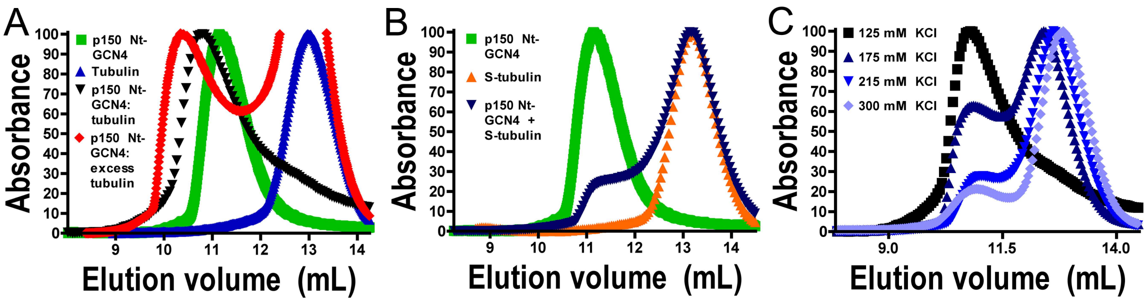

Figure 3. ***p150^{Glued}* *forms a complex with soluble tubulin.*** (A) Size exclusion chromatograms for p150 Nt-GCN4 run alone or pre-incubated with tubulin reveal that p150 forms a stable complex with tubulin. For the red trace, maximum absorbance is scaled to the complex peak. (B) Size exclusion chromatograms for subtilisin-treated tubulin incubated with p150 Nt-GCN4 suggest that the p150^{Glued} binds tubulin C-termini in solution as complex formation is not observed . (C) Size exclusion chromatograms for p150 Nt-GCN4 incubated with tubulin and eluted in increasing ionic strengths indicate that electrostatic interactions between tubulin and the p150 basic domain helps stabilize the p150-tubulin complex because reduced complex formation is observed in increasing ionic strength.

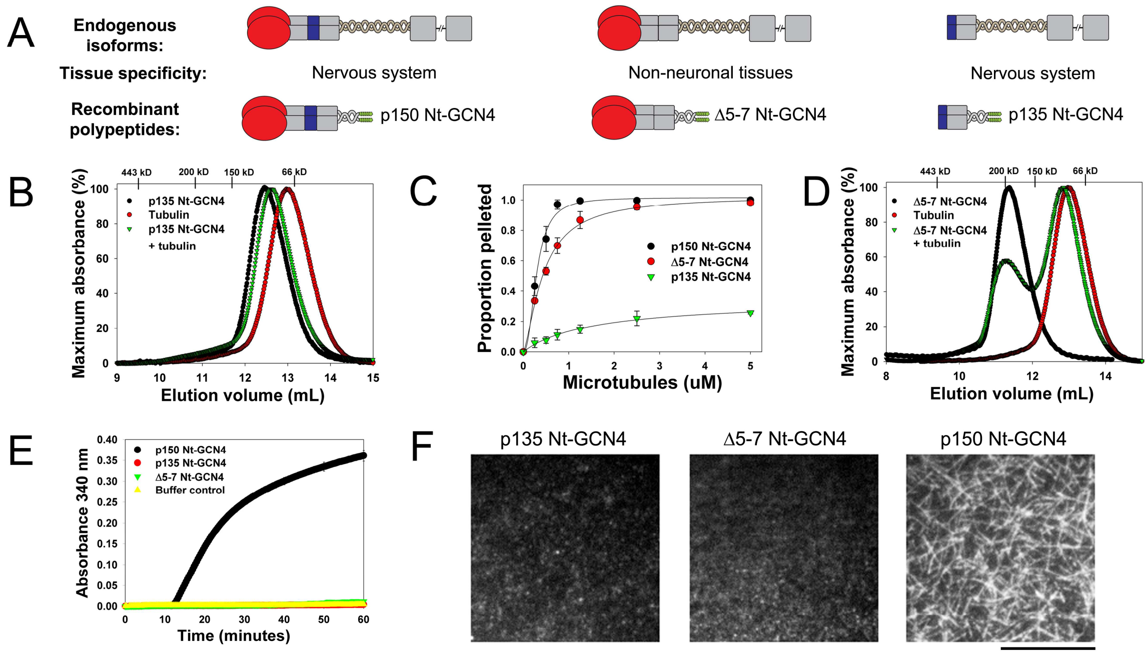

Figure 4. ***Tissue-specific p150^{Glued} isoforms differentially modify microtubule assembly dynamics.*** (A) Schematic depicting p150^{Glued} spliceforms (and corresponding recombinant proteins): the neuronally-enriched p135 (p135 Nt-GCN4) and the ubiquitous isoform lacking the basic region (exons 5-7, Δ5-7 Nt-GCN4). (B, D) Size exclusion chromatography with (B) p135 Nt-GCN4 or (D) Δ5-7 Nt-GCN4 indicates that they cannot form stable complexes with tubulin. (C) Microtubule affinity of 400 nM dimeric polypeptides for increasing concentrations of Taxol-stabilized microtubules demonstrate that these constructs bind microtubules. (E) Light scattering traces for 1 µM constructs suggest that only the brain-specific full-length p150 isoform can promote microtubule formation. Error bars (± SEM) are smaller than the symbols. (F) Single frames from 6 minutes post-tubulin perfusion contrasting the inability of Δ5-7 Nt-GCN4 or p135 Nt-GCN4 to nucleate microtubules with the full-length p150 Nt-GCN4. Scale bar, 12.5 um.

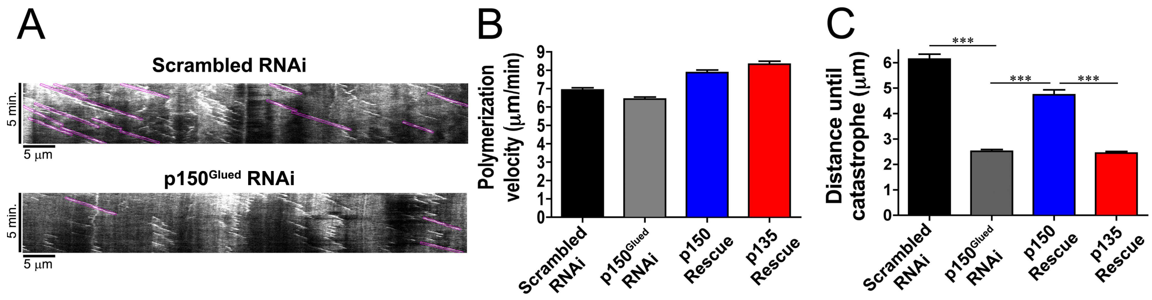

Figure 5. *p150^{Glued} stabilizes microtubules in neurons.* (A) Kymographs of GFP-EB3 comets in cultured dorsal root ganglion neurons treated with either scrambled or p150^{Glued} RNAi reveal that in neurons, p150^{Glued} inhibits catastrophe. Pink traces are added for clarity and indicate polymerization of greater than 5 μm. (B, C) Quantitation of kymographs from neurons under the stated experimental conditions reveal that in neurons, p150^{Glued} acts to stabilize microtubules by inhibiting catastrophe without markedly affecting polymerization rates. Bars represent mean of comet parameters ± SEM. Statistical testing was performed via T-test with correction for multiple comparisons. ***, $p < 0.001$.

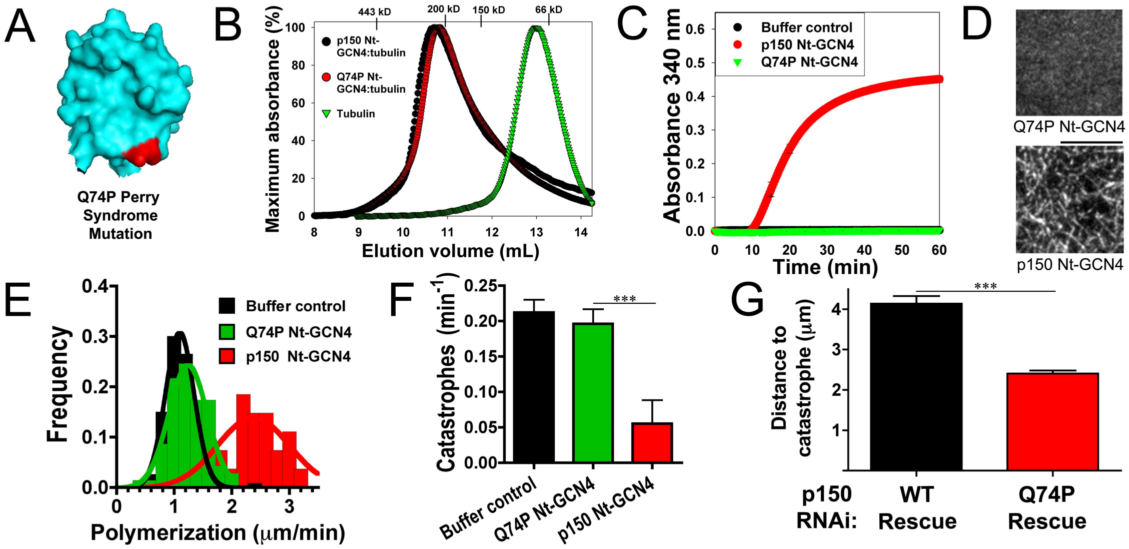

Figure 6. A *Parkinson syndrome mutation abrogates p150^{Glued} activity.* (A) Depiction of the Q74P amino acid substitution identified as a causative mutation for Perry syndrome. (B) Size exclusion chromatograms for p150 Nt-GCN4 or Q74P Nt-GCN4 with tubulin reveal that both can form a stable complex. (C) Light scattering traces suggest that Q74P Nt-GCN4 is defective at promoting microtubule formation. (D) Single frames from 6 minutes post-tubulin perfusion confirm that Q74P Nt-GCN4 cannot catalyze microtubule nucleation. Scale bar, 10 um (E) Polymerization and (F) catastrophe rates demonstrate that Q74P p150 Nt-GCN4 cannot encourage polymerization from pre-formed microtubule seeds. Data from the wild-type construct are graphed for comparison. (G) Transfection of Q74P p150 in neurons expressing GFP-EB3 and depleted for p150^{Glued} shows that the disease mutant cannot substitute for wild-type p150. All bars in this figure repsent mean ± SEM, with statistical testing performed via T-test. ***, $p < 0.001$.

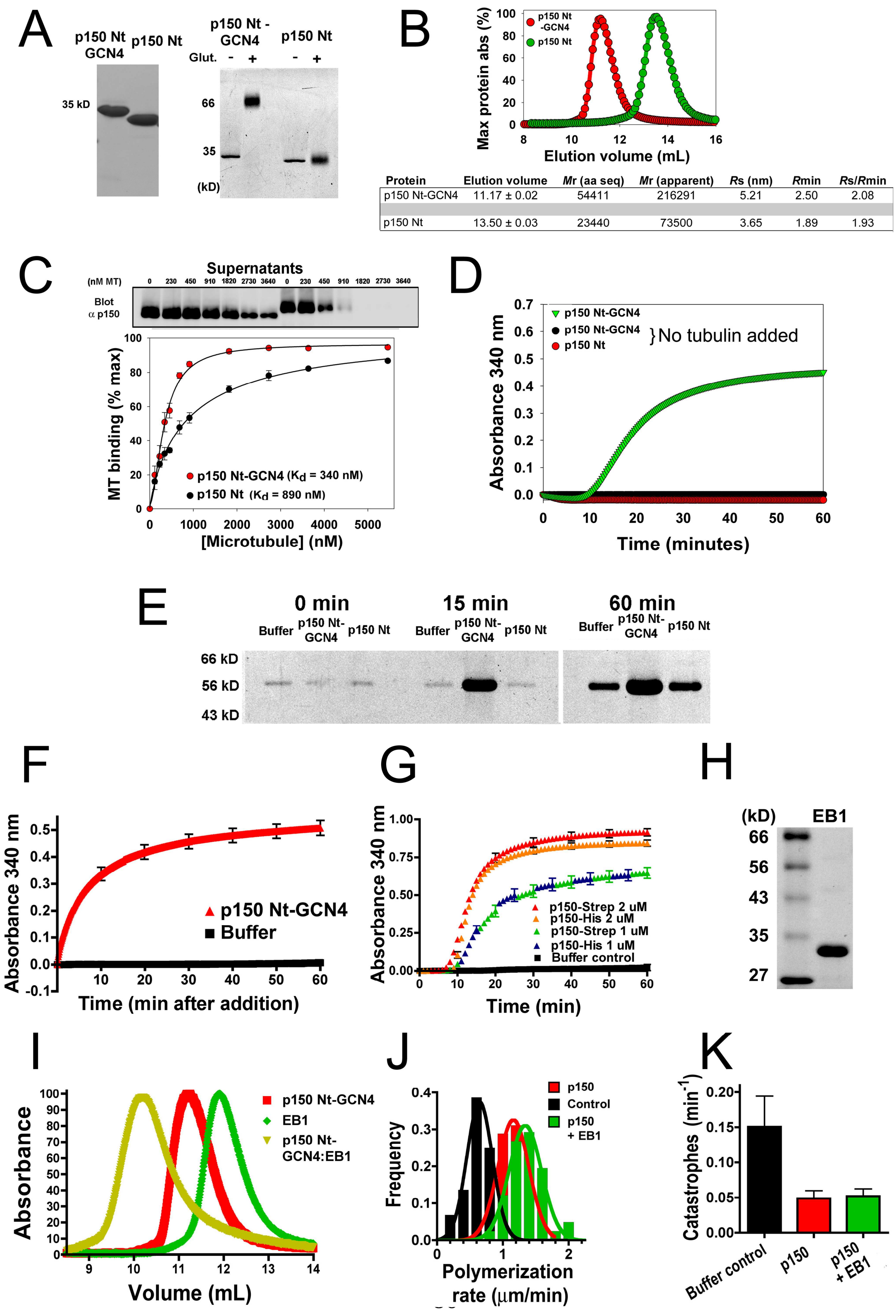

Protein	Elution volume	*Mr* (aa seq)	*Mr* (apparent)	*Rs* (nm)	*R*min	*Rs*/*R*min
p150 Nt-GCN4	11.17 ± 0.02	54411	216291	5.21	2.50	2.08
p150 Nt	13.50 ± 0.03	23440	73500	3.65	1.89	1.93

Figure S1, related to Figure 1. ***Characterization of recombinant dimeric and monomeric p150 polypeptides.*** (A) Coomassie staining demonstrates purity of recombinant polypeptides used in experiments, and at right, dimerization of p150 Nt-GCN4 confirmed by glutaraldehyde cross-linking. (B) Hydrodynamic analysis of the p150 Nt-GCN4 and p150 Nt confirms monodispersion and suggests elongated shape. From left: mean elution volume ± SEM for at least 3 separate column runs; expected molecular mass from the primary amino acid sequence; apparent molecular mass from the calibrated column; calculated Stokes radius from the calibrated column; minimal Stokes radius of a perfectly spherical protein of the expected molecular mass; ratio of Rs/Rmin (Globular 1.2-1.3; moderately elongated 1.5-1.9; highly elongated >2.0) (Erickson, 2009). (C) Microtubule pelleting curves for 100 nM C-terminal GFP-tagged constructs incubated with increasing concentrations of Taxol-stabilized microtubules shows both constructs bind microtubules with moderate affinity. Percent binding was determined fluorimetrically from the fraction of construct in the pellet. Below, validation of fluorimetry by Western blotting the supernatants for p150. (D) Light scattering traces for recombinant polypeptides incubated alone or with 20 μM tubulin and warmed to 37 C confirm that constructs do not contribute to light scattering in the absence of tubulin. (E) Pellets of assembly reactions from Fig 1B confirm microtubule formation. (F) Light scattering traces for buffer control or recombinant polypeptides demonstrate that p150 Nt-GCN4 causes the instant appearance of light scattering when added to pre-warmed tubulin. All error bars indicate the SEM for 3 or more independent experiments. (G) Light scattering traces for buffer control or recombinant polypeptides incubated with 20 μM tubulin and warmed to 37C confirm that the ability of p150 to promote microtubule formation does not result from excess charge on the His-tag. Note that since they otherwise would be indistinguishable, the traces for the 1 μM His- or Strep-tagged p150 Nt-GCN4 alternate. (H) Coomassie staining of purified full-length EB1 used in experiments. (I) Size exclusion chromatograms for EB1 and p150 Nt-GCN4 run alone, or pre-incubated in a 1:2 ratio indicate that they form a stable complex. (J, K) Polymerization rates and catastrophe frequencies from seeded assembly shows that p150 Nt-GCN4 promotes polymerization and inhibits catastrophe independently of EB1.

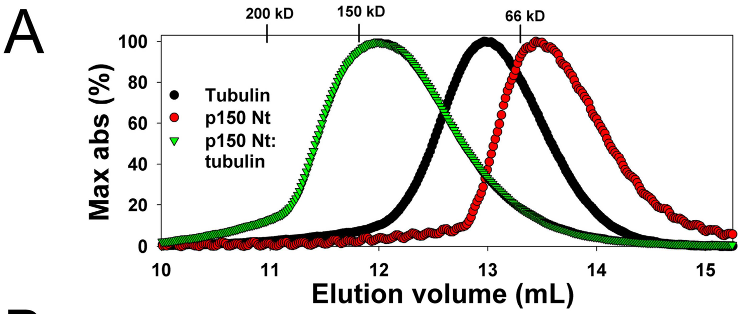

B

Polypeptide	Elution volume	*Mr* (aa seq)	*Mr* (apparent)	*Rs* (nm)	*R*min	*Rs*/ *R*min
Tubulin	12.91 ± 0.06	110000	94821	4.04	3.16	1.28
p150 Nt-GCN4	11.17 ± 0.02	54411	216291	5.21	2.50	2.08
p150 Nt	13.50 ± 0.03	23440	73500	3.65	1.89	1.93
p150 Nt-GCN4:tubulin	10.45 ± 0.03	164411	270761	5.49	3.62	1.52
p150 Nt:tubulin	12.11 ± 0.05	134510	134510	4.56	3.56	1.28

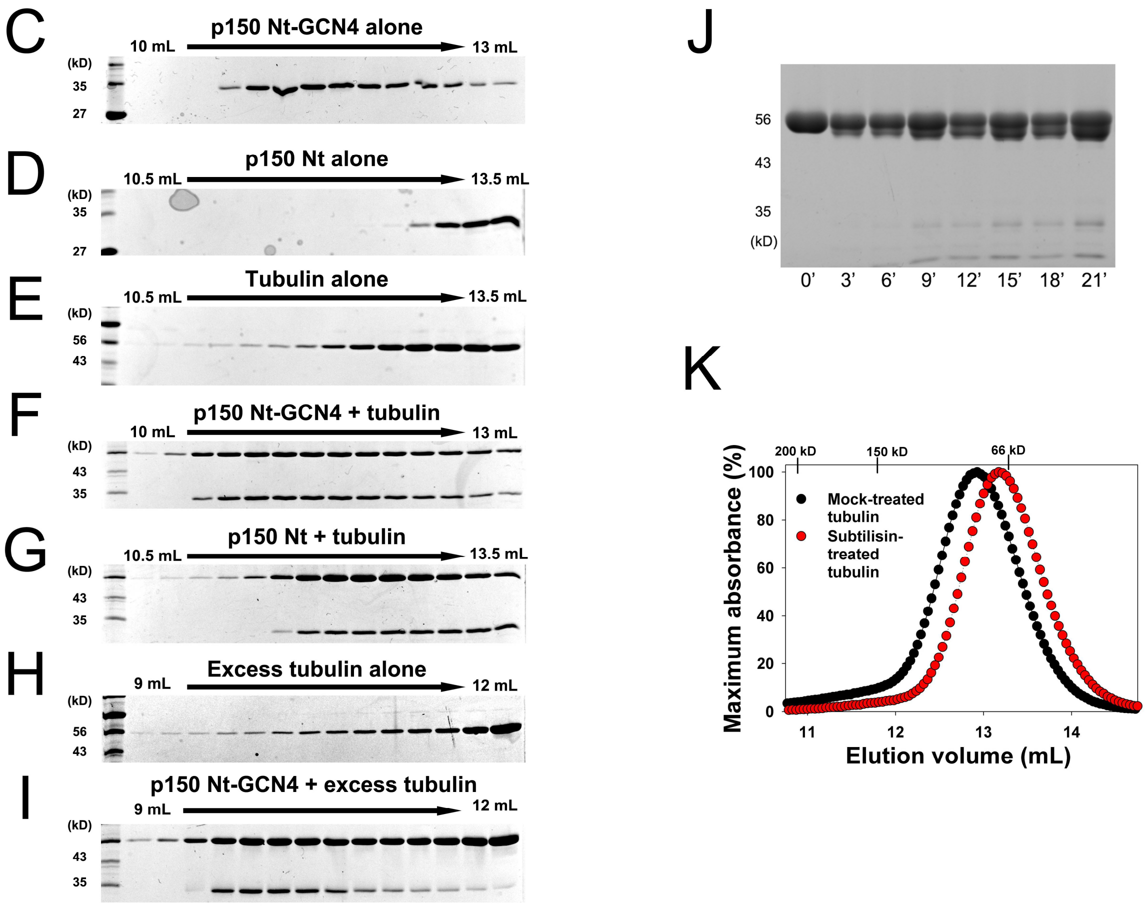

Figure S2, related to Figure 3. ***Characterization of complex formation between the p150 Nt and tuublin.*** (A) Size exclusion chromatograms for p150 Nt run alone or pre-incubated with tubulin reveal that p150 forms a stable complex with tubulin. (B) Hydrodynamic analysis of the p150 Nt-GCN4 and p150 Nt complexes with tubulin suggest the formation of a globular complex. From left: mean elution volume ± SEM for at least 3 separate column runs; expected molecular mass from the primary amino acid sequence; apparent molecular mass from the calibrated column; calculated Stokes radius from the calibrated column; minimal Stokes radius of a perfectly spherical protein of the expected molecular mass; ratio of Rs/Rmin (Globular 1.2-1.3; moderately elongated 1.5-1.9; highly elongated >2.0) (Erickson, 2009). (C-I) Individual SEC fractions for the indicated conditions were subjected to SDS-PAGE and colloidal Coomassie staining. (J) Subtilisin was incubated in a 1:350 weight ratio with tubulin at room temperature for the indicated times, then inactivated with 4 mM PMSF and heat denatured. 20 minutes cleavage was chosen for further experiments because separation of the β-tubulin band has plateaued and internal cleavage products have begun to form. (K) Size exclusion chromatograms of mock-treated tubulin or subtilisin-treated tubulin.

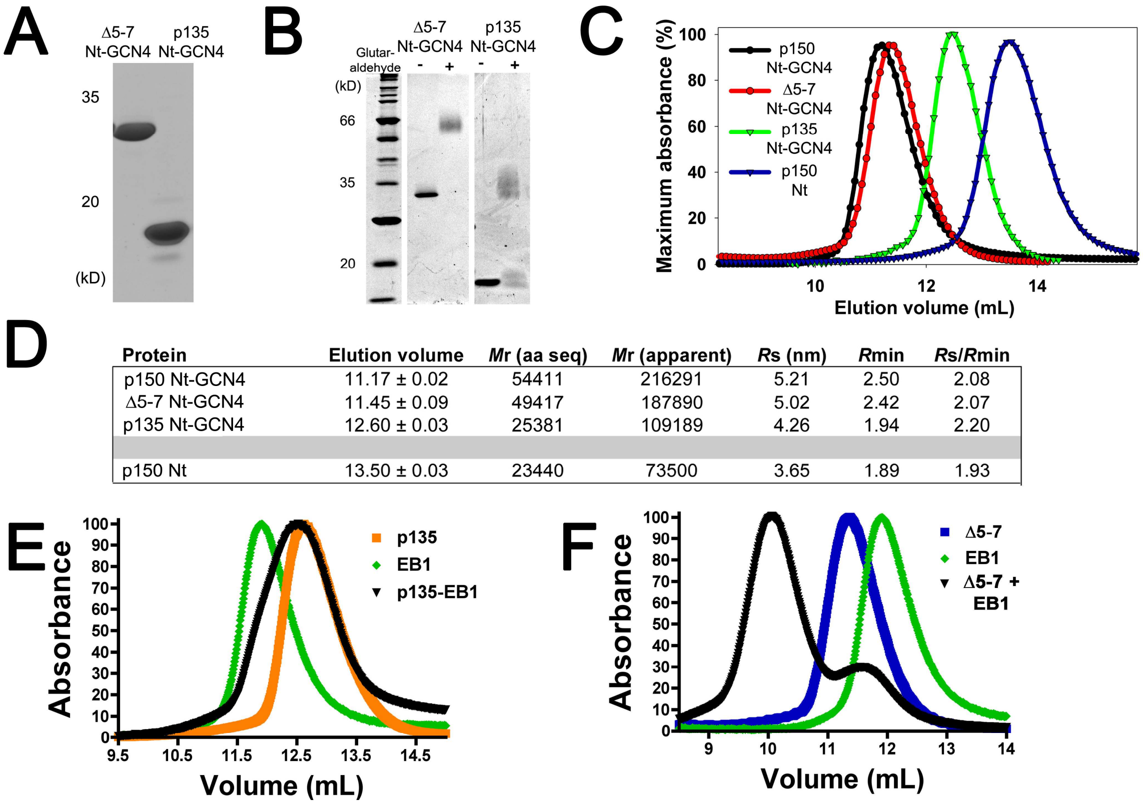

Protein	Elution volume	*Mr* (aa seq)	*Mr* (apparent)	*R*s (nm)	*R*min	*R*s/*R*min
p150 Nt-GCN4	11.17 ± 0.02	54411	216291	5.21	2.50	2.08
Δ5-7 Nt-GCN4	11.45 ± 0.09	49417	187890	5.02	2.42	2.07
p135 Nt-GCN4	12.60 ± 0.03	25381	109189	4.26	1.94	2.20
p150 Nt	13.50 ± 0.03	23440	73500	3.65	1.89	1.93

Figure S3, related to Figure 4. ***Characterization of recombinant Δ5-7 Nt-GCN4 and p135 Nt-GCN4 representing endogenous isoforms.*** (A) Coomassie staining of purified polypeptides used in experiments. (B) Coomassie stain of the recombinant dimers in the absence or presence of 0.5% glutaraldehyde demonstrates dimerization. (C) Size exclusion chromatograms of p150 Nt-GCN4, p150 Nt, Δ5-7 Nt-GCN4, and p135 Nt-GCN4 together to allow comparison. (D) Hydrodynamic analysis of the p150 polypeptides. From left: mean elution volume ± SEM for at least 3 separate column runs; expected molecular mass from the primary amino acid sequence; apparent molecular mass from the calibrated column; calculated Stokes radius from the calibrated column; minimal Stokes radius of a perfectly spherical protein of the expected molecular mass; ratio of Rs/Rmin (Globular 1.2-1.3; moderately elongated 1.5-1.9; highly elongated >2.0) (Erickson, 2009). (E, F) Size exclusion chromatograms for EB1 and Δ5-7 Nt-GCN4 or p135 Nt-GCN4 run alone, or pre-incubated in a 1:2 ratio indicate that Δ5-7 Nt-GCN4, which contains the CAP-Gly domain, but not p135 Nt-GCN4, which does not, can form a stable complex with EB1.

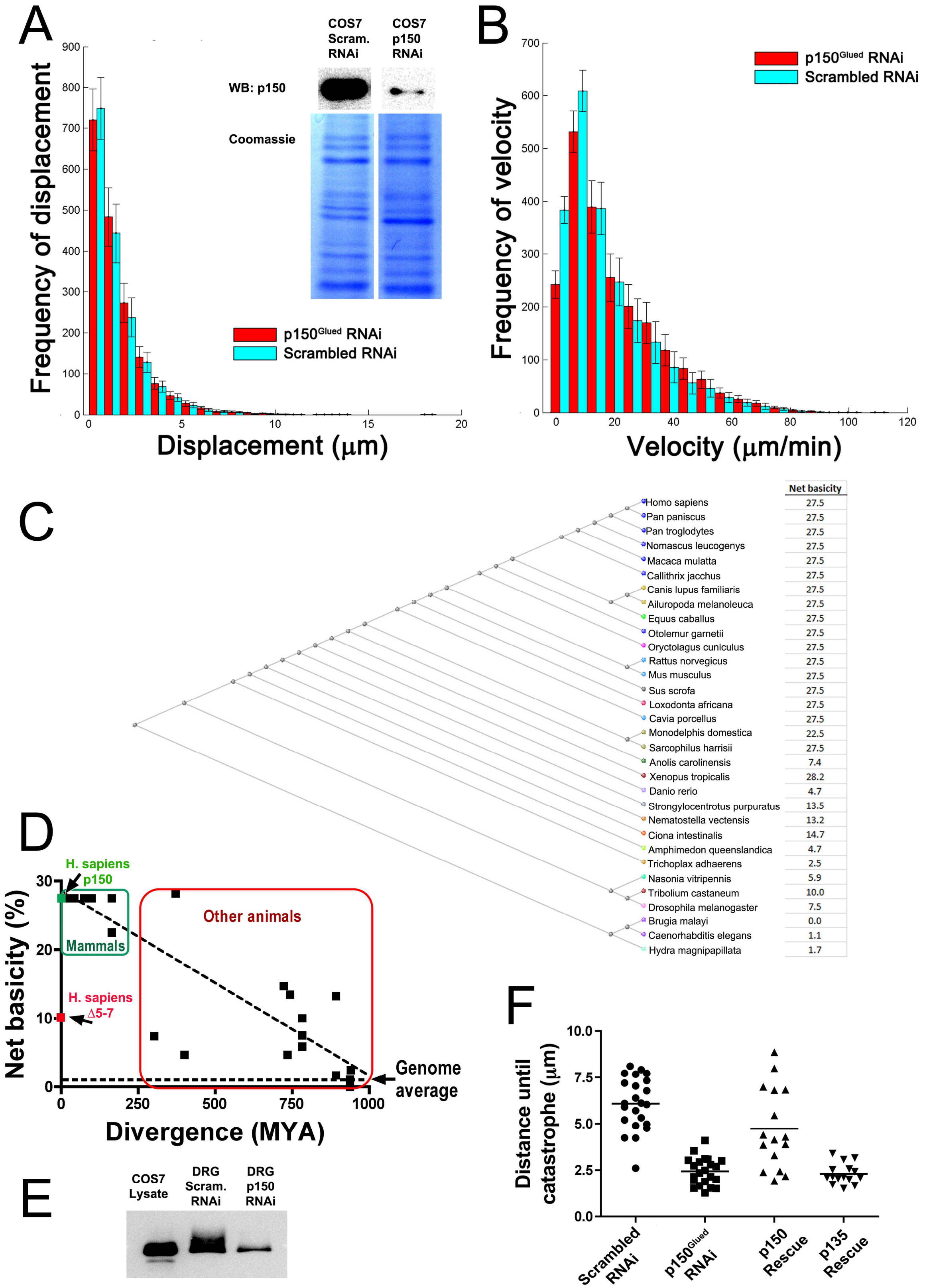
A
COS7 Scram. RNAi
COS7 p150 RNAi
WB: p150
Coomassie
Frequency of displacement
900
800
700
600
500
400
300
200
100
0
0
5
10
15
20
Displacement (μm)
p150Glued RNAi
Scrambled RNAi
B
Frequency of velocity
700
600
500
400
300
200
100
0
0
20
40
60
80
100
120
Velocity (μm/min)
p150Glued RNAi
Scrambled RNAi
C
Net basicity
Homo sapiens 27.5
Pan paniscus 27.5
Pan troglodytes 27.5
Nomascus leucogenys 27.5
Macaca mulatta 27.5
Callithrix jacchus 27.5
Canis lupus familiaris 27.5
Ailuropoda melanoleuca 27.5
Equus caballus 27.5
Otolemur garnetii 27.5
Oryctolagus cuniculus 27.5
Rattus norvegicus 27.5
Mus musculus 27.5
Sus scrofa 27.5
Loxodonta africana 27.5
Cavia porcellus 27.5
Monodelphis domestica 22.5
Sarcophilus harrisii 27.5
Anolis carolinensis 7.4
Xenopus tropicalis 28.2
Danio rerio 4.7
Strongylocentrotus purpuratus 13.5
Nematostella vectensis 13.2
Ciona intestinalis 14.7
Amphimedon queenslandica 4.7
Trichoplax adhaerens 2.5
Nasonia vitripennis 5.9
Tribolium castaneum 10.0
Drosophila melanogaster 7.5
Brugia malayi 0.0
Caenorhabditis elegans 1.1
Hydra magnipapillata 1.7
D
H. sapiens p150
Mammals
H. sapiens Δ5-7
Other animals
Genome average
Net basicity (%)
30
20
10
0
0
250
500
750
1000
Divergence (MYA)
E
COS7 Lysate
DRG Scram. RNAi
DRG p150 RNAi
F
Distance until catastrophe (μm)
10.0
7.5
5.0
2.5
0.0
Scrambled RNAi
p150Glued RNAi
p150 Rescue
p135 Rescue

Figure S4, related to Figure 5. *Characterization of p150^{Glued} role in modulating microtubule dynamics in cells.* (A) At right, Western blot for p150^{Glued} in COS7 cells in the setting of scrambled and p150^{Glued} RNAi. Below, Coomassie staining to show equal protein loading. At left, PlusTipTracker quantitation of EB3-GFP comet displacement before catastrophe shows that knockdown does not alter parameters of microtubule dynamics. (B) PlusTipTracker quantitation of EB3-GFP comet velocities shows that knockdown does not alter parameters of microtubule dynamics. (C) Bioinformatics analysis of p150^{Glued} homologues in diverse metazoans characterizes the basicity downstream of the CAP-Gly domain. Using Homo sapiens p150^{Glued} as a search term, PSI-BLAST was performed to identify as many metazoan homologues as possible (Altschul et al., 1997). Then, full-length cDNA or, to avoid biases due to splicing, genomic DNA computationally spliced using GENSCAN (Burge and Karlin, 1997), was pairwise aligned using Clustal Omega (Sievers et al., 2011), and peptide characteristics computed using ExPASy ProtParam (Gasteiger et al., 2005). (D) Basicity vs. divergence time plot indicates that over Metazoan evolution, the region downstream of the p150^{Glued} CAP-Gly has evolved progressively more basicity. Divergence times calculated using TimeTree (Kumar and Hedges, 2011). (E) Western Blot of p150^{Glued} in COS7 cells compared to in mouse dorsal root ganglion neurons suggests that, in agreement with previous findings, a higher molecular weight pool exists in mammalian neurons. (F) GFP-EB3 comet distance to catastrophe was analyzed using kymograph analysis on a per-neuron basis to control for variable rescue transfection efficiency.

A

Protein	Elution volume	*Mr* (aa seq)	*Mr* (apparent)	*Rs* (nm)	*R*min	*Rs*/*R*min
p150 NT-GCN4	11.17 ± 0.02	54411	216291	5.21	2.50	2.08
Q74P NT-GCN4	11.32 ± 0.03	54349	205388	5.14	2.50	2.06

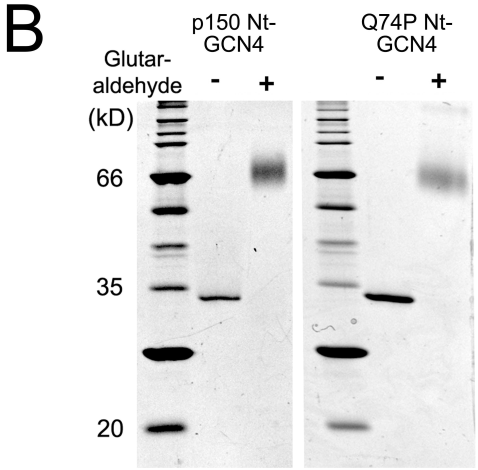

Figure S5. Related to Figure 6. Characterization of *Q74P mutant construct.* (A) Hydrodynamic analysis of the p150 polypeptides shows that the mutant construct is similar to the wild-type construct. From left: mean elution volume ± SEM for at least 3 separate column runs; expected molecular mass from the primary amino acid sequence; apparent molecular mass from the calibrated column; calculated Stokes radius from the calibrated column; minimal Stokes radius of a perfectly spherical protein of the expected molecular mass; ratio of Rs/Rmin (Globular 1.2-1.3; moderately elongated 1.5-1.9; highly elongated >2.0) (Erickson, 2009). (B) Coomassie stain of the recombinant dimers in the absence or presence of 0.5% glutaraldehyde shows that the mutant construct is correctly dimerized.

5.4 Discussion

Here we show *in vitro* that p150^{Glued} promotes microtubule formation by catalyzing nucleation, increasing the microtubule polymerization rate, and inhibiting catastrophe. These activities are dependent on the ability of p150^{Glued} to form a stable complex with tubulin through interactions with both the N-terminal CAP-Gly and basic domains, and require dimerization. In primary neurons, we observe that the dominant role of p150^{Glued} on microtubule dynamics is the suppression of catastrophe. Finally, we discover that a single point mutation within the CAP-Gly domain of p150^{Glued} causative for a a fatal familial Parkinson syndrome leaves p150^{Glued} unable to promote microtubule assembly either *in vitro* or in neurons.

Dynactin was originally identified as a large protein complex that supported dynein-mediated vesicle transport (Gill et al., 1991; Schroer and Sheetz, 1991). The N-terminus of the 150 kDa subunit binds microtubules independently of dynein (Waterman-Storer et al., 1995), and increases the processivity of dynein *in vitro* (Culver-Hanlon et al., 2006; King and Schroer, 2000). Recently, however, it has been demonstrated that the microtubule-binding N-terminus of p150^{Glued} is dispensable for organelle localization and vesicular motility (Dixit et al., 2008a; Kim et al., 2007; Moughamian and Holzbaur, 2012) . One function of the microtubule-binding CAP-Gly domain of dynactin is to promote the initial association of dynein with the microtubule, particularly at the growing plus-end in neurons (Lloyd et al., 2012; Moughamian and Holzbaur, 2012). A plus end-localized pool of p150^{Glued} may serve to load dynein onto the microtubule (Vaughan et al., 2002). However biochemical analyses and immunolocalization suggest that a large proportion of dynactin may in fact not be in complex with dynein (Gill et al., 1991; Habermann et al., 2001; Morgan et al., 2011). Enriched at the plus end, this population of dynactin would be perfectly poised to affect microtubule dynamics.

Recently, it has been suggested that the kinetics of tubulin association and dissociation with the microtubule may be much faster than previously appreciated (Gardner et al., 2011a). This makes it increasingly plausible that one mode whereby MAPs alter microtubule dynamics is by modulating the off-rate of tubulin subunits from microtubule plus ends. Since p150 can bind both to microtubules and to soluble tubulin, and because dimerization appears necessary for p150 to robustly modify dynamics, we speculate that p150 may be acting in this capacity by binding to both microtubules and tubulin at the same time, decreasing the off-rate and inhibiting catastrophe. Interestingly, this mechanism is distinct from the mode by which we have recently discovered that cytoplasmic dynein inhibits catastrophe (Hendricks et al., 2012). Areas of the distal neuron where both cytoplasmic dynein and dynactin are localized could be sites of particularly robust microtubule stabilization.

The regulation of these microtubule-modifying abilities of $p150^{Glued}$ may be multifactorial. We have shown that the basic region is necessary for the modification of microtubule dynamics by $p150^{Glued}$, likely by ensuring a stable complex with the distributed acidic nature of tubulin. The basic region is also serine- and threonine-rich, and has been shown to be the target of phosphorylation by regulatory kinases (Li et al., 2010; Rome et al., 2010), which might further modulate the p150-tubulin interaction during mitosis, or during development. In the cell, $p150^{Glued}$ also binds to CLIP-170

(Goodson et al., 2003; Hayashi et al., 2005; Honnappa et al., 2006; Ligon et al., 2003), which could also further modify the behavior of $p150^{Glued}$ *in vivo.*

Only the $p150^{Glued}$ isoform expressed in neurons includes both the full CAP-Gly and basic domains that we have shown are necessary to modify microtubule assembly dynamics. We have recently shown that young, developing neurons depleted of $p150^{Glued}$ are morphologically normal (Moughamian and Holzbaur, 2012). In fact, profound depletion of both EB1 and EB3, which should completely disrupt the entire plus-end complex, has no gross effects on neurite outgrowth (Moughamian and Holzbaur, 2012). It may be that, as recent evidence suggests, only as neurons age, lengthen, and elaborate their processes, does the centrosome lose its function as a microtubule organizing center and microtubule dynamics become particularly reliant on plus-end regulation (Nguyen et al., 2011; Stiess et al., 2010). It is perhaps telling that human patients with the Q74P $p150^{Glued}$ mutation which we have shown is a complete loss of function, do not show disease onset until the 5th decade of life (Farrer et al., 2009). It may also be that regulation of microtubule dynamics in aging neurons is a more universal challenge, as we are beginning to learn from sporadic Parkinson's and Alzheimer's disease.

In summary, we have identified and characterized a novel role for $p150^{Glued}$ in the tissue-specific stabilization of microtubules, and implicated defects in neurodegeneration. Further studies to disentangle the effects of the mutation on axonal transport and microtubule stability in neurons will be required to clarify the pathogenesis involved.

CHAPTER 6.

Dynein activation by dynactin

Contributions:

Mariko Tokito performed all cloning for constructs used in these experiments and performed the yeast 2 hybrid assay. Tien-Ming Lin in the lab of Mike Ostap generated baculovirus and infected and harvested Sf9 cells for protein purification. DIC1-GFP mice were generated by Jun Zhang in the lab of Xin Xiang and bred and maintained by Karen Wallace. I purified all proteins and performed all biochemistry described in this chapter. My characterization of the dynein-dynactin complex in the DIC1-GFP mice is included in a study led by Eran Perlson on which I am co-author that is currently in revision in the EMBO Journal.

6.1 Introduction

Microtubules serve as crucial tracks for long-range cellular transport. Numerous plus end-directed kinesins have evolved to perform various functions in the cell, but there is only one major minus end-directed microtubule motor: cytoplasmic dynein (Kardon and Vale, 2009; Paschal and Vallee, 1987). This one motor must navigate through an array of cellular environments and interact with a wide diversity of vesicles and organelles. Fundamentally, the motor properties of dynein are more flexible than those of kinesin (Gennerich and Vale, 2009), but another crucial way that dynein is aided in its tasks is by a small group of crucial cofactors.

The first to be discovered came to be known as dynactin (Gill et al., 1991) because it served to activate dynein transport in vitro (Schroer and Sheetz, 1991). Subsequently, it was found that the integrity of dynactin was necessary for most dynein functions in the cell (Schroer, 2004). It was originally proposed that the primary way that dynactin assisted dynein was by binding to microtubules independently of dynein through the N-terminus of its p150^{Glued} subunit. This would allow the relatively non-processive dynein motor to stay bound to the microtubule during aborted retrograde runs (King and Schroer, 2000; Waterman-Storer et al., 1995).

However, during the past 5 years, we have found that this may not be the case. When dynein cargoes are imaged in cells lacking the p150^{Glued} N-terminus, cargo run length, the percentage of anterograde runs, and cargo velocity are not appreciably affected (Dixit et al., 2008a; Kardon et al., 2009; Kim et al., 2007; Lloyd et al., 2012; Moore et al., 2009; Moughamian and Holzbaur, 2012). It may be that dynactin allows dynein to exert higher maximal forces, such as during spindle orientation in mitosis or nuclear migration (Kim et al., 2007; Moore et al., 2009). Alternatively, instead of having a constitutive effect on processivity, the p150^{Glued} N-terminus may instead be particularly important in the initiation of dynein transport, particularly at the microtubule plus end, where we have shown that dynactin alters microtubule dynamics and where it may bind to EB1 or CLIP-170 (Lloyd et al., 2012; Moore et al., 2009; Moughamian and Holzbaur, 2012; Vaughan et al., 2002; Xiang et al., 2000; Zhang et al., 2003).

Here, we describe preliminary data that will allow us to test these hypotheses.

6.2 Results

To create recombinant dynactin constructs that could interact with dynein, we first sought to define the minimum essential region of $p150^{Glued}$ that interacted with dynein. Earlier studies indicated that dynein bound to the first $p150^{Glued}$ coiled coil (CC1) and an extended C-terminal region (Karki and Holzbaur, 1995; Vaughan and Vallee, 1995; Vaughan et al., 2002). To confirm these results we transfected Cos7 cells with FLAG-tagged $p150^{Glued}$ constructs, and determined their ability to co-immunoprecipitate dynein.

As in previous studies, we found that when we immunoprecipitated AA 1-880 of $p150^{Glued}$, we were able to detect both endogenous dynein intermediate chain and dynein heavy chain on the beads (Figure 1, left). In contrast, we found that AA 1-210, which encodes the $p150^{Glued}$ N-terminus without CC1, did not co-immunoprecipitate dynein (Figure 1, middle). We also did not find that the region C-terminal to CC1, AA 550-880, was sufficient alone to immunoprecipitate dynein (Figure 1, right).

To further narrow down the minimal dynein binding region, we performed a yeast two-hybrid screen with the dynein intermediate chain as bait. Then, we screened the $p150^{Glued}$ fragments that were found, and aligned them to define a region of overlap (Figure 2, top). All of the fragments that we found encoded the CC1 region (Figure 2, bottom), suggesting that, like previous studies, this might be sufficient to bind dynein (King et al., 2003). Interestingly, the putative minimum essential region identified from this screen encompassed a region of CC1 that is predicted to form a break in the coiled coil. This break appears to be conserved from humans, to Xenopus, to Drosophila (Figure 3).

To determine if the entire CC1 region was necessary for dynein binding, or if a smaller sub-region was sufficient, we designed N-terminal p150^{Glued} fragments terminated at various points in CC1. We then transfected these fragments and a plasmid encoding a tagged dynein intermediate chain into Cos7 cells and assayed for co-immunoprecipitation as above. We found that both AA 1-880, and 1-547 of p150^{Glued} could immunoprecipitate both exogenous DIC and endogenous dynein complex (Figure 4, left). CC1 truncations displayed a gradient of exogenous DIC binding, with shorter constructs progressively co-immunoprecipitating less DIC (Figure 4, middle). This likely indicates that the interface between the p150^{Glued} CC1 and DIC is quite extended. Importantly though, CC1 truncations were not able to co-immunoprecipitate endogenous dynein heavy chain, indicating that the entire domain is necessary for authentic interaction.

DIC is actually the product of two different genes, which are themselves each alternatively spliced into 3 separate isoforms (Kuta et al., 2010). Using the Cos7 system above to express these different isoforms, we sought to define the minimal region on dynein sufficient for dynactin interaction, and to determine if dynein-dynactin binding might be regulated by alternative splicing.

The N-terminus of DIC has previously been implicated in binding to p150^{Glued}, with AA 1-70 identified as being sufficient to mediate this interaction (McKenney et al., 2011). Using the different DIC isoforms as probes, we asked if there were further binding determinants more C-terminal. The region of greatest homology between the DIC1 and DIC2 gene products lies in the N-terminal DIC coiled coil, with divergence after AA 50

(Figure 5). The first DIC splice site removes AA 75-95 in the “b” and “c” isoforms. An additional region encompassing AA 125-145 is further removed in the “c” isoforms. “a” isoforms are unspliced.

When we immunoprecipitated FLAG-tagged p150^{Glued} and blotted for HA-tagged DIC isoforms, we observed a highly significant difference in the amount of DIC that co-immunoprecipitated (Fig 6, top). In general, p150^{Glued} co-IPs more DIC1 isoforms than DIC2 isoforms, indicating that binding encompasses regions downstream of the first DIC coiled coil. There is also a large difference observed between the “a” isoforms and the “b” and “c” isoforms, implying that there are binding determinants at least as far as AA 100. In contrast, we do not observe differences between the “b” and the “c” isoforms, suggesting that the interface does not last past AA 120. These data also make it attractive to speculate that the dynein-dynactin interaction may be stronger or weaker in different body tissues. For example, DIC1 is only expressed in brain (Kuta et al., 2010).

With the minimal regions for dynein-dynactin binding defined, we designed reagents that would allow us to examine their interaction in vitro. So that we could visualize and detect mammalian dynein in subsequent experiments, collaborators generated mice with GFP and FLAG tags at the endogenous DIC1 locus. Homozygotes are viable and fertile. We sought to determine if this genetic alteration perturbed the normal organization of the dynein-dynactin complex.

To test this we fist immunoprecipitated DIC and assayed for dynein subunits and the presence of dynactin. When we used either a FLAG antibody or an antibody specifically to DIC, we detected the dynein heavy chain, and both the unmodified DIC2 gene, and DIC1-GFP (Figure 7). This suggests that DIC1-GFP is correctly incorporated into the dynein complex, and that in fact it and the unmodified DIC2 can heterodimerize. When we IP'd with FLAG, we also observed the presence of dynactin, indicating that the incorporation of DIC1-GFP into the dynein complex does not disrupt the dynein-dynactin interaction. We did not detect dynactin when we IP'd with the DIC antibody, but that it is because the antibody epitope lies in the first 100 AA of DIC, which would disrupt the dynein-dynactin interaction. We also did not detect co-immunoprecipitation when we used a c-Myc antibody as negative control (Figure 7, right).

To confirm the structural integrity of the complex, we performed sucrose gradient density centrifugation and observed the subsequent distribution of the complexes. Similar to in wild-type mice, we observe that the dynein and dynactin complexes co-migrate through the gradient (Figure 8). DIC1-GFP overlapped completely with DIC2, indicating again that it is correctly incorporated into the complex.

Finally, we designed a recombinant p150^{Glued} construct that would be sufficient to bind dynein. This construct encompasses the p150^{Glued} N-terminus and CC1. We expressed and purified it from Sf9 cells. Characterization by analytical size exclusion chromatography indicates that it is monodisperse and that its elution volume is consistent with previous, smaller, p150^{Glued} constructs. We then sought to confirm if this construct could bind to dynein.

We incubated native cytoplasmic dynein from bovine brain with either this construct, p150 Nt-CC1 (Figure 9, right), or a previously characterized construct which does not contain the dynein binding site in CC1, but contains the dimerized N-terminus

(Figure 9, left, p150 Nt-GCN4). We found that p150 Nt-CC1, but not p150 Nt-GCN4 could bind dynein (Figure 9).

6.3 Figures

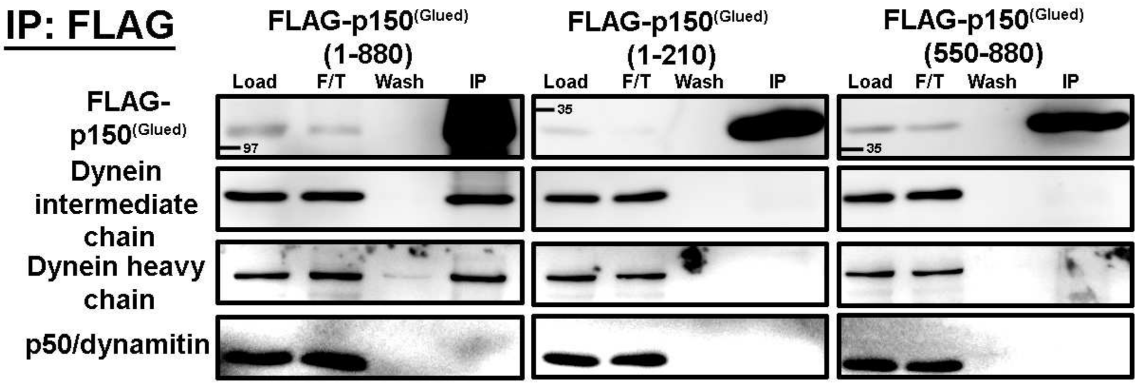
IP: FLAG
FLAG-p150(Glued) (1-880)
FLAG-p150(Glued) (1-210)
FLAG-p150(Glued) (550-880)
Load
F/T
Wash
IP
FLAG-p150(Glued)
Dynein intermediate chain
Dynein heavy chain
p50/dynamitin
97
35
35

Figure 1. Coarse mapping of the p150^{Glued} binding region for dynein. FLAG-p150^{Glued} 1-880, 1-210, or 550-880 were transfected into Cos7 cells and assayed for the ability to co-immunoprecipitate endogenous dynein complex. p50/dynamitin is a constituent of the dynactin complex. Its lack of binding indicates that it binds to p150^{Glued}, as expected, C-terminal to AA 880.

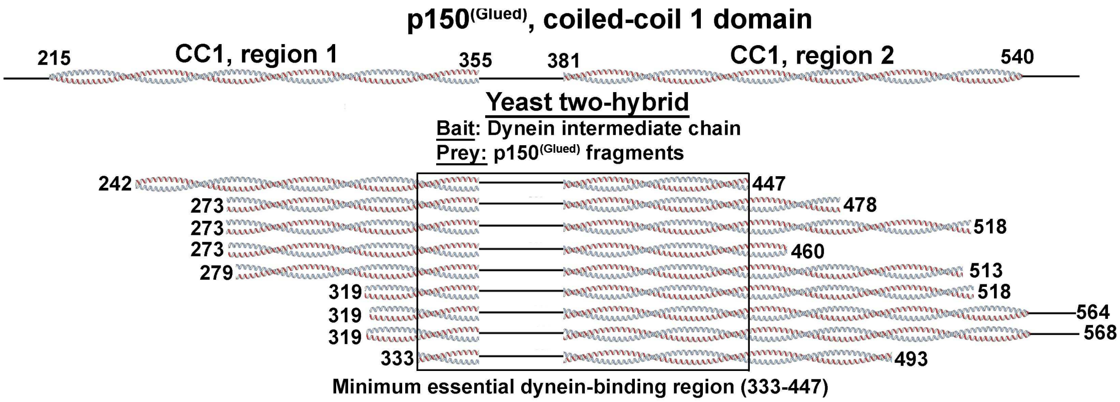
p150(Glued), coiled-coil 1 domain
215
CC1, region 1
355
381
CC1, region 2
540
Yeast two-hybrid
Bait: Dynein intermediate chain
Prey: p150(Glued) fragments
242
447
273
478
273
518
273
460
279
513
319
518
319
564
319
568
333
493
Minimum essential dynein-binding region (333-447)

Figure 2. Yeast 2 hybrid analysis of the p150^{Glued} binding region for dynein. Yeast expression constructs were screened with DIC as bait. p150^{Glued} fragments were aligned to determine a putative minimum region in the p150^{Glued} CC1, depicted in full above. AA 355-381 are predicted to be a break in helical character in CC1.

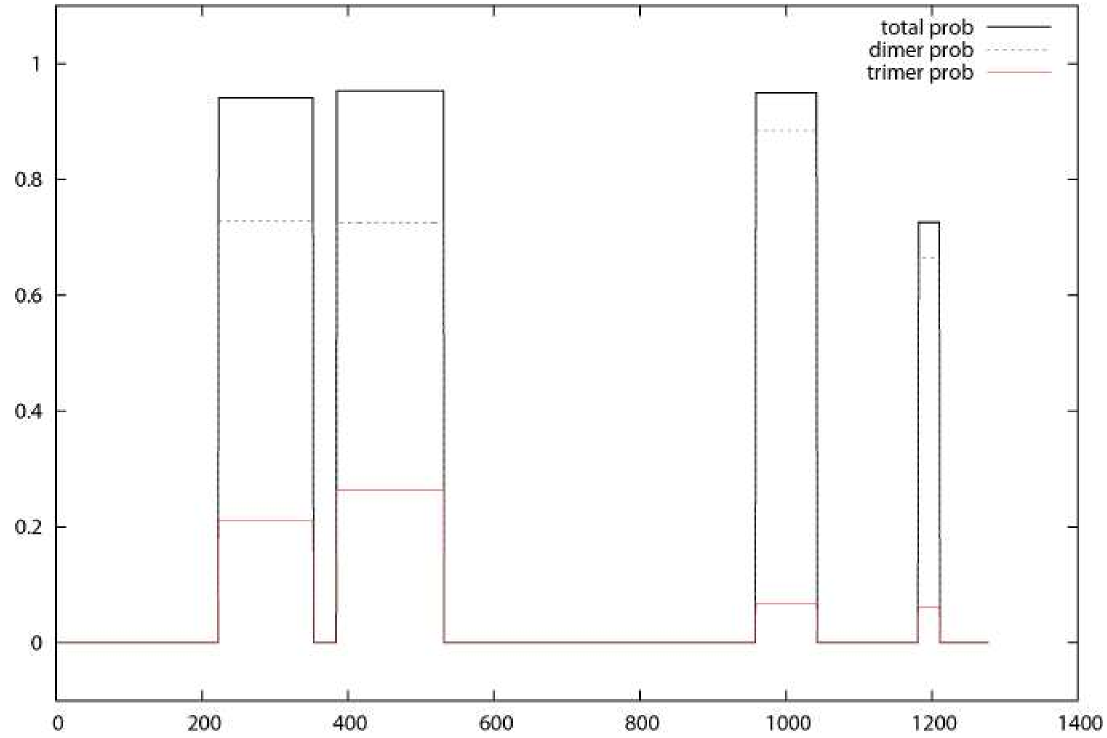

MultiCoil score for DCTN1 human

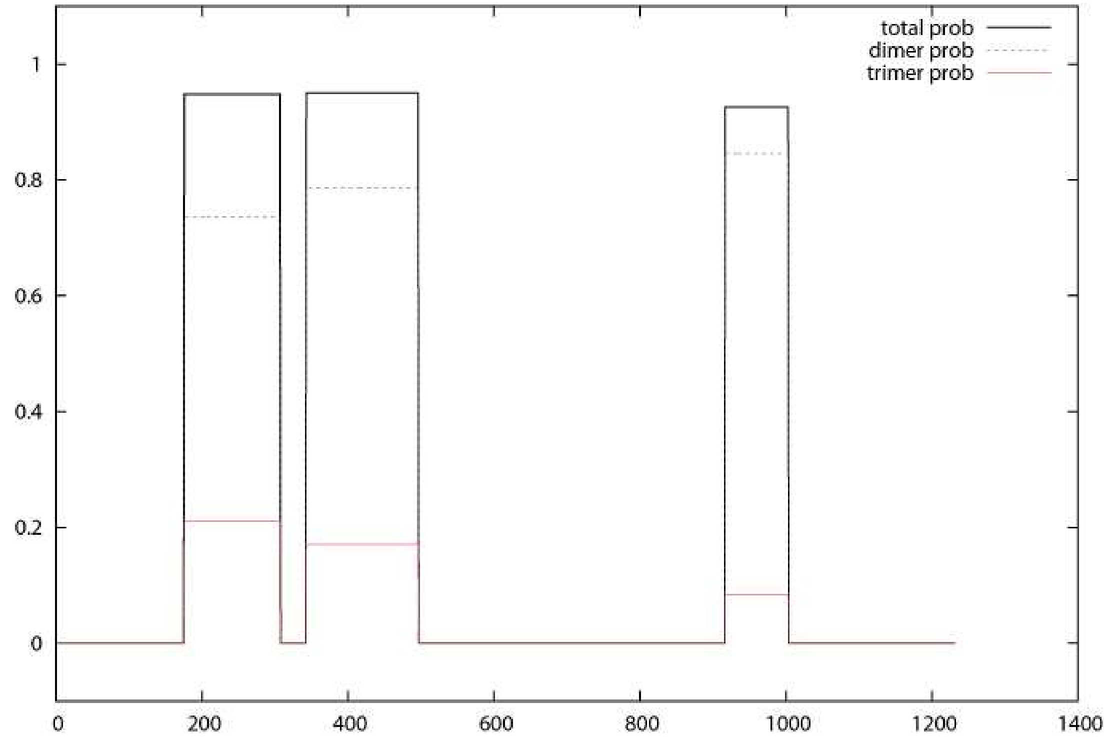

MultiCoil score for DCTN1 xenopus

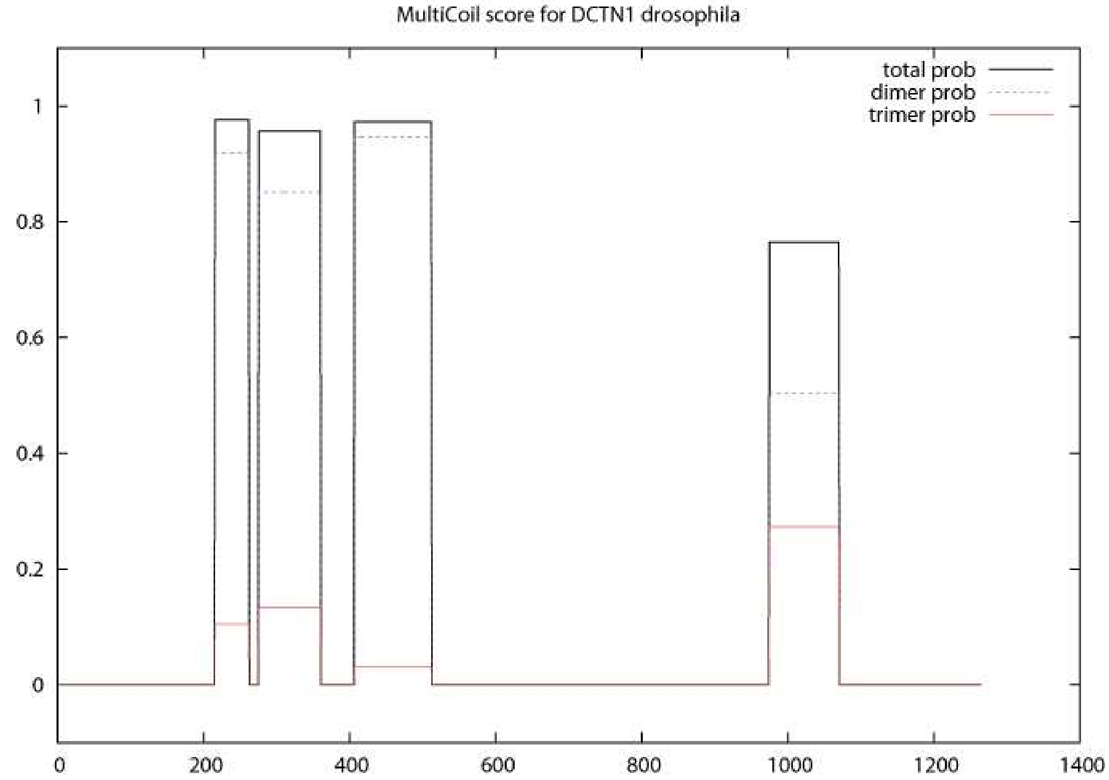

Figure 3. Secondary structure prediction for p150^{Glued}. There is predicted to be a break in coiled coil character in CC1 (AA 210-550) from humans, Xenopus, and Drosophila.

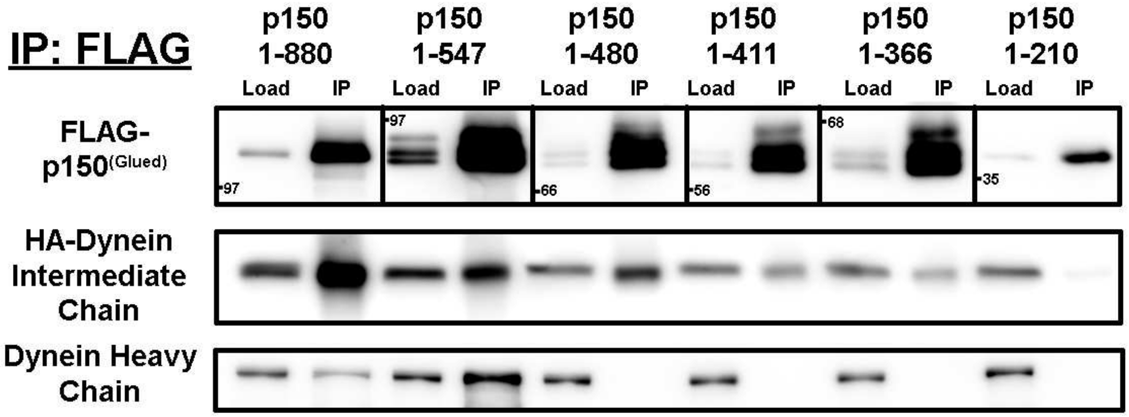
IP: FLAG
p150 1-880
p150 1-547
p150 1-480
p150 1-411
p150 1-366
p150 1-210
Load
IP
FLAG-p150(Glued)
HA-Dynein Intermediate Chain
Dynein Heavy Chain
97
97
66
56
68
35

Figure 4. Fine mapping of the p150^{Glued} binding region for dynein. FLAG-p150^{Glued} constructs were transfected into Cos7 cells and assayed for the ability to co-immunoprecipitate endogenous dynein complex or exogenous HA-DIC.

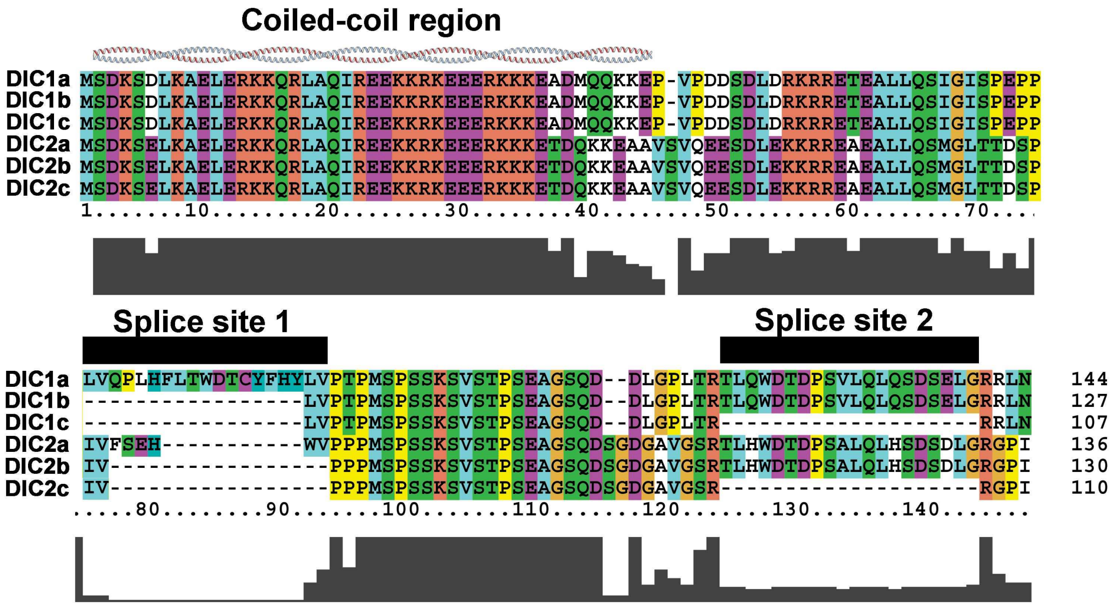
Coiled-coil region
DIC1a MSDKSDLKAELERKKQRLAQIREEKKRKEEERKKKEADMQQKKEP-VPDDSDLDRKRRETEALLQSIGISPEPP
DIC1b MSDKSDLKAELERKKQRLAQIREEKKRKEEERKKKEADMQQKKEP-VPDDSDLDRKRRETEALLQSIGISPEPP
DIC1c MSDKSDLKAELERKKQRLAQIREEKKRKEEERKKKEADMQQKKEP-VPDDSDLDRKRRETEALLQSIGISPEPP
DIC2a MSDKSELKAELERKKQRLAQIREEKKRKEEERKKKETDQKKEAAVSVQEESDLEKKRREAEALLQSMGLTTDSP
DIC2b MSDKSELKAELERKKQRLAQIREEKKRKEEERKKKETDQKKEAAVSVQEESDLEKKRREAEALLQSMGLTTDSP
DIC2c MSDKSELKAELERKKQRLAQIREEKKRKEEERKKKETDQKKEAAVSVQEESDLEKKRREAEALLQSMGLTTDSP
1.......10........20........30........40........50........60........70....
Splice site 1
Splice site 2
DIC1a LVQPLHFLTWDTCYFHYLVPTPMSPSSKSVSTPSEAGSQD--DLGPLTRTLQWDTDPSVLQLQSDSELGRRLN 144
DIC1b -----------------LVPTPMSPSSKSVSTPSEAGSQD--DLGPLTRTLQWDTDPSVLQLQSDSELGRRLN 127
DIC1c -----------------LVPTPMSPSSKSVSTPSEAGSQD--DLGPLTR--------------------RRLN 107
DIC2a IVFSEH-----------WVPPPMSPSSKSVSTPSEAGSQDSGDGAVGSRTLHWDTDPSALQLHSDSDLGRGPI 136
DIC2b IV-----------------PPPMSPSSKSVSTPSEAGSQDSGDGAVGSRTLHWDTDPSALQLHSDSDLGRGPI 130
DIC2c IV-----------------PPPMSPSSKSVSTPSEAGSQDSGDGAVGSR--------------------RGPI 110
.....80........90.......100.......110.......120.......130.......140.......

Figure 5. Depiction of splicing of the DIC1 and DIC2 genes. Homology scores are below, in grey.

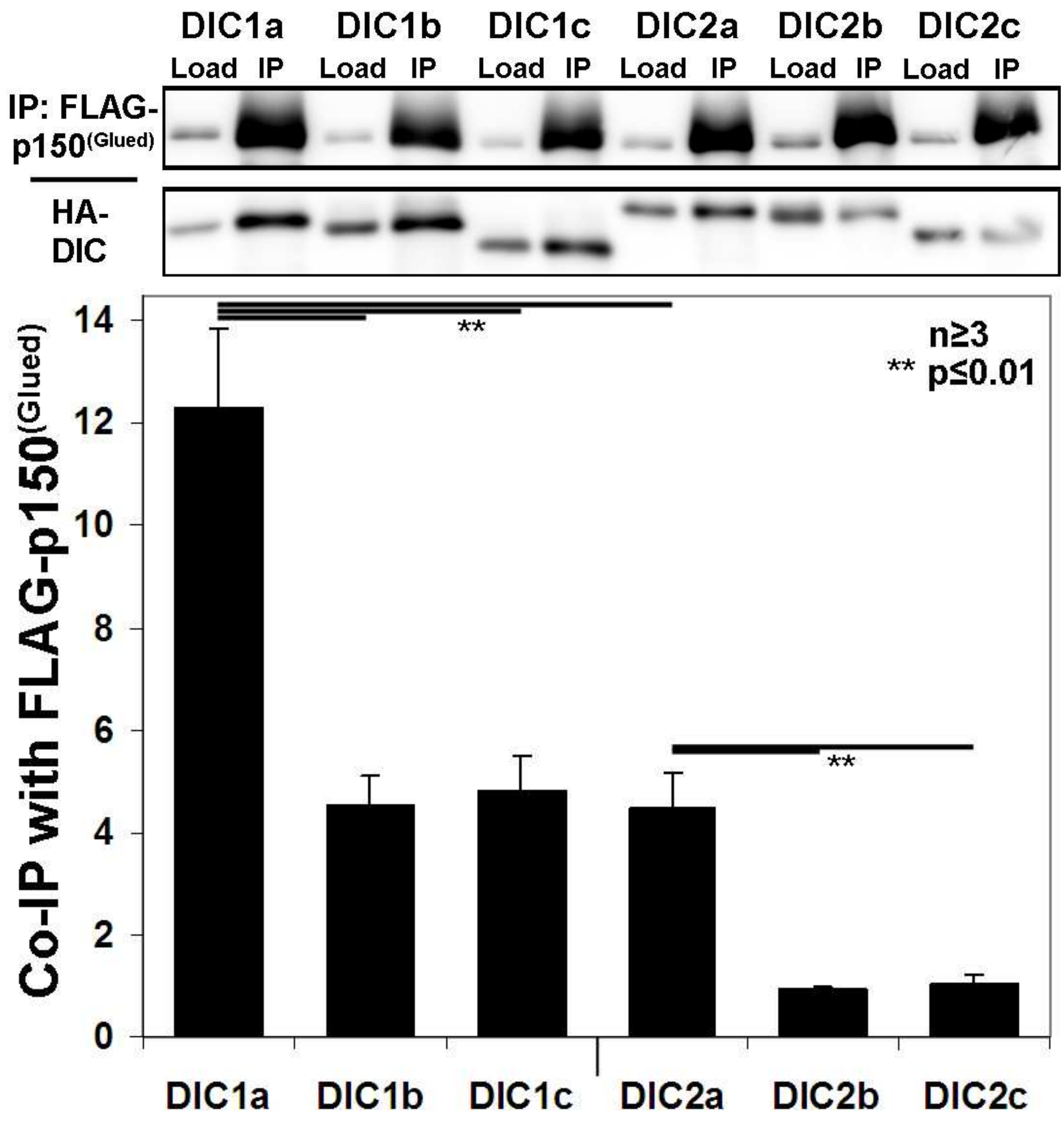

Figure 6. Isoform-specific differences in dynein-dynactin binding. FLAG-p150^{Glued} was assayed for its ability to co-IP HA-tagged DIC isoforms transfected into Cos7 cells.

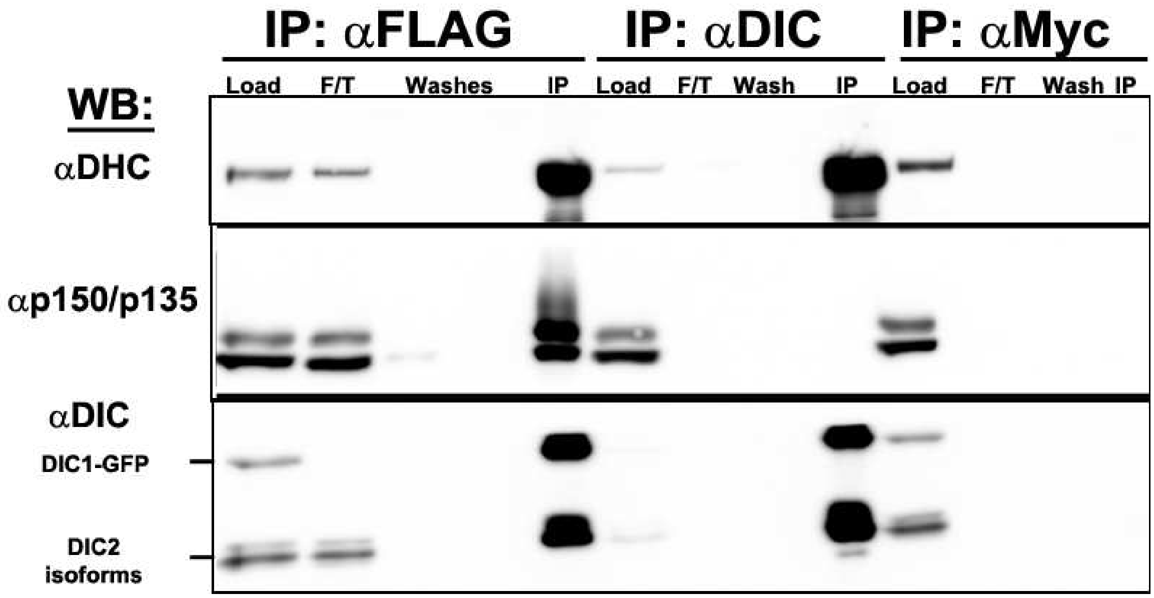
IP: αFLAG
IP: αDIC
IP: αMyc
Load
F/T
Washes
IP
Load
F/T
Wash
IP
Load
F/T
Wash
IP
WB:
αDHC
αp150/p135
αDIC
DIC1-GFP
DIC2 isoforms

Figure 7. Characterization of DIC1-GFP-FLAG knock-in mice by immunopreciptiation. Brain lysates from mice were clarified and subjected to immunoprecipitation by either anti-FLAG, –DIC, or –Myc antibody.

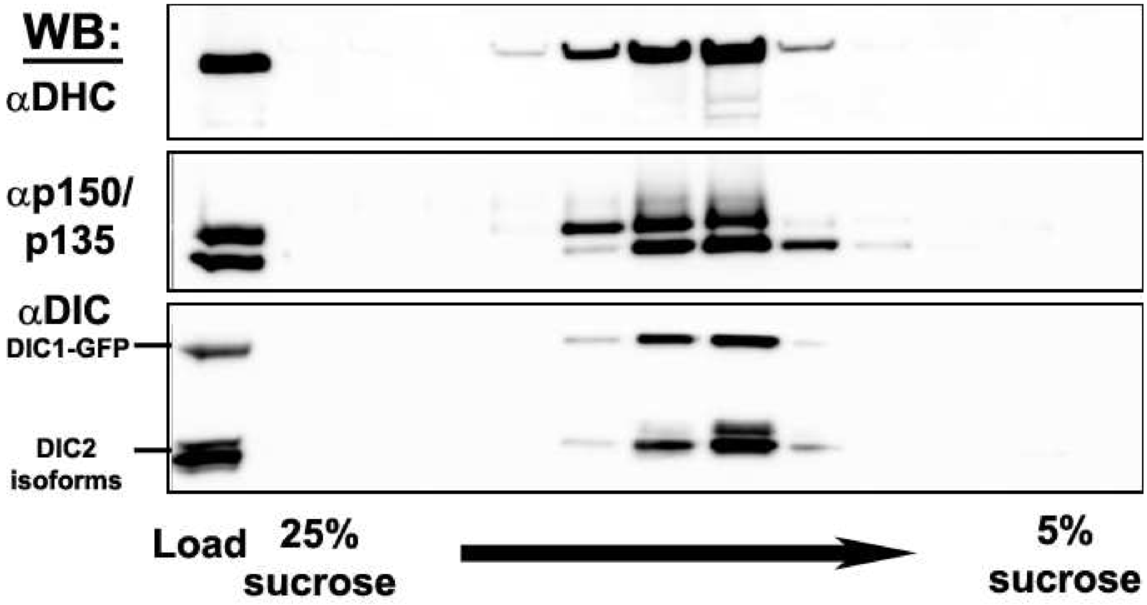
WB:
αDHC
αp150/
p135
αDIC
DIC1-GFP
DIC2
isoforms
Load
25%
sucrose
5%
sucrose

Figure 8. Characterization of DIC1-GFP-FLAG knock-in mice by density centrifugation. Brain lysates from mice were clarified and subjected to sucrose density centrifugation. Fractions were collected and analyzed by Western blot.

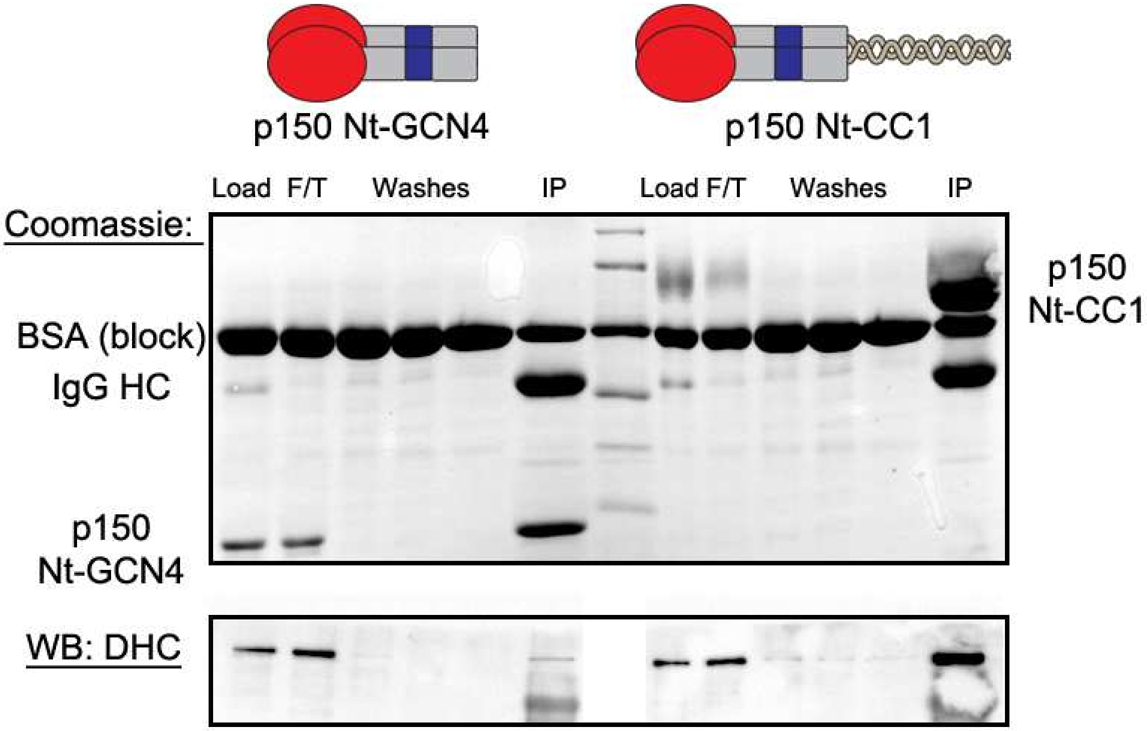
p150 Nt-GCN4
p150 Nt-CC1
Load
F/T
Washes
IP
Load
F/T
Washes
IP
Coomassie:
BSA (block)
IgG HC
p150 Nt-GCN4
p150 Nt-CC1
WB: DHC

Figure 9. Characterization of the ability of recombinant p150^{Glued} to bind native dynein. Recombinant p150^{Glued} either lacking (left) or containing (right) the dynein binding site were blocked with BSA and incubated with cytoplasmic dynein purified from bovine brain. Recombinant constructs were then immunoprecipitated, and the presence of dynein was assayed by Western blot.

6.4 Discussion

Here, we have shown that the binding of dynactin to dynein is influenced by differential splicing of the DIC N-terminus. We have also characterized the minimum essential binding regions of dynactin for dynein and vice versa. As a step toward reconstituting the interaction in vitro, we have also generated and performed the initial characterization of a recombinant p150^{Glued} polypeptide and the dynein complex from a new knockin mouse that will enable us to directly observe the influence of dynactin on the stepping and force-generating ability of dynein.

We discuss future directions for these studies in more detail in Chapter 8.

7. Conclusion

Here, we have reconstituted microtubule dynamic instability in vitro and imaged microtubule assembly and disassembly using TIRF microscopy. This has allowed us to finally test long-standing hypotheses about the microtubule plus end complex and how dynein and dynactin act there. First, we discovered that the mammalian EB1 protein localizes to the microtubule plus-end irrespective of other factors. Then, using techniques developed during this project, we demonstrated in vitro, and in the case of dynactin, also in primary neurons, that dynein and dynactin directly modify microtubule dynamics. Thus, in addition to the traditional role for dynein-dynactin in retrograde transport, we now know they act to directly alter the properties of the cytoskeleton. Primarily, we have found that they stabilize microtubules from depolymerization.

7.1 Microtubule plus end reconstitution

First, we and others (Bieling et al., 2008) demonstrated that mammalian EB1 is sufficient to recognize the growing microtubule plus end. This had previously been shown in yeast (Bieling et al., 2007). Therefore, EB1 is a conserved eukaryotic microtubule plus end-recognition factor. Though other proteins have subsequently been found to localize independently to the growing microtubule (Bechstedt and Brouhard, 2012; Brouhard et al., 2008), unlike EB1 and the closely related EB2 and EB3, they do not seem to be adapted primarily to binding other proteins. Instead, they likely modify microtubule dynamics directly.

The specificity of EB1 for the microtubule plus-end observed here in a minimal system indicates that EB1 binds preferentially there relative to the overall polymer lattice, due to either biochemical or structural differences at the microtubule tip. It remains an open question what exactly about the microtubule plus end EB1 recognizes. We and others (Zanic et al., 2009) proposed that EB1 might recognize the cap of GTP tubulin that exists at the microtubule plus end and canonically, is thought to prevent microtubules from depolymerizing.

We based this conclusion primarily on the fact that, when we polymerized microtubules in the presence of GMPCPP, a slowly-hydrolyzable GTP analogue, CLIP-170 was no longer localized to the plus end. Instead, we observed it bound nonspecifically to the entire microtubule. However, though our dwell time analysis was consistent with earlier data we took, and indicated that CLIP-170 was in complex with EB1, we did not image EB1 directly. Therefore, the non-selective binding of CLIP-170 to the microtubule lattice could simply represent CLIP-170 acting in its normal, non-discriminating manner in the absence of EB1 binding. This is likely the case, since in earlier experiments with GMPCPP microtubule seeds and GTP tubulin, we did not see preferential binding of fluorescent EB1 to the GMPCPP seed. Other groups did see preferential binding of EB1 to GMPCPP seeds (Zanic et al., 2009), but only when EB1 was His-tagged and only in the presence of low salt. In our hands and in others (Maurer et al., 2011; Zhu et al., 2009), we know that these factors individually, and especially in combination drastically reduce the specificity of EB1 for the growing microtubule plus end.

Therefore, we suspected that EB1 might not be recognizing GTP tubulin, and instead, that it might be more complicated, and potentially more interesting than this. In fact, spatially, the GTP cap is too small to fully account for the length of the EB1 comet; theoretical studies calculate that a GTP cap only a few layers thick is probably sufficient to prevent catastrophe, and estimations of large cap sizes put the upper limit at no more than 50 tubulin layers (Schek et al., 2007; Seetapun et al., 2012; VanBuren et al., 2002). At 8 nm per tubulin layer, this would not be large enough to account for an EB1 comet that is 2 microns long.

We considered that it might be that EB1 recognizes a large GTP tubulin cap, but after nucleotide hydrolysis, there is a slow unbinding of EB1 from the microtubule that gives the comet a more elongated appearance. However, our dwell-time analysis indicated EB1 binds and unbinds from the microtubule plus end rapidly, typically in less than a second. Others calculated that the residence time might be even less than that (Bieling et al., 2008). In vitro, the rate of microtubule polymerization is rarely higher than 0.1 μm/second, so this would not be enough to account for the difference in lengths between the GTP cap and the comet length.

Interestingly, Bieling et al. (2007) found that EB1 comet tails were longer at higher rates of microtubule polymerization. This is consistent with GTP-tubulin being the structural recognition unit for EB1; as tubulin subunits are added faster to the growing microtubule, GTP hydrolysis lags, and there are a greater number of tubulin layers that have not hydrolyzed GTP, and so the comet is larger. However, it is also consistent with

EB1 instead recognizing GDP-P_i-tubulin or a related hydrolysis intermediate. Though the matter is still controversial, recent evidence indicates that this may be true.

A new study (Maurer et al., 2012) reports that EB1 recognizes microtubules bound to the nucleotides GTPγS, or to GDP-BeF_3^- with 10-fold great specificity than GMPCPP. GTPγS and GDP-BeF_3^- represent a GDP-P_i transition state and are not GTP-tubulin analogs. This suggests to us one of two new possibilities: EB1 recognizes tubulin-GDP-P_i, and the extended comet corresponds to slow phosphate release from the microtubule; or EB1 recognizes a particular hydrolysis intermediate, and the extended comet might represent fast phosphate release with slower structural rearrangements at the microtubule tip structure, with subsequent EB1 unbinding.

This would have a rather surprising implication; EB1 might not be at the very end of the microtubule at all, because these tubulin subunits would have not yet hydrolyzed their GTP or relaxed to the recognized structural intermediate. A recent tubulin crystal structure informs on this possibility.

High-resolution crystal structures of tubulin are extraordinarily limited because of the tendency of tubulin to polymerize at the high concentrations required for protein crystallization (Ayaz et al., 2012). Therefore, models of GTP-bound tubulin have been derived from computational analysis of cryo-EM of microtubule structures. These structures have yielded the canonical view that GTP-tubulin is relatively straight in solution, and maintenance of this straight conformation upon polymerization is what allows the GTP cap to prevent microtubule catastrophe.

However, structures of GTP-tubulin crystallized in the presence of a binding protein have shown that, like the GDP-tubulin seen in electron micrographs of depolymerizing microtubules (Mandelkow et al., 1991), GTP-tubulin might also be curved (Gigant et al., 2005; Pecqueur et al., 2012). Therefore, GTP tubulin might not stabilize microtubules by straightening them at all; instead the straightness of the microtubule may instead be enforced on it by the requirements for lateral protofilament bonding (Pecqueur et al., 2012). The result from this would be that, at the very tip of the microtubule, perhaps no more than a few layers thick, tubulin is not straight, but instead still curved.

The implications of such a model for EB1 binding are rather unexpected. At the very tip of the microtubule, where GTP hydrolysis has yet to occur, and tubulin is curved, EB1 would not be expected to bind. Close to the tip, but not at the tip, where hydrolysis had occurred but P_i had not been released yet, EB1 would bind. Farther back, after phosphate release, or further tubulin structural rearrangement, EB1 would not bind. Experiments to test this would be challenging, but careful super-resolution microscopy using fluorescently labeled tubulin and EB1 might make it possible. This model would keep the very tip of the tubulin uncovered with EB1 or its myriad binders, so that the microtubule can interact with proteins at the cortex.

7.2 Dynein tethering

We have long known that a population of cytoplasmic dynein localizes to the cell cortex, and investigators have speculated that immobilized there, it could tether and stabilize growing microtubules. Particularly strong evidence came from studies done in yeast because in yeast, dynein does not act as a cargo transporter. Instead, it acts primarily to drag the spindle pole body into the mother-daughter bud neck by binding to and pulling growing cortical microtubules (Heil-Chapdelaine et al., 2000; Moore and Cooper, 2010).

A similar role has also been proposed for dynein in multicellular eukaryotes. In C. elegans, Drosophila, and in human cells, a pool of dynein at the cortex has been implicated in positioning the mitotic spindle (Gonczy et al., 1999; Samora et al.; Siller and Doe, 2009). We have also long been interested in an analogous mechanism in interphase cells. We previously proposed that dynein might capture and tethering microtubules, primarily at sites of cell-cell interaction such as adherens junctions and the immunological synapse (Combs et al., 2006; Ligon et al., 2001). There, we speculated that it could stabilize microtubules and allow a preferred route for delivery or recycling of components to a particular cortical micro-domain.

In vitro, we have now found that such proposals were correct; mammalian dynein can act as a tether for dynamic microtubules. Normally, when microtubules grow into a rigid barrier, they have a tendency to undergo catastrophe. This has been shown in vitro with microfabricated chambers (Janson et al., 2003), and in cells, it has been found that microtubules have a tendency to undergo catastrophe as they grow out and encounter the plasma membrane (Wadsworth, 1999; Waterman-Storer and Salmon, 1997).

Here, we showed that when dynein is present, catastrophe was delayed. Importantly, this stabilization was not due just to the ability of dynein to bind microtubules; in the absence of ATP, dynein binds microtubules very tightly, but they are not preferentially stabilized, indicating that active force generation was required. Modeling studies confirmed this result, and suggested that dynein accomplishes this by exerting tension and straightening individual microtubule protofilaments. This would counteract the initial deforming force on microtubules when they encounter an organelle or the plasma membrane. It might also inhibit bending of the lattice, and might even feed back directly to the nucleotide hydrolyzing properties of the tubulins in the GTP cap, or slow the rates of phosphate release, stabilizing the microtubule in that way.

We have speculated that mammalian dynein might be particularly well-suited for such a role for multiple reasons. Unlike yeast dynein, which has a high unitary stall force of around 6 pN and may be specialized for pulling microtubules and orienting the spindle, mammalian dynein stalls around 1 pN (Mallik et al., 2005; Schroeder et al., 2010; Soppina et al., 2009). This would allow dynein to straighten microtubule protofilaments, and hold the microtubule in place, without causing undue strain to the lattice. The flexibility of mammalian dynein – its tendency to step backward and even sideways along the microtubule (Ross et al., 2008; Ross et al., 2006) – may specifically allow an immobilized dynein to remain attached to a polymerizing microtubule.

A recent study on immobilized yeast dynein allows us to directly compare our results from mammalian dynein (Laan et al., 2012). While the differences are illuminating, the similarities are also satisfying. The authors also find that yeast cytoplasmic dynein, when immobilized at a barrier, is able to interact with dynamic microtubules, and with laser tweezers, they measure directly that dynein is able to exert force. However, the geometry of their system is fundamentally quite different than ours, and their dynein is stronger, so the force it exerts manifests differently.

We sought to reconstitute the interaction of a growing microtubule with the plasma membrane or a large organelle in the cytoplasm. In this situation, the microtubule will encounter the rigid membrane, but if it survives this initial encounter without undergoing catastrophe, it is free to continue to polymerize by either bending or flexing. In this way, microtubules that initially encounter our rigid dynein-coated beads are free to polymerize around the beads if they do not depolymerize.

The other group reconstituted their interaction with a rigid wall that also contained an overhang so that microtubules that grew into the wall were trapped and could not continue to polymerize. It traps the microtubule, so that it must stall, or catastrophe.

They find that in this situation, dynein actually serves to increase catastrophe. Here, when dynein is coupled to an inescapable barrier, it increases catastrophe because after counteracting the initial deforming force, it can continue to interact with the growing microtubule in an end-on manner and actually hold it perilously straight as it rams with maximal tension into the wall. We observed similar encounters in our bead experiments with dynein in the absence of nucleotide. When dynein bound rigidly to the growing microtubule, forcing it to grow square into the bead, catastrophe was very frequent.

As alluded to earlier, the experiments are also different because, fundamentally, we are examining different dyneins. One possibility is that the higher maximal force exerted by the yeast dynein not only stabilizes the lattice, but strains it. The yeast dynein that they used for their experiments was also not truly authentic yeast dynein. It was a truncated, GST-dimerized construct, that while processive, lacks the normal communication between the motor domains. This strategy allowed them to very stably immobilize the dynein at the barrier with a biotin-streptavidin linkage, but this only serves to exacerbate the inflexibility in this dynein and magnify the differences between it and our authentic, mammalian dynein.

However, what their experiments shows quite nicely, once again, is that microtubules that grow into a rigid barrier are prone to catastrophe (Dogterom and Yurke, 1997; Janson et al., 2003; Janson and Dogterom, 2004a, b; Kerssemakers et al., 2006; Laan et al., 2008; Laan et al., 2012). In cells, perhaps different dyneins, in different geometries, can either hasten or avert catastrophe.

7.3 Dynactin plus end regulation

Though our study shows that a non-motor MAP could not act by the same mechanism as cytoplasmic dynein in altering microtubule dynamics, they likely still have some role to play in microtubule tethering. Enrichment of +TIPs with cortical binding partners could help guide the growing microtubule into regions of high local dynein concentration. By acting through other mechanisms, +TIPs that inhibit microtubule catastrophe could act to ensure that polymerizing microtubules actually make it into these zones of high cortical dynein.

We have discovered that dynactin is one of those +TIPs. Here, we show that in vitro, the $p150^{Glued}$ subunit of dynactin increases the microtubule polymerization rate and inhibits catastrophe. We went on to dissect the molecular mechanism, and found that $p150^{Glued}$ dimerization is necessary, and that these activities are dependent on the ability of $p150^{Glued}$ to complex with tubulin through interactions with both the N-terminal CAP-Gly and basic domains. When we pursued these observations in cells, we observed that the $p150^{Glued}$ anti-catastrophe activity likely predominates in vivo. Finally, we discovered that a disease mutation in the $p150^{Glued}$ CAP-Gly causative for a fatal familial Parkinson syndrome leaves $p150^{Glued}$ unable to promote microtubule assembly either in vitro or in neurons.

We have long known that there was a pool of plus end-localized dynactin in the cell (Vaughan et al., 2002). Indeed, biochemical analyses and immunoelectron microscopy suggest that a large proportion of dynactin may in fact not be in complex with dynein (Gill et al., 1991; Habermann et al., 2001; Morgan et al., 2011). Localized to the microtubule plus end, dynactin could modify microtubule dynamics. We speculated here that because $p150^{Glued}$ can bind both to microtubules and to soluble tubulin, and because dimerization appears necessary for $p150^{Glued}$ to robustly modify dynamics, that $p150^{Glued}$ might be inhibiting catastrophe by decreasing the off-rate of tubulin at the end of the microtubule.

This mechanism is fundamentally different from the way that dynein inhibits catastrophe. It is fascinating that these two cooperating complexes would both act to prevent microtubule depolymerization, but in completely different ways. Areas of the distal neuron where both cytoplasmic dynein and dynactin are localized could be sites of particularly robust microtubule stabilization.

This microtubule stabilization could be particularly important in the setting of neurodegenerative disease. Tau, a MAP implicated in the development of both Alzheimer disease and Parkinson disease, normally exists in a highly soluble form that stabilizes microtubules in axons (Brunden et al., 2012). However, in the setting of disease, tau becomes hyperphosphorylated (Matsuo et al., 1994), which decreases its ability to bind and stabilize microtubules (Wagner et al., 1996). It also becomes sequestered in large aggregates, which further decreases its ability to stabilize microtubules (Hasegawa, 2006).

While data from our lab suggests that dynein is more resilient than kinesin to disruption by tau, tau patches still caused dynein to reverse directions nearly 50% of the time (Dixit et al., 2008b). Therefore, tau can clearly affect dynein-as-cargo-transporter. What effect does it have on dynein-as-tether? If it decreases its ability to tether and stabilize microtubules in the setting of disease, this would further exacerbate the microtubule defects seen in Alzheimer and Parkinson disease. We might expect that aggregated tau would also decrease the ability of dynactin to bind and stabilize growing microtubules plus ends, particularly if aggregated tau not only binds microtubules but also competes with dynactin for soluble tubulin. Future experiments to explore this possibility may be particularly illuminating.

8. Future directions

8.1 Dynein tethering

We have demonstrated that cytoplasmic dynein is a dynamic microtubule tether, and that this is dependent on the dynein ATPase. We have suggested that mammalian dynein, because of its mechanochemical properties, may be particularly well-suited for these activities.

There are numerous routes to extend this study. One of the most interesting and feasible would be to test if another minus end-directed motor, used in the place of dynein, can similarly tether microtubules. An attractive candidate is the Kinesin-14 motor, Ncd. Truncated, functional Ncd motors can be expressed and purified from bacteria. Additionally, mutations to alter the length of the Ncd lever arm, its mechanochemistry, and dimerization are well-characterized (Endres et al., 2006). Finally, recombinant purification would allow us to site-specifically attach biotin, which would aid considerably in attaching the motor to the beads, and the beads to the coverslip, which was a difficult obstacle in our original study. As another minus end-directed motor, Ncd might, like dynein, tether and stabilize microtubules. However, it is not a processive motor, and it is much smaller, and likely also stronger than dynein. While it may be able to dampen lateral microtubule fluctuations, it might not be nearly as well suited to preventing catastrophe.

In vivo, dynein binds to dynactin, and the p150^{Glued} subunit of dynactin contains an additional microtubule-binding site for the amalgamated motor complex (Waterman-Storer et al., 1995). Would dynein-dynactin tether microtubules more effectively than dynein alone? It might, by increasing the efficiency of dynein binding and tethering. Or, it might not, by introducing the more inelastic dynactin microtubule binding domain into the system. We could most simply address this question by repeating the procedure described in Chapter 2, but instead of adsorbing FPLC-purified dynein to the beads, adsorb sucrose gradient-isolated dynein and dynactin (Bingham et al., 1998). Because we have shown that dynactin influences microtubule dynamics in solution, we would need to ensure that the dynactin was stably bound to the beads. We could do this by subjecting the beads to variable amounts of washes, and then boiling off and assaying the retained dynactin. We could also carefully quantitate microtubule dynamics away from the beads in the presence or absence of dynactin.

Mutations to the tail domain of cytoplasmic dynein have been shown to cause neurodegeneration, and to alter its ability to transport vesicles (Hafezparast et al., 2003). Interestingly, these mutations seem to disrupt coordination between the two dynein subunits without altering its basic parameters; in the best characterized F580Y (Loa) mutation, average velocities and stall forces were unaltered, but processivity was greatly decreased (Ori-McKenney et al., 2010). Would dynein still be able to tether microtubules in the setting of normal force generation, but altered stepping? These experiments would probably be best performed in accompaniment to those described above, as dynein-dynactin is much easier to purify from the small amounts of tissue available from Loa homozygous mouse pups. The results could implicate new kinds of dynein defects in neurodegenerative disease.

8.2 Dynactin plus end regulation

We have shown that the p150^{Glued} subunit of dynactin modifies microtubule dynamics, acting predominantly to stabilize microtubules by inhibiting catastrophe.

We have shown that in vitro, the presence of the basic domain is necessary for p150^{Glued} to bind tubulin and promote microtubule formation. However, in neurons, we did not test whether an isoform completely lacking the basic domain would rescue microtubule defects in RNAi cells, though we would predict that it would not. Additionally, the basic domain consists of 3 separate exons, and alternative splicing generates the full diversity of possible spliceforms in non-neuronal tissues (Dixit et al., 2008a). Recombinant dimeric p150^{Glued} polypeptides lacking 1 or 2 of those exons in combination could be easily tested to see if they promote microtubule formation. This would allow us to more fully delineate the minimal requirement for stable tubulin binding by p150^{Glued}, and definitely test if microtubule regulation by dynactin is truly neuron-specific.

Similarly, p150^{Glued} is subject to phosphoregulation by mitotic kinases (Li et al., 2010; Rome et al., 2010). Does p150^{Glued} undergo differential splicing or phosphoregulation during neurodevelopment? If exons 5, 6, or 7, are phosphorylated, we might predict that p150^{Glued} would no longer be able to bind tubulin and promote microtubule formation. Perhaps the relative expression of p150^{Glued} isoforms differ during development, or even in different brain regions or neuron subtypes. This would have the effect of moderating or magnifying the strong inhibition of p150^{Glued} on microtubule catastrophe.

Finally, though we have shown that p150^{Glued} modifies microtubule dynamics independently of EB1, a more thorough investigation of their interplay would be informative. There is conflicting evidence whether EB1 might be sufficient to bring p150^{Glued} to the microtubule plus end. By analogy to the CAP-Gly-containing CLIP-170, EB1 may be sufficient to localize p150^{Glued} to the microtubule plus end (Bieling et al., 2008; Bieling et al., 2007; Dixit et al., 2009), though reports from cells suggest that the interaction between p150^{Glued} and CLIP-170 might also assist (Ligon et al., 2006; Watson and Stephens, 2006). Using fluorescent constructs similar to those used for Chapter 5, we are currently conducting experiments to test these possibilities. Preliminary data suggest EB1 may not be sufficient to localize p150^{Glued} to the microtubule plus end.

8.3 Dynein activation by dynactin

How does dynein activate dynein? In Chapter 6, we described the mapping of the minimal binding determinants of dynein for dynactin and vice versa, and the initial characterization of a recombinant p150^{Glued} polypeptide and a knockin mouse that will allow us to investigate this fundamental question.

This project can be divided into 4 major sections. The first examines the hypothesis that dynactin helps dynein load onto the microtubule i.e. with its initial attachment. The simplest way to test this hypothesis would be to examine the landing rates for the GFP-dynein on Taxol-stabilized microtubules. At a fixed dynein concentration and microtubule density, this could be defined simply as the number of fluorescent spots observed per microtubule length per unit time. We could then test how dynactin alters this by pre-incubating the dynein with recombinant p150^{Glued}. As a non-microtubule-binding control, a recombinant p135 construct, or just the CC1 region of p150^{Glued} could also be pre-incubated with dynein before assaying landing rates. A more elaborate system would make use of fluorescent p150^{Glued}, so that dynein landing events that co-occur with fluorescent p150^{Glued} could be scored differently than dynein landing events alone. The construct we expressed and purified has a C-terminal AviTag which allows site-specific biotinylation, after which we could bind it to fluorescent Neutravidin. We are testing the feasibility of that strategy currently. As an alternative, we could express a p150^{Glued} construct with a HaloTag, which would allow direct fluorescent labeling, but this would have the disadvantage of requiring translation of a larger p150 construct, which have a tendency to be improperly folded and insoluble.

The second major section of the project investigates the hypothesis that dynactin facilitates the plus end-localization of dynein. The simplest way to accomplish this experiment would be to first determine what factors are necessary to localize p150^{Glued} to the plus end of dynamic microtubules. As we discussed above, EB1 may be sufficient, or it may require assistance from the CLIP-170 C-terminus. If this is the case, recombinant expression and purification of full length CLIP-170 would be required from Sf9 cells (Telley et al., 2011), as bacteria are incapable of producing CLIP-170 constructs that encompass both the N- and C-terminus (Scheel et al., 1999). With plus end-tracking of p150^{Glued} reconstituted, we could then ask, does it localize dynein to the microtubule plus end?

The third major section of the project investigates the stepping behavior of dynein in the presence of dynactin. Dynactin binds to DIC, which associates with the tail domain of the dynein heavy chain. Mutations to the dynein heavy chain alter the processivity of dynein (Ori-McKenney et al., 2010). In yeast, there was a recent report that dynactin increases the processivity of dynein, but the microtubule-binding N-terminus of $p150^{Glued}$ was not required for this (Kardon et al., 2009). Perhaps dynactin increases the processivity of dynein directly via structural rearrangements to the dynein tail. By pre-incubating dynein with dynactin, and then performing high-resolution tracking of GFP-dynein that is, or is not co-occuring with fluorescent $p150^{Glued}$, we could test that hypothesis. If the GFP on DIC is insufficiently bright to allow high-resolution tracking of dynein, we could bind a quantum dot to the GFP or to the DIC C-terminal FLAG tag.

The final major section of the project tests the hypothesis that the N-terminus of $p150^{Glued}$ alters the force-generating properties of dynein. A previous report from yeast showed that removing the N-terminus of $p150^{Glued}$ caused defects in high load dynein-dependent transport such as nuclear migration and spindle positioning (Moore et al., 2009). We also know that, while the maximum stall force of mutant dynein is not affected (Ori-McKenney et al., 2010), there are nevertheless neuronal migration defects in these mice (Ori-McKenney and Vallee, 2011). These might arise from defects in nuclear migration, or in spindle position defects, which we know dynein also is important for in eukaryotes (Kiyomitsu and Cheeseman, 2012). We can test the hypothesis that the N-terminus of $p150^{Glued}$ alters the force generating properties of dynein by specifically binding biotinylated $p150^{Glued}$ to streptavidin-coated beads, then assaying the force-generating properties of dynein using laser tweezers. The presence of dynactin may allow dynein to generate higher stall forces, or to sustain them for longer periods before detaching.

Every organism with cytoplasmic dynein has a dynactin complex (Hammesfahr and Kollmar, 2012). These proposed studies, should finally allow us to clarify why this complex has persisted over hundreds of millions of years, and how it activates dynein.

Bibliography

Ahmed, S., Sun, S., Siglin, A.E., Polenova, T., and Williams, J.C. (2010). Disease-associated mutations in the p150(Glued) subunit destabilize the CAP-gly domain. Biochemistry *49*, 5083-5085.

Akhmanova, A., and Hoogenraad, C.C. (2005). Microtubule plus-end-tracking proteins: mechanisms and functions. Curr. Opin. Cell Biol. *17*, 47-54.

Akhmanova, A., and Steinmetz, M.O. (2008). Tracking the ends: a dynamic protein network controls the fate of microtubule tips. Nat. Rev. Mol. Cell Biol. *9*, 309-322.

Al-Bassam, J., Kim, H., Brouhard, G., van Oijen, A., Harrison, S.C., and Chang, F. (2010). CLASP promotes microtubule rescue by recruiting tubulin dimers to the microtubule. Dev. Cell *19*, 245-258.

Altschul, S.F., Madden, T.L., Schaffer, A.A., Zhang, J., Zhang, Z., Miller, W., and Lipman, D.J. (1997). Gapped BLAST and PSI-BLAST: a new generation of protein database search programs. Nucleic Acids Res. *25*, 3389-3402.

Applegate, K.T., Besson, S., Matov, A., Bagonis, M.H., Jaqaman, K., and Danuser, G. (2011). plusTipTracker: Quantitative image analysis software for the measurement of microtubule dynamics. J. Struct. Biol. *176*, 168-184.

Arnal, I., Heichette, C., Diamantopoulos, G.S., and Chretien, D. (2004). CLIP-170/tubulin-curved oligomers coassemble at microtubule ends and promote rescues. Curr. Biol. *14*, 2086-2095.

Ayaz, P., Ye, X., Huddleston, P., Brautigam, C.A., and Rice, L.M. (2012). A TOG:alphabeta-tubulin Complex Structure Reveals Conformation-Based Mechanisms for a Microtubule Polymerase. Science *337*, 857-860.

Barten, D.M., Fanara, P., Andorfer, C., Hoque, N., Wong, P.Y., Husted, K.H., Cadelina, G.W., Decarr, L.B., Yang, L., Liu, V., *et al.* (2012). Hyperdynamic microtubules, cognitive deficits, and pathology are improved in tau transgenic mice with low doses of the microtubule-stabilizing agent BMS-241027. J. Neurosci. *32*, 7137-7145.

Bechstedt, S., and Brouhard, G.J. (2012). Doublecortin recognizes the 13-protofilament microtubule cooperatively and tracks microtubule ends. Dev. Cell *23*, 181-192.

Berrueta, L., Tirnauer, J.S., Schuyler, S.C., Pellman, D., and Bierer, B.E. (1999). The APC-associated protein EB1 associates with components of the dynactin complex and cytoplasmic dynein intermediate chain. Curr. Biol. *9*, 425-428.

Bibring, T., and Baxandall, J. (1971). Selective extraction of isolated mitotic apparatus. Evidence that typical microtubule protein is extracted by organic mercurial. J. Cell Biol. *48*, 324-339.

Bieling, P., Kandels-Lewis, S., Telley, I.A., van Dijk, J., Janke, C., and Surrey, T. (2008). CLIP-170 tracks growing microtubule ends by dynamically recognizing composite EB1/tubulin-binding sites. J. Cell Biol. *183*, 1223-1233.

Bieling, P., Laan, L., Schek, H., Munteanu, E.L., Sandblad, L., Dogterom, M., Brunner, D., and Surrey, T. (2007). Reconstitution of a microtubule plus-end tracking system in vitro. Nature *450*, 1100-1105.

Bingham, J.B., King, S.J., and Schroer, T.A. (1998). Purification of dynactin and dynein from brain tissue. Methods Enzymol. *298*, 171-184.

Bingham, J.B., and Schroer, T.A. (1999). Self-regulated polymerization of the actin-related protein Arp1. Curr. Biol. *9*, 223-226.

Borisy, G.G., and Taylor, E.W. (1967a). The mechanism of action of colchicine. Binding of colchincine-3H to cellular protein. J. Cell Biol. *34*, 525-533.

Borisy, G.G., and Taylor, E.W. (1967b). The mechanism of action of colchicine. Colchicine binding to sea urchin eggs and the mitotic apparatus. J. Cell Biol. *34*, 535-548.

Brouhard, G.J., Stear, J.H., Noetzel, T.L., Al-Bassam, J., Kinoshita, K., Harrison, S.C., Howard, J., and Hyman, A.A. (2008). XMAP215 is a processive microtubule polymerase. Cell *132*, 79-88.

Browning, H., Hackney, D.D., and Nurse, P. (2003). Targeted movement of cell end factors in fission yeast. Nat. Cell Biol. *5*, 812-818.

Browning, H., Hayles, J., Mata, J., Aveline, L., Nurse, P., and McIntosh, J.R. (2000). Tea2p is a kinesin-like protein required to generate polarized growth in fission yeast. J. Cell Biol. *151*, 15-28.

Brunden, K.R., Ballatore, C., Lee, V.M., Smith, A.B., and Trojanowski, J.Q. (2012). Brain-penetrant microtubule-stabilizing compounds as potential therapeutic agents for tauopathies. Biochem. Soc. Trans. *40*, 661-666.

Brunner, D., and Nurse, P. (2000). CLIP170-like tip1p spatially organizes microtubular dynamics in fission yeast. Cell *102*, 695-704.

Bryan, J., and Wilson, L. (1971). Are cytoplasmic microtubules heteropolymers? Proc. Natl. Acad. Sci. U. S. A. *68*, 1762-1766.

Burge, C., and Karlin, S. (1997). Prediction of complete gene structures in human genomic DNA. J. Mol. Biol. *268*, 78-94.

Burkhardt, J.K., Echeverri, C.J., Nilsson, T., and Vallee, R.B. (1997). Overexpression of the dynamitin (p50) subunit of the dynactin complex disrupts dynein-dependent maintenance of membrane organelle distribution. J. Cell Biol. *139*, 469-484.

Busch, K.E., and Brunner, D. (2004). The microtubule plus end-tracking proteins mal3p and tip1p cooperate for cell-end targeting of interphase microtubules. Curr. Biol. *14*, 548-559.

Caplow, M., Ruhlen, R.L., and Shanks, J. (1994). The free energy for hydrolysis of a microtubule-bound nucleotide triphosphate is near zero: all of the free energy for hydrolysis is stored in the microtubule lattice. J. Cell Biol. *127*, 779-788.

Carlier, M.F., Hill, T.L., and Chen, Y. (1984). Interference of GTP hydrolysis in the mechanism of microtubule assembly: an experimental study. Proc. Natl. Acad. Sci. U. S. A. *81*, 771-775.

Cartelli, D., Ronchi, C., Maggioni, M.G., Rodighiero, S., Giavini, E., and Cappelletti, G. (2010). Microtubule dysfunction precedes transport impairment and mitochondria damage in MPP+ -induced neurodegeneration. J. Neurochem. *115*, 247-258.

Carter, A.P., Garbarino, J.E., Wilson-Kubalek, E.M., Shipley, W.E., Cho, C., Milligan, R.A., Vale, R.D., and Gibbons, I.R. (2008). Structure and functional role of dynein's microtubule-binding domain. Science *322*, 1691-1695.

Castoldi, M., and Popov, A.V. (2003). Purification of brain tubulin through two cycles of polymerization-depolymerization in a high-molarity buffer. Protein Expr. Purif. *32*, 83-88.

Clark, S.W., and Meyer, D.I. (1992). Centractin is an actin homologue associated with the centrosome. Nature *359*, 246-250.

Cleveland, D.W., Kirschner, M.W., and Cowan, N.J. (1978). Isolation of separate mRNAs for alpha- and beta-tubulin and characterization of the corresponding in vitro translation products. Cell *15*, 1021-1031.

Cleveland, D.W., Lopata, M.A., MacDonald, R.J., Cowan, N.J., Rutter, W.J., and Kirschner, M.W. (1980). Number and evolutionary conservation of alpha- and beta-tubulin and cytoplasmic beta- and gamma-actin genes using specific cloned cDNA probes. Cell *20*, 95-105.

Combs, J., Kim, S.J., Tan, S., Ligon, L.A., Holzbaur, E.L., Kuhn, J., and Poenie, M. (2006). Recruitment of dynein to the Jurkat immunological synapse. Proc. Natl. Acad. Sci. U. S. A. *103*, 14883-14888.

Culver-Hanlon, T.L., Lex, S.A., Stephens, A.D., Quintyne, N.J., and King, S.J. (2006). A microtubule-binding domain in dynactin increases dynein processivity by skating along microtubules. Nat. Cell Biol. *8*, 264-270.

Dammermann, A., Desai, A., and Oegema, K. (2003). The minus end in sight. Curr. Biol. *13*, R614-624.

DeWitt, M.A., Chang, A.Y., Combs, P.A., and Yildiz, A. (2012). Cytoplasmic dynein moves through uncoordinated stepping of the AAA+ ring domains. Science *335*, 221-225.

Diamantopoulos, G.S., Perez, F., Goodson, H.V., Batelier, G., Melki, R., Kreis, T.E., and Rickard, J.E. (1999). Dynamic localization of CLIP-170 to microtubule plus ends is coupled to microtubule assembly. J. Cell Biol. *144*, 99-112.

Dixit, R., Barnett, B., Lazarus, J.E., Tokito, M., Goldman, Y.E., and Holzbaur, E.L. (2009). Microtubule plus-end tracking by CLIP-170 requires EB1. Proc. Natl. Acad. Sci. U. S. A. *106*, 492-497.

Dixit, R., Levy, J.R., Tokito, M., Ligon, L.A., and Holzbaur, E.L. (2008a). Regulation of dynactin through the differential expression of p150Glued isoforms. J. Biol. Chem. *283*, 33611-33619.

Dixit, R., Ross, J.L., Goldman, Y.E., and Holzbaur, E.L. (2008b). Differential regulation of dynein and kinesin motor proteins by tau. Science *319*, 1086-1089.

Dogterom, M., and Yurke, B. (1997). Measurement of the force-velocity relation for growing microtubules. Science *278*, 856-860.

Dragestein, K.A., van Cappellen, W.A., van Haren, J., Tsibidis, G.D., Akhmanova, A., Knoch, T.A., Grosveld, F., and Galjart, N. (2008). Dynamic behavior of GFP-CLIP-170 reveals fast protein turnover on microtubule plus ends. J. Cell Biol. *180*, 729-737.

Echeverri, C.J., Paschal, B.M., Vaughan, K.T., and Vallee, R.B. (1996). Molecular characterization of the 50-kD subunit of dynactin reveals function for the complex in chromosome alignment and spindle organization during mitosis. J. Cell Biol. *132*, 617-633.

Endres, N.F., Yoshioka, C., Milligan, R.A., and Vale, R.D. (2006). A lever-arm rotation drives motility of the minus-end-directed kinesin Ncd. Nature *439*, 875-878.

Erickson, H.P. (2009). Size and shape of protein molecules at the nanometer level determined by sedimentation, gel filtration, and electron microscopy. Biol. Proced. Online *11*, 32-51.

Euteneuer, U., Koonce, M.P., Pfister, K.K., and Schliwa, M. (1988). An ATPase with properties expected for the organelle motor of the giant amoeba, Reticulomyxa. Nature *332*, 176-178.

Evans, L., Mitchison, T., and Kirschner, M. (1985). Influence of the centrosome on the structure of nucleated microtubules. J. Cell Biol. *100*, 1185-1191.

Farrer, M.J., Hulihan, M.M., Kachergus, J.M., Dachsel, J.C., Stoessl, A.J., Grantier, L.L., Calne, S., Calne, D.B., Lechevalier, B., Chapon, F., *et al.* (2009). DCTN1 mutations in Perry syndrome. Nat. Genet. *41*, 163-165.

Feit, H., Slusarek, L., and Shelanski, M.L. (1971). Heterogeneity of tubulin subunits. Proc. Natl. Acad. Sci. U. S. A. *68*, 2028-2031.

Folker, E.S., Baker, B.M., and Goodson, H.V. (2005). Interactions between CLIP-170, tubulin, and microtubules: implications for the mechanism of Clip-170 plus-end tracking behavior. Mol. Biol. Cell *16*, 5373-5384.

Fourniol, F.J., Sindelar, C.V., Amigues, B., Clare, D.K., Thomas, G., Perderiset, M., Francis, F., Houdusse, A., and Moores, C.A. (2010). Template-free 13-protofilament microtubule-MAP assembly visualized at 8 A resolution. J. Cell Biol. *191*, 463-470.

Gao, Y., Vainberg, I.E., Chow, R.L., and Cowan, N.J. (1993). Two cofactors and cytoplasmic chaperonin are required for the folding of alpha- and beta-tubulin. Mol. Cell. Biol. *13*, 2478-2485.

Gardner, M.K., Charlebois, B.D., Janosi, I.M., Howard, J., Hunt, A.J., and Odde, D.J. (2011a). Rapid microtubule self-assembly kinetics. Cell *146*, 582-592.

Gardner, M.K., Pearson, C.G., Sprague, B.L., Zarzar, T.R., Bloom, K., Salmon, E.D., and Odde, D.J. (2005). Tension-dependent regulation of microtubule dynamics at kinetochores can explain metaphase congression in yeast. Mol Biol Cell *16*, 3764-3775.

Gardner, M.K., Zanic, M., Gell, C., Bormuth, V., and Howard, J. (2011b). Depolymerizing kinesins Kip3 and MCAK shape cellular microtubule architecture by differential control of catastrophe. Cell *147*, 1092-1103.

Gasteiger, E., Hoogland, C., Gattiker, A., Duvaud, S., Wilkins, M.R., Appel, R.D., and Bairoch, A. (2005). Protein Identification and Analysis Tools on the ExPASy Server. In The Proteomics Protocols Handbook, W. JM, ed. (Humana Press), pp. 571-607.

Gee, M.A., Heuser, J.E., and Vallee, R.B. (1997). An extended microtubule-binding structure within the dynein motor domain. Nature *390*, 636-639.

Gell, C., Bormuth, V., Brouhard, G.J., Cohen, D.N., Diez, S., Friel, C.T., Helenius, J., Nitzsche, B., Petzold, H., Ribbe, J., *et al.* (2010). Microtubule dynamics reconstituted in vitro and imaged by single-molecule fluorescence microscopy. Methods Cell Biol. *95*, 221-245.

Gennerich, A., Carter, A.P., Reck-Peterson, S.L., and Vale, R.D. (2007). Force-induced bidirectional stepping of cytoplasmic dynein. Cell *131*, 952-965.

Gennerich, A., and Vale, R.D. (2009). Walking the walk: how kinesin and dynein coordinate their steps. Curr. Opin. Cell Biol. *21*, 59-67.

Gibbons, I.R. (1963). Studies on the Protein Components of Cilia from Tetrahymena Pyriformis. Proc. Natl. Acad. Sci. U. S. A. *50*, 1002-1010.

Gigant, B., Wang, C., Ravelli, R.B., Roussi, F., Steinmetz, M.O., Curmi, P.A., Sobel, A., and Knossow, M. (2005). Structural basis for the regulation of tubulin by vinblastine. Nature *435*, 519-522.

Gill, S.R., Cleveland, D.W., and Schroer, T.A. (1994). Characterization of DLC-A and DLC-B, two families of cytoplasmic dynein light chain subunits. Mol. Biol. Cell *5*, 645-654.

Gill, S.R., Schroer, T.A., Szilak, I., Steuer, E.R., Sheetz, M.P., and Cleveland, D.W. (1991). Dynactin, a conserved, ubiquitously expressed component of an activator of vesicle motility mediated by cytoplasmic dynein. J. Cell Biol. *115*, 1639-1650.

Gonczy, P., Pichler, S., Kirkham, M., and Hyman, A.A. (1999). Cytoplasmic dynein is required for distinct aspects of MTOC positioning, including centrosome separation, in the one cell stage Caenorhabditis elegans embryo. J Cell Biol *147*, 135-150.

Goodson, H.V., Skube, S.B., Stalder, R., Valetti, C., Kreis, T.E., Morrison, E.E., and Schroer, T.A. (2003). CLIP-170 interacts with dynactin complex and the APC-binding protein EB1 by different mechanisms. Cell Motil Cytoskeleton *55*, 156-173.

Grimstone, A.V., and Klug, A. (1966). Observations on the substructure of flagellar fibres. J. Cell Sci. *1*, 351-362.

Grishchuk, E.L., Efremov, A.K., Volkov, V.A., Spiridonov, I.S., Gudimchuk, N., Westermann, S., Drubin, D., Barnes, G., McIntosh, J.R., and Ataullakhanov, F.I. (2008).

The Dam1 ring binds microtubules strongly enough to be a processive as well as energy-efficient coupler for chromosome motion. Proc Natl Acad Sci U S A *105*, 15423-15428.

Grishchuk, E.L., Molodtsov, M.I., Ataullakhanov, F.I., and McIntosh, J.R. (2005). Force production by disassembling microtubules. Nature *438,* 384-388.

Gupta, K.K., Joyce, M.V., Slabbekoorn, A.R., Zhu, Z.C., Paulson, B.A., Boggess, B., and Goodson, H.V. (2010). Probing interactions between CLIP-170, EB1, and microtubules. J. Mol. Biol. *395*, 1049-1062.

Gupta, K.K., Paulson, B.A., Folker, E.S., Charlebois, B., Hunt, A.J., and Goodson, H.V. (2009). Minimal plus-end tracking unit of the cytoplasmic linker protein CLIP-170. J. Biol. Chem. *284*, 6735-6742.

Habermann, A., Schroer, T.A., Griffiths, G., and Burkhardt, J.K. (2001). Immunolocalization of cytoplasmic dynein and dynactin subunits in cultured macrophages: enrichment on early endocytic organelles. J. Cell Sci. *114,* 229-240.

Hafezparast, M., Klocke, R., Ruhrberg, C., Marquardt, A., Ahmad-Annuar, A., Bowen, S., Lalli, G., Witherden, A.S., Hummerich, H., Nicholson, S., *et al.* (2003). Mutations in dynein link motor neuron degeneration to defects in retrograde transport. Science *300*, 808-812.

Hammesfahr, B., and Kollmar, M. (2012). Evolution of the eukaryotic dynactin complex, the activator of cytoplasmic dynein. BMC Evol. Biol. *12*, 95.

Hasegawa, M. (2006). Biochemistry and molecular biology of tauopathies. Neuropathology *26*, 484-490.

Hayashi, I., Wilde, A., Mal, T.K., and Ikura, M. (2005). Structural basis for the activation of microtubule assembly by the EB1 and p150Glued complex. Mol. Cell *19*, 449-460.

Heil-Chapdelaine, R.A., Oberle, J.R., and Cooper, J.A. (2000). The cortical protein Num1p is essential for dynein-dependent interactions of microtubules with the cortex. J Cell Biol *151*, 1337-1344.

Helenius, J., Brouhard, G., Kalaidzidis, Y., Diez, S., and Howard, J. (2006). The depolymerizing kinesin MCAK uses lattice diffusion to rapidly target microtubule ends. Nature *441*, 115-119.

Hendricks, A.G., Lazarus, J.E., Perlson, E., Gardner, M.K., Odde, D.J., Goldman, Y.E., and Holzbaur, E.L. (2012). Dynein tethers and stabilizes dynamic microtubule plus ends. Curr. Biol. *22*, 632-637.

Hodgkinson, J.L., Peters, C., Kuznetsov, S.A., and Steffen, W. (2005). Three-dimensional reconstruction of the dynactin complex by single-particle image analysis. Proc. Natl. Acad. Sci. U. S. A. *102,* 3667-3672.

Holleran, E.A., Ligon, L.A., Tokito, M., Stankewich, M.C., Morrow, J.S., and Holzbaur, E.L. (2001). beta III spectrin binds to the Arp1 subunit of dynactin. J. Biol. Chem. *276,* 36598-36605.

Holleran, E.A., Tokito, M.K., Karki, S., and Holzbaur, E.L. (1996). Centractin (ARP1) associates with spectrin revealing a potential mechanism to link dynactin to intracellular organelles. J. Cell Biol. *135*, 1815-1829.

Holy, T.E., and Leibler, S. (1994). Dynamic instability of microtubules as an efficient way to search in space. Proc. Natl. Acad. Sci. U. S. A. *91*, 5682-5685.

Holzbaur, E.L., Hammarback, J.A., Paschal, B.M., Kravit, N.G., Pfister, K.K., and Vallee, R.B. (1991). Homology of a 150K cytoplasmic dynein-associated polypeptide with the Drosophila gene Glued. Nature *351*, 579-583.

Holzbaur, E.L., Hammarback, J.A., Paschal, B.M., Kravit, N.G., Pfister, K.K., and Vallee, R.B. (1992). Homology of a 150K cytoplasmic dynein-associated polypeptide with the Drosophila gene Glued. Nature *360*, 695.

Honnappa, S., Okhrimenko, O., Jaussi, R., Jawhari, H., Jelesarov, I., Winkler, F.K., and Steinmetz, M.O. (2006). Key interaction modes of dynamic +TIP networks. Mol. Cell *23*, 663-671.

Horio, T., and Hotani, H. (1986). Visualization of the dynamic instability of individual microtubules by dark-field microscopy. Nature *321*, 605-607.

Howard, J., and Hyman, A.A. (2003). Dynamics and mechanics of the microtubule plus end. Nature *422*, 753-758.

Hughes, S.M., Vaughan, K.T., Herskovits, J.S., and Vallee, R.B. (1995). Molecular analysis of a cytoplasmic dynein light intermediate chain reveals homology to a family of ATPases. J. Cell Sci. *108 (Pt 1)*, 17-24.

Hyman, A.A., Salser, S., Drechsel, D.N., Unwin, N., and Mitchison, T.J. (1992). Role of GTP hydrolysis in microtubule dynamics: information from a slowly hydrolyzable analogue, GMPCPP. Mol. Biol. Cell *3*, 1155-1167.

Imai, H., Narita, A., Schroer, T.A., and Maeda, Y. (2006). Two-dimensional averaged images of the dynactin complex revealed by single particle analysis. J. Mol. Biol. *359*, 833-839.

Janson, M.E., de Dood, M.E., and Dogterom, M. (2003). Dynamic instability of microtubules is regulated by force. J. Cell Biol. *161*, 1029-1034.

Janson, M.E., and Dogterom, M. (2004a). A bending mode analysis for growing microtubules: evidence for a velocity-dependent rigidity. Biophys. J. *87*, 2723-2736.

Janson, M.E., and Dogterom, M. (2004b). Scaling of microtubule force-velocity curves obtained at different tubulin concentrations. Phys Rev Lett *92*, 248101.

Jaworski, J., Hoogenraad, C.C., and Akhmanova, A. (2008). Microtubule plus-end tracking proteins in differentiated mammalian cells. Int. J. Biochem. Cell Biol. *40*, 619-637.

Kardon, J.R., Reck-Peterson, S.L., and Vale, R.D. (2009). Regulation of the processivity and intracellular localization of Saccharomyces cerevisiae dynein by dynactin. Proc. Natl. Acad. Sci. U. S. A. *106*, 5669-5674.

Kardon, J.R., and Vale, R.D. (2009). Regulators of the cytoplasmic dynein motor. Nat. Rev. Mol. Cell Biol. *10*, 854-865.

Karki, S., and Holzbaur, E.L. (1995). Affinity chromatography demonstrates a direct binding between cytoplasmic dynein and the dynactin complex. J. Biol. Chem. *270*, 28806-28811.

Karki, S., LaMonte, B., and Holzbaur, E.L. (1998). Characterization of the p22 subunit of dynactin reveals the localization of cytoplasmic dynein and dynactin to the midbody of dividing cells. J. Cell Biol. *142*, 1023-1034.

Kerssemakers, J.W., Munteanu, E.L., Laan, L., Noetzel, T.L., Janson, M.E., and Dogterom, M. (2006). Assembly dynamics of microtubules at molecular resolution. Nature *442*, 709-712.

Kim, H., Ling, S.C., Rogers, G.C., Kural, C., Selvin, P.R., Rogers, S.L., and Gelfand, V.I. (2007). Microtubule binding by dynactin is required for microtubule organization but not cargo transport. J. Cell Biol. *176*, 641-651.

King, S.J., Brown, C.L., Maier, K.C., Quintyne, N.J., and Schroer, T.A. (2003). Analysis of the dynein-dynactin interaction in vitro and in vivo. Mol. Biol. Cell *14*, 5089-5097.

King, S.J., and Schroer, T.A. (2000). Dynactin increases the processivity of the cytoplasmic dynein motor. Nat. Cell Biol. *2*, 20-24.

Kirschner, M., and Mitchison, T. (1986). Beyond self-assembly: from microtubules to morphogenesis. Cell *45*, 329-342.

Kiyomitsu, T., and Cheeseman, I.M. (2012). Chromosome- and spindle-pole-derived signals generate an intrinsic code for spindle position and orientation. Nat. Cell Biol. *14*, 311-317.

Knipling, L., Hwang, J., and Wolff, J. (1999). Preparation and properties of pure tubulin S. Cell Motil Cytoskeleton *43*, 63-71.

Kobayashi, T., Shiroguchi, K., Edamatsu, M., and Toyoshima, Y.Y. (2006). Microtubule-binding properties of dynactin p150 expedient for dynein motility. Biochem. Biophys. Res. Commun. *340*, 23-28.

Kollman, J.M., Merdes, A., Mourey, L., and Agard, D.A. (2011). Microtubule nucleation by gamma-tubulin complexes. Nat. Rev. Mol. Cell Biol. *12*, 709-721.

Komarova, Y., Lansbergen, G., Galjart, N., Grosveld, F., Borisy, G.G., and Akhmanova, A. (2005). EB1 and EB3 control CLIP dissociation from the ends of growing microtubules. Mol. Biol. Cell *16*, 5334-5345.

Komarova, Y.A., Akhmanova, A.S., Kojima, S., Galjart, N., and Borisy, G.G. (2002). Cytoplasmic linker proteins promote microtubule rescue in vivo. J. Cell Biol. *159*, 589-599.

Koshland, D.E., Mitchison, T.J., and Kirschner, M.W. (1988). Polewards chromosome movement driven by microtubule depolymerization in vitro. Nature *331*, 499-504.

Kull, F.J., Sablin, E.P., Lau, R., Fletterick, R.J., and Vale, R.D. (1996). Crystal structure of the kinesin motor domain reveals a structural similarity to myosin. Nature *380*, 550-555.

Kumar, S., and Hedges, S.B. (2011). TimeTree2: species divergence times on the iPhone. Bioinformatics *27*, 2023-2024.

Kuta, A., Deng, W., Morsi El-Kadi, A., Banks, G.T., Hafezparast, M., Pfister, K.K., and Fisher, E.M. (2010). Mouse cytoplasmic dynein intermediate chains: identification of new isoforms, alternative splicing and tissue distribution of transcripts. PLoS One *5*, e11682.

Laan, L., Husson, J., Munteanu, E.L., Kerssemakers, J.W., and Dogterom, M. (2008). Force-generation and dynamic instability of microtubule bundles. Proc. Natl. Acad. Sci. U. S. A. *105*, 8920-8925.

Laan, L., Pavin, N., Husson, J., Romet-Lemonne, G., van Duijn, M., Lopez, M.P., Vale, R.D., Julicher, F., Reck-Peterson, S.L., and Dogterom, M. (2012). Cortical dynein controls microtubule dynamics to generate pulling forces that position microtubule asters. Cell *148*, 502-514.

Lansbergen, G., and Akhmanova, A. (2006). Microtubule plus end: a hub of cellular activities. Traffic *7*, 499-507.

Lansbergen, G., Komarova, Y., Modesti, M., Wyman, C., Hoogenraad, C.C., Goodson, H.V., Lemaitre, R.P., Drechsel, D.N., van Munster, E., Gadella, T.W., Jr., *et al.* (2004). Conformational changes in CLIP-170 regulate its binding to microtubules and dynactin localization. J. Cell Biol. *166*, 1003-1014.

Lee, J.C., and Timasheff, S.N. (1977). In vitro reconstitution of calf brain microtubules: effects of solution variables. Biochemistry *16*, 1754-1764.

Lees-Miller, J.P., Helfman, D.M., and Schroer, T.A. (1992). A vertebrate actin-related protein is a component of a multisubunit complex involved in microtubule-based vesicle motility. Nature *359*, 244-246.

Levy, J.R., and Holzbaur, E.L. (2007). Special delivery: dynamic targeting via cortical capture of microtubules. Dev. Cell *12*, 320-322.

Lewis, J.H., Greenberg, M.J., Laakso, J.M., Shuman, H., and Ostap, E.M. (2012). Calcium regulation of myosin-I tension sensing. Biophys. J. *102*, 2799-2807.

Li, H., Liu, X.S., Yang, X., Song, B., Wang, Y., and Liu, X. (2010). Polo-like kinase 1 phosphorylation of p150Glued facilitates nuclear envelope breakdown during prophase. Proc. Natl. Acad. Sci. U. S. A. *107*, 14633-14638.

Ligon, L.A., Karki, S., Tokito, M., and Holzbaur, E.L. (2001). Dynein binds to beta-catenin and may tether microtubules at adherens junctions. Nat. Cell Biol. *3*, 913-917.

Ligon, L.A., Shelly, S.S., Tokito, M., and Holzbaur, E.L. (2003). The microtubule plus-end proteins EB1 and dynactin have differential effects on microtubule polymerization. Mol. Biol. Cell *14*, 1405-1417.

Ligon, L.A., Shelly, S.S., Tokito, M.K., and Holzbaur, E.L. (2006). Microtubule binding proteins CLIP-170, EB1, and p150Glued form distinct plus-end complexes. FEBS Lett. *580*, 1327-1332.

Lloyd, T.E., Machamer, J., O'Hara, K., Kim, J.H., Collins, S.E., Wong, M.Y., Sahin, B., Imlach, W., Yang, Y., Levitan, E.S., *et al.* (2012). The p150(Glued) CAP-Gly domain regulates initiation of retrograde transport at synaptic termini. Neuron *74*, 344-360.

Lu, Q., and Wood, J.G. (1993). Functional studies of Alzheimer's disease tau protein. J. Neurosci. *13*, 508-515.

Lye, R.J., Porter, M.E., Scholey, J.M., and McIntosh, J.R. (1987). Identification of a microtubule-based cytoplasmic motor in the nematode C. elegans. Cell *51*, 309-318.

Mallik, R., Carter, B.C., Lex, S.A., King, S.J., and Gross, S.P. (2004). Cytoplasmic dynein functions as a gear in response to load. Nature *427*, 649-652.

Mallik, R., Petrov, D., Lex, S.A., King, S.J., and Gross, S.P. (2005). Building complexity: an in vitro study of cytoplasmic dynein with in vivo implications. Curr. Biol. *15*, 2075-2085.

Mandelkow, E.M., Mandelkow, E., and Milligan, R.A. (1991). Microtubule dynamics and microtubule caps: a time-resolved cryo-electron microscopy study. J. Cell Biol. *114*, 977-991.

Manna, T., Honnappa, S., Steinmetz, M.O., and Wilson, L. (2008). Suppression of microtubule dynamic instability by the +TIP protein EB1 and its modulation by the CAP-Gly domain of p150glued. Biochemistry *47*, 779-786.

Margolis, R.L., and Wilson, L. (1981). Microtubule treadmills--possible molecular machinery. Nature *293*, 705-711.

Markus, S.M., and Lee, W.L. (2011). Regulated offloading of cytoplasmic dynein from microtubule plus ends to the cortex. Dev. Cell *20*, 639-651.

Matsuo, E.S., Shin, R.W., Billingsley, M.L., Van deVoorde, A., O'Connor, M., Trojanowski, J.Q., and Lee, V.M. (1994). Biopsy-derived adult human brain tau is phosphorylated at many of the same sites as Alzheimer's disease paired helical filament tau. Neuron *13*, 989-1002.

Maurer, S.P., Bieling, P., Cope, J., Hoenger, A., and Surrey, T. (2011). GTPgammaS microtubules mimic the growing microtubule end structure recognized by end-binding proteins (EBs). Proc. Natl. Acad. Sci. U. S. A. *108*, 3988-3993.

Maurer, S.P., Fourniol, F.J., Bohner, G., Moores, C.A., and Surrey, T. (2012). EBs recognize a nucleotide-dependent structural cap at growing microtubule ends. Cell *149*, 371-382.

McIntosh, J.R., Morphew, M.K., Grissom, P.M., Gilbert, S.P., and Hoenger, A. (2009). Lattice structure of cytoplasmic microtubules in a cultured Mammalian cell. J. Mol. Biol. *394*, 177-182.

McKenney, R.J., Weil, S.J., Scherer, J., and Vallee, R.B. (2011). Mutually exclusive cytoplasmic dynein regulation by NudE-Lis1 and dynactin. J. Biol. Chem. *286*, 39615-39622.

Mikami, A., Paschal, B.M., Mazumdar, M., and Vallee, R.B. (1993). Molecular cloning of the retrograde transport motor cytoplasmic dynein (MAP 1C). Neuron *10*, 787-796.

Mishima, M., Maesaki, R., Kasa, M., Watanabe, T., Fukata, M., Kaibuchi, K., and Hakoshima, T. (2007). Structural basis for tubulin recognition by cytoplasmic linker protein 170 and its autoinhibition. Proc. Natl. Acad. Sci. U. S. A. *104*, 10346-10351.

Mitchison, T., and Kirschner, M. (1984). Dynamic instability of microtubule growth. Nature *312*, 237-242.

Mitchison, T.J., and Kirschner, M.W. (1985). Properties of the kinetochore in vitro. I. Microtubule nucleation and tubulin binding. J. Cell Biol. *101*, 755-765.

Mocz, G., and Gibbons, I.R. (2001). Model for the motor component of dynein heavy chain based on homology to the AAA family of oligomeric ATPases. Structure *9*, 93-103.

Molodtsov, M.I., Grishchuk, E.L., Efremov, A.K., McIntosh, J.R., and Ataullakhanov, F.I. (2005). Force production by depolymerizing microtubules: a theoretical study. Proc. Natl. Acad. Sci. U. S. A. *102*, 4353-4358.

Moore, J.K., and Cooper, J.A. (2010). Coordinating mitosis with cell polarity: Molecular motors at the cell cortex. Semin. Cell Dev. Biol. *21*, 283-289.

Moore, J.K., Sept, D., and Cooper, J.A. (2009). Neurodegeneration mutations in dynactin impair dynein-dependent nuclear migration. Proc. Natl. Acad. Sci. U. S. A. *106*, 5147-5152.

Morgan, J.L., Song, Y., and Barbar, E. (2011). Structural dynamics and multiregion interactions in dynein-dynactin recognition. J. Biol. Chem. *286*, 39349-39359.

Moughamian, A., and Holzbaur, E.L. (2011). Cytoplasmic Dynein Dysfunction and Neurodegenerative Disease. In Dyneins: Structure, Biology and Disease, S.M. King, ed. (London.: Elsevier.), pp. 584-601.

Moughamian, A.J., and Holzbaur, E.L. (2012). Dynactin is required for transport initiation from the distal axon. Neuron *74*, 331-343.

Muller-Reichert, T., Chretien, D., Severin, F., and Hyman, A.A. (1998). Structural changes at microtubule ends accompanying GTP hydrolysis: information from a slowly hydrolyzable analogue of GTP, guanylyl (alpha,beta)methylenediphosphonate. Proc. Natl. Acad. Sci. U. S. A. *95*, 3661-3666.

Muresan, V., Stankewich, M.C., Steffen, W., Morrow, J.S., Holzbaur, E.L., and Schnapp, B.J. (2001). Dynactin-dependent, dynein-driven vesicle transport in the absence of membrane proteins: a role for spectrin and acidic phospholipids. Mol. Cell *7*, 173-183.

Nguyen, M.M., Stone, M.C., and Rolls, M.M. (2011). Microtubules are organized independently of the centrosome in Drosophila neurons. Neural Dev *6*, 38.

Nogales, E., Whittaker, M., Milligan, R.A., and Downing, K.H. (1999). High-resolution model of the microtubule. Cell *96*, 79-88.

Nogales, E., Wolf, S.G., and Downing, K.H. (1998). Structure of the alpha beta tubulin dimer by electron crystallography. Nature *391*, 199-203.

Olmsted, J.B., and Borisy, G.G. (1975). Ionic and nucleotide requirements for microtubule polymerization in vitro. Biochemistry *14*, 2996-3005.

Ori-McKenney, K.M., and Vallee, R.B. (2011). Neuronal migration defects in the Loa dynein mutant mouse. Neural Dev *6*, 26.

Ori-McKenney, K.M., Xu, J., Gross, S.P., and Vallee, R.B. (2010). A cytoplasmic dynein tail mutation impairs motor processivity. Nat. Cell Biol. *12*, 1228-1234.

Paschal, B.M., Mikami, A., Pfister, K.K., and Vallee, R.B. (1992). Homology of the 74-kD cytoplasmic dynein subunit with a flagellar dynein polypeptide suggests an intracellular targeting function. J. Cell Biol. *118*, 1133-1143.

Paschal, B.M., Shpetner, H.S., and Vallee, R.B. (1987). MAP 1C is a microtubule-activated ATPase which translocates microtubules in vitro and has dynein-like properties. J. Cell Biol. *105*, 1273-1282.

Paschal, B.M., and Vallee, R.B. (1987). Retrograde transport by the microtubule-associated protein MAP 1C. Nature *330*, 181-183.

Pecqueur, L., Duellberg, C., Dreier, B., Jiang, Q., Wang, C., Pluckthun, A., Surrey, T., Gigant, B., and Knossow, M. (2012). A designed ankyrin repeat protein selected to bind to tubulin caps the microtubule plus end. Proc. Natl. Acad. Sci. U. S. A. *109*, 12011-12016.

Perez, F., Diamantopoulos, G.S., Stalder, R., and Kreis, T.E. (1999). CLIP-170 highlights growing microtubule ends in vivo. Cell *96*, 517-527.

Perlson, E., Jeong, G.B., Ross, J.L., Dixit, R., Wallace, K.E., Kalb, R.G., and Holzbaur, E.L. (2009). A switch in retrograde signaling from survival to stress in rapid-onset neurodegeneration. J. Neurosci. *29*, 9903-9917.

Perlson, E., Maday, S., Fu, M.M., Moughamian, A.J., and Holzbaur, E.L. (2010). Retrograde axonal transport: pathways to cell death? Trends Neurosci. *33*, 335-344.

Pierre, P., Scheel, J., Rickard, J.E., and Kreis, T.E. (1992). CLIP-170 links endocytic vesicles to microtubules. Cell *70*, 887-900.

Qiu, W., Derr, N.D., Goodman, B.S., Villa, E., Wu, D., Shih, W., and Reck-Peterson, S.L. (2012). Dynein achieves processive motion using both stochastic and coordinated stepping. Nat. Struct. Mol. Biol. *19*, 193-200.

Riehemann, K., and Sorg, C. (1993). Sequence homologies between four cytoskeleton-associated proteins. Trends Biochem. Sci. *18*, 82-83.

Roberts, A.J., Malkova, B., Walker, M.L., Sakakibara, H., Numata, N., Kon, T., Ohkura, R., Edwards, T.A., Knight, P.J., Sutoh, K., *et al.* (2012). ATP-Driven Remodeling of the Linker Domain in the Dynein Motor. Structure.

Roberts, A.J., Numata, N., Walker, M.L., Kato, Y.S., Malkova, B., Kon, T., Ohkura, R., Arisaka, F., Knight, P.J., Sutoh, K., *et al.* (2009). AAA+ Ring and linker swing mechanism in the dynein motor. Cell *136*, 485-495.

Rome, P., Montembault, E., Franck, N., Pascal, A., Glover, D.M., and Giet, R. (2010). Aurora A contributes to p150(glued) phosphorylation and function during mitosis. J. Cell Biol. *189*, 651-659.

Ross, J.L., Shuman, H., Holzbaur, E.L., and Goldman, Y.E. (2008). Kinesin and dynein-dynactin at intersecting microtubules: motor density affects dynein function. Biophys. J. *94*, 3115-3125.

Ross, J.L., Wallace, K., Shuman, H., Goldman, Y.E., and Holzbaur, E.L. (2006). Processive bidirectional motion of dynein-dynactin complexes in vitro. Nat. Cell Biol. *8*, 562-570.

Sabatini, D.D., Bensch, K., and Barrnett, R.J. (1963). Cytochemistry and electron microscopy. The preservation of cellular ultrastructure and enzymatic activity by aldehyde fixation. J. Cell Biol. *17*, 19-58.

Salmon, T., Walker, R.A., and Pryer, N.K. (1989). Video-enhanced differential interference contrast light microscopy. BioTechniques *7*, 624-633.

Samora, C.P., Mogessie, B., Conway, L., Ross, J.L., Straube, A., and McAinsh, A.D. MAP4 and CLASP1 operate as a safety mechanism to maintain a stable spindle position in mitosis. Nat Cell Biol *13*, 1040-1050.

Sandblad, L., Busch, K.E., Tittmann, P., Gross, H., Brunner, D., and Hoenger, A. (2006). The Schizosaccharomyces pombe EB1 homolog Mal3p binds and stabilizes the microtubule lattice seam. Cell *127*, 1415-1424.

Schafer, D.A., Gill, S.R., Cooper, J.A., Heuser, J.E., and Schroer, T.A. (1994). Ultrastructural analysis of the dynactin complex: an actin-related protein is a component of a filament that resembles F-actin. J. Cell Biol. *126*, 403-412.

Scheel, J., Pierre, P., Rickard, J.E., Diamantopoulos, G.S., Valetti, C., van der Goot, F.G., Haner, M., Aebi, U., and Kreis, T.E. (1999). Purification and analysis of authentic CLIP-170 and recombinant fragments. J. Biol. Chem. *274*, 25883-25891.

Schek, H.T., 3rd, Gardner, M.K., Cheng, J., Odde, D.J., and Hunt, A.J. (2007). Microtubule assembly dynamics at the nanoscale. Curr. Biol. *17*, 1445-1455.

Schnapp, B.J. (1986). Viewing single microtubules by video light microscopy. Methods Enzymol. *134*, 561-573.

Schnapp, B.J., and Reese, T.S. (1989). Dynein is the motor for retrograde axonal transport of organelles. Proc. Natl. Acad. Sci. U. S. A. *86*, 1548-1552.

Schroeder, H.W., 3rd, Mitchell, C., Shuman, H., Holzbaur, E.L., and Goldman, Y.E. (2010). Motor number controls cargo switching at actin-microtubule intersections in vitro. Curr. Biol. *20*, 687-696.

Schroer, T.A. (2004). Dynactin. Annu. Rev. Cell Dev. Biol. *20*, 759-779.

Schroer, T.A., and Sheetz, M.P. (1991). Two activators of microtubule-based vesicle transport. J. Cell Biol. *115*, 1309-1318.

Schroer, T.A., Steuer, E.R., and Sheetz, M.P. (1989). Cytoplasmic dynein is a minus end-directed motor for membranous organelles. Cell *56*, 937-946.

Seetapun, D., Castle, B.T., McIntyre, A.J., Tran, P.T., and Odde, D.J. (2012). Estimating the Microtubule GTP Cap Size In Vivo. Curr. Biol.

Shelanski, M.L., and Taylor, E.W. (1967). Isolation of a protein subunit from microtubules. J. Cell Biol. *34*, 549-554.

Shpetner, H.S., Paschal, B.M., and Vallee, R.B. (1988). Characterization of the microtubule-activated ATPase of brain cytoplasmic dynein (MAP 1C). J. Cell Biol. *107*, 1001-1009.

Siegrist, S.E., and Doe, C.Q. (2007). Microtubule-induced cortical cell polarity. Genes Dev. *21*, 483-496.

Sievers, F., Wilm, A., Dineen, D., Gibson, T.J., Karplus, K., Li, W., Lopez, R., McWilliam, H., Remmert, M., Soding, J., *et al.* (2011). Fast, scalable generation of high-quality protein multiple sequence alignments using Clustal Omega. Mol Syst Biol *7*, 539.

Siller, K.H., and Doe, C.Q. (2009). Spindle orientation during asymmetric cell division. Nat Cell Biol *11*, 365-374.

Slep, K.C., and Vale, R.D. (2007). Structural basis of microtubule plus end tracking by XMAP215, CLIP-170, and EB1. Mol. Cell *27*, 976-991.

Soppina, V., Rai, A.K., Ramaiya, A.J., Barak, P., and Mallik, R. (2009). Tug-of-war between dissimilar teams of microtubule motors regulates transport and fission of endosomes. Proc. Natl. Acad. Sci. U. S. A. *106*, 19381-19386.

Stebbings, H. (1988). Microtubule motors. Cytoplasmic dynein graduates. Nature *336*, 14-15.

Steinmetz, M.O., and Akhmanova, A. (2008). Capturing protein tails by CAP-Gly domains. Trends Biochem. Sci. *33*, 535-545.

Stephens, R.E., Renaud, F.L., and Gibbons, I.R. (1967). Guanine nucleotide associated with the protein of the outer fibers of flagella and cilia. Science *156*, 1606-1608.

Stiess, M., Maghelli, N., Kapitein, L.C., Gomis-Ruth, S., Wilsch-Brauninger, M., Hoogenraad, C.C., Tolic-Norrelykke, I.M., and Bradke, F. (2010). Axon extension occurs independently of centrosomal microtubule nucleation. Science *327*, 704-707.

Takagi, Y., Homsher, E.E., Goldman, Y.E., and Shuman, H. (2006). Force generation in single conventional actomyosin complexes under high dynamic load. Biophys. J. *90*, 1295-1307.

Telley, I.A., Bieling, P., and Surrey, T. (2011). Reconstitution and quantification of dynamic microtubule end tracking in vitro using TIRF microscopy. Methods Mol. Biol. *777*, 127-145.

Tirnauer, J.S., Grego, S., Salmon, E.D., and Mitchison, T.J. (2002). EB1-microtubule interactions in Xenopus egg extracts: role of EB1 in microtubule stabilization and mechanisms of targeting to microtubules. Mol. Biol. Cell *13*, 3614-3626.

Toba, S., Watanabe, T.M., Yamaguchi-Okimoto, L., Toyoshima, Y.Y., and Higuchi, H. (2006). Overlapping hand-over-hand mechanism of single molecular motility of cytoplasmic dynein. Proc. Natl. Acad. Sci. U. S. A. *103*, 5741-5745.

Tokito, M.K., Howland, D.S., Lee, V.M., and Holzbaur, E.L. (1996). Functionally distinct isoforms of dynactin are expressed in human neurons. Mol. Biol. Cell *7*, 1167-1180.

Trybus, K.M., Freyzon, Y., Faust, L.Z., and Sweeney, H.L. (1997). Spare the rod, spoil the regulation: necessity for a myosin rod. Proc. Natl. Acad. Sci. U. S. A. *94,* 48-52.

Vale, R.D., Reese, T.S., and Sheetz, M.P. (1985). Identification of a novel force-generating protein, kinesin, involved in microtubule-based motility. Cell *42*, 39-50.

Valetti, C., Wetzel, D.M., Schrader, M., Hasbani, M.J., Gill, S.R., Kreis, T.E., and Schroer, T.A. (1999). Role of dynactin in endocytic traffic: effects of dynamitin overexpression and colocalization with CLIP-170. Mol. Biol. Cell *10*, 4107-4120.

VanBuren, V., Cassimeris, L., and Odde, D.J. (2005). Mechanochemical model of microtubule structure and self-assembly kinetics. Biophys J *89*, 2911-2926.

VanBuren, V., Odde, D.J., and Cassimeris, L. (2002). Estimates of lateral and longitudinal bond energies within the microtubule lattice. Proc. Natl. Acad. Sci. U. S. A. *99*, 6035-6040.

Varga, V., Helenius, J., Tanaka, K., Hyman, A.A., Tanaka, T.U., and Howard, J. (2006). Yeast kinesin-8 depolymerizes microtubules in a length-dependent manner. Nat. Cell Biol. *8*, 957-962.

Vaughan, K.T. (2005). TIP maker and TIP marker; EB1 as a master controller of microtubule plus ends. J. Cell Biol. *171*, 197-200.

Vaughan, K.T., and Vallee, R.B. (1995). Cytoplasmic dynein binds dynactin through a direct interaction between the intermediate chains and p150Glued. J. Cell Biol. *131*, 1507-1516.

Vaughan, P.S., Miura, P., Henderson, M., Byrne, B., and Vaughan, K.T. (2002). A role for regulated binding of p150(Glued) to microtubule plus ends in organelle transport. J. Cell Biol. *158*, 305-319.

Vitre, B., Coquelle, F.M., Heichette, C., Garnier, C., Chretien, D., and Arnal, I. (2008). EB1 regulates microtubule dynamics and tubulin sheet closure in vitro. Nat. Cell Biol. *10*, 415-421.

Voter, W.A., O'Brien, E.T., and Erickson, H.P. (1991). Dilution-induced disassembly of microtubules: relation to dynamic instability and the GTP cap. Cell Motil Cytoskeleton *18*, 55-62.

Wadsworth, P. (1999). Regional regulation of microtubule dynamics in polarized, motile cells. Cell Motil Cytoskeleton *42*, 48-59.

Wagner, U., Utton, M., Gallo, J.M., and Miller, C.C. (1996). Cellular phosphorylation of tau by GSK-3 beta influences tau binding to microtubules and microtubule organisation. J. Cell Sci. *109 (Pt 6)*, 1537-1543.

Walker, R.A., O'Brien, E.T., Pryer, N.K., Soboeiro, M.F., Voter, W.A., Erickson, H.P., and Salmon, E.D. (1988). Dynamic instability of individual microtubules analyzed by video light microscopy: rate constants and transition frequencies. J. Cell Biol. *107*, 1437-1448.

Wang, H.W., and Nogales, E. (2005). Nucleotide-dependent bending flexibility of tubulin regulates microtubule assembly. Nature *435*, 911-915.

Wang, Z., Khan, S., and Sheetz, M.P. (1995). Single cytoplasmic dynein molecule movements: characterization and comparison with kinesin. Biophys. J. *69*, 2011-2023.

Waterman-Storer, C.M., Karki, S., and Holzbaur, E.L. (1995). The p150Glued component of the dynactin complex binds to both microtubules and the actin-related protein centractin (Arp-1). Proc. Natl. Acad. Sci. U. S. A. *92*, 1634-1638.

Waterman-Storer, C.M., and Salmon, E.D. (1997). Actomyosin-based retrograde flow of microtubules in the lamella of migrating epithelial cells influences microtubule dynamic instability and turnover and is associated with microtubule breakage and treadmilling. J. Cell Biol. *139*, 417-434.

Watson, P., and Stephens, D.J. (2006). Microtubule plus-end loading of p150(Glued) is mediated by EB1 and CLIP-170 but is not required for intracellular membrane traffic in mammalian cells. J. Cell Sci. *119*, 2758-2767.

Weisbrich, A., Honnappa, S., Jaussi, R., Okhrimenko, O., Frey, D., Jelesarov, I., Akhmanova, A., and Steinmetz, M.O. (2007). Structure-function relationship of CAP-Gly domains. Nat. Struct. Mol. Biol. *14*, 959-967.

Westermann, S., Avila-Sakar, A., Wang, H.W., Niederstrasser, H., Wong, J., Drubin, D.G., Nogales, E., and Barnes, G. (2005). Formation of a dynamic kinetochore-microtubule interface through assembly of the Dam1 ring complex. Mol. Cell *17*, 277-290.

Westermann, S., Wang, H.W., Avila-Sakar, A., Drubin, D.G., Nogales, E., and Barnes, G. (2006). The Dam1 kinetochore ring complex moves processively on depolymerizing microtubule ends. Nature *440*, 565-569.

Xiang, X., Han, G., Winkelmann, D.A., Zuo, W., and Morris, N.R. (2000). Dynamics of cytoplasmic dynein in living cells and the effect of a mutation in the dynactin complex actin-related protein Arp1. Curr. Biol. *10*, 603-606.

Yanagisawa, T., Hasegawa, S., and Mohri, H. (1968). The bound nucleotides of the isolated microtubules of sea-urchin sperm flagella and their possible role in flagellar movement. Exp. Cell Res. *52*, 86-100.

Yeh, T.Y., Quintyne, N.J., Scipioni, B.R., Eckley, D.M., and Schroer, T.A. (2012). Dynactin's pointed end complex is a cargo-targeting module. Mol. Biol. Cell.

Yildiz, A., Tomishige, M., Gennerich, A., and Vale, R.D. (2008). Intramolecular strain coordinates kinesin stepping behavior along microtubules. Cell *134*, 1030-1041.

Yildiz, A., Tomishige, M., Vale, R.D., and Selvin, P.R. (2004). Kinesin walks hand-over-hand. Science *303*, 676-678.

Zanic, M., Stear, J.H., Hyman, A.A., and Howard, J. (2009). EB1 recognizes the nucleotide state of tubulin in the microtubule lattice. PLoS One *4*, e7585.

Zhang, B., Carroll, J., Trojanowski, J.Q., Yao, Y., Iba, M., Potuzak, J.S., Hogan, A.M., Xie, S.X., Ballatore, C., Smith, A.B., 3rd, *et al.* (2012). The microtubule-stabilizing agent, epothilone D, reduces axonal dysfunction, neurotoxicity, cognitive deficits, and Alzheimer-like pathology in an interventional study with aged tau transgenic mice. J. Neurosci. *32*, 3601-3611.

Zhang, J., Li, S., Fischer, R., and Xiang, X. (2003). Accumulation of cytoplasmic dynein and dynactin at microtubule plus ends in Aspergillus nidulans is kinesin dependent. Mol. Biol. Cell *14*, 1479-1488.

Zhang, J., Yao, X., Fischer, L., Abenza, J.F., Penalva, M.A., and Xiang, X. (2011). The p25 subunit of the dynactin complex is required for dynein-early endosome interaction. J. Cell Biol. *193*, 1245-1255.

Zhapparova, O.N., Bryantseva, S.A., Dergunova, L.V., Raevskaya, N.M., Burakov, A.V., Bantysh, O.B., Shanina, N.A., and Nadezhdina, E.S. (2009). Dynactin subunit p150Glued isoforms notable for differential interaction with microtubules. Traffic *10*, 1635-1646.

Zhu, Z.C., Gupta, K.K., Slabbekoorn, A.R., Paulson, B.A., Folker, E.S., and Goodson, H.V. (2009). Interactions between EB1 and microtubules: dramatic effect of affinity tags and evidence for cooperative behavior. J. Biol. Chem. *284*, 32651-32661.